DE GRUYTER
OPEN

Contributions to Geophysics and Geodesy Vol. 48/1, 2018 (1–21)

Applications of shallow seismic refraction measurements in the Western Carpathians (Slovakia): case studies

Bibiana BRIXOVÁ, Andrea MOSNÁ, René PUTIŠKA

Comenius University in Bratislava, Faculty of Natural Sciences,
Department of Applied and Environmental Geophysics,
Mlynská dolina, Ilkovičova 6, SK-84215 Bratislava, Slovak Republic;
e-mail: kytkova1@gmail.com

Abstract: Shallow seismic measurement, specifically seismic refraction tomography, is an effective geophysical method that has applications in various sectors. It enables the search for and determination of the course of the interfaces, thus helping to resolve geological, environmental, hydrogeological, engineering, geotechnical and other problems. The paper demonstrates the possibilities of using these methods through examples of shallow seismic measurements that have been performed at various four locations in the Western Carpathian Mountains. The first case study describes Monastery Pond at Katarínka. It was found that, the basement of the Monastery pond is at a depth of 2–3 m below the surface and the results were also confirmed by electrical resistivity tomography (ERT). The next measurement through the thermal power station waste storage showed that the storage area base runs at a depth of about 20 m under the measured profile. The third case study addresses the depth of groundwater depth in the area of Borská nížina. The measurement confirmed the assumed depth of ground water level at 3.35 m below the surface. In the last case study, border fault between the Turiec Basin and the Malá Fatra Mts. was mapped by application of shallow refraction methods. The results show that shallow seismic methods shed light on the problem and in combination with other geophysical methods are an effective tool with great potential. They provide very useful data for shallow mapping applications.

Key words: refraction seismics, seismic refraction tomography, shallow seismic measurements, Western Carpathians, case study

1. Introduction

In the past, seismic methods were mainly associated with hydrocarbon exploration, whose main benefit is their large depth range. On the other hand

doi: 10.2478/congeo-2018-0001

the shallow refraction measurements were used to determine the parameters of the low-velocity layer for the treatment of processing for deep reflection seismic profiles.

Shallow seismic methods have historical roots dating back to the 1930s, when limited shallow refraction work was performed using the Intercept-Time method (*Steeples, 2000*). The development of technology in both the acquisition and processing has led to substantial progress in the use of shallow seismic measurements since 1980 (*Steeples, 2000; Steeples and Miller, 1990*).

The use of surface waves has also evolved. These waves which overlap the useful signal and have to be filtered out in reflection and refraction processing (especially in the shallow parts of the profiles), have found application in shallow research methods such as a SASW (Spectral Analysis of Surface Waves – *Nazarian et al., 1983*) and MASW (Multichannel Analysis of Surface Waves – *Park et al., 1998, 1999; Xia et al., 1999, 2000*). The use of shallow seismic measurements is excellent, particularly for determining the depth or course of geological interfaces for different purposes: (a) for geo-engineering, geotechnical investigation and the assessment of landslide areas (e.g., *Beng et al., 1982; Shtivelman, V., 2003; Cardarelli et al., 2014; Coulouma et al., 2012; Hack, 2000; McClymont et al., 2016*); (b) for hydrogeological purposes (e.g., *Haeni, 1986; Gordon, 1997; Gabr et al., 2012; Osumeje and Kudamnya, 2014; Pandula, 2000; Shtivelman, 2003; Prekopová et al., 2016*); and (c) for archaeological exploration (e.g., *Tsokas et al., 1995; Shtivelman, 2003; Henley, 2003; Shahrukh et al., 2012*).

The basic parameter for the successful use of seismic methods for any purpose is to achieve the possibilities and limitations of these methods. In some cases, the geological layers cannot be detected (*Soske, 1954* and *Sander, 1978* in *Haeni, 1986*). One of the criteria is an insufficient velocity contrast of layer or thickness in order to return first arrival energy (*Haeni, 1986*). This is related to the vertical resolution of the method. Seismic method vertical resolution depends on the generally accepted one-quarter wavelength axiom (after *Widess, 1973* in *Nanda, 2016*). If the thickness of a layer is less than one-quarter of a wavelength of the incidence wave, the thin bed will not be visible on the time–distance graph (*Reynolds, 1997*). Because the wavelength is a ratio of wave velocity and frequency, in a rock environment with a wave velocity of 2000 m/s and a frequency of 50 Hz, the

vertical resolution will be approximately 10 m. Layers thinner than 10 m will not be detected. The vertical resolution decreases with depth because of the attenuation signal of the higher frequency component and higher velocities (*Nanda, 2016*). Better resolution can be expected in shallow parts of the environment. Vertical resolution is attainable with a reflection of about 10 cm as described in *Steeples (1998)*. The vertical resolution is sometimes referred to as a percentage of the practical survey depth. For refraction measurement it is presented as 10–20% of depth (*Enviroscan, 2018*). Survey depth for refraction seismic is deposed as 1/5 to 1/4 of the maximum offset (shot-geophone separation) (*Enviroscan, 2018*). The appropriate spacing of geophones is an important parameter for layer detection by seismic refraction (*Reynolds, 1997*). If the distance between geophones is too large, there is not enough sampling for an identification of the layer on time-distance graphs. This is another layer problem. In planning for the use of seismic refraction measurement, one must be aware of another limitation of this method. Based on the principles of the propagation of seismic waves and the conditions for critically refracted wave occurrence, refraction seismic measurements are only able to detect layers when velocity increases with depth (*Reynolds, 1997*).

The most commonly used shallow geophysical methods, especially for non-demanding terrain measurement, are electrical resistivity tomography (ERT) and georadar. However, as one of the selected case studies has shown, these methods are not always successful. Therefore, the aim of this article is to demonstrate that shallow seismic methods have a wide range of applications and are equivalent methods for various shallow survey application. This paper provides case studies from four different locations in the Western Carpathians (Fig. 1). The first case study relates to an archaeological research on the marginal part of the Malé Karpaty Mts. The goal is to map the basment of Monastery Pond. The next case study deals with an environmental issue, namely, waste storage at a thermal power station. The third case study maps the tectonic contact of the Turiec Basin with the Malá Fatra Mts. The last case study features an example of using the shallow seismic methods for hydrogeological purposes. It is aimed at searching for the surface of underground water levels.

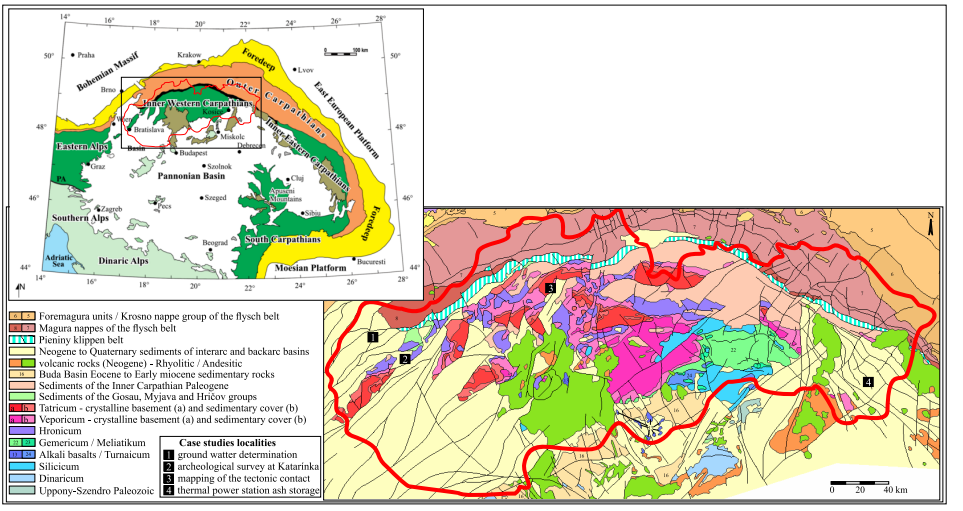

Fig. 1: Geological scheme of the Western Carpathians (after *Bielik, 1998* and *Geological map of Slovakia, 2013*) with marked case studies localities. MK – Malé Karpaty Mts., BN – Borská nížina, TB – Turiec Basin, MF – Malá Fatra Mts.

2. Methodology

Refraction seismic methods use controlled source seismic waves, specifically refraction waves, to determine depths to the interface within the subsurface and the velocities of the layer between the interfaces (Lillie, 1999). In seismic refraction surveys on land, a number of geophones are laid out along a cable in a straight line. In the simplest case, the seismic source (shot) is located at the beginning and end of a geophone line. The source can also be positioned at a location along the geophone spread, or at a discrete distance from the end of the spread. The positioning of shots provides adequate lateral resolution (*Reylnolds, 1997*).

The seismic refraction tomography profile (SRT) requires a higher density of sources and receivers than in conventional surveys to obtain high resolution profile.

The seismic waves spread from the source and the arrival of each wave is detected along the set of geophones. Direct waves and waves critically refracted from interfaces are useful for refraction seismic interpretation. The

direct wave comes to geophones as the first to the offset known as the crossover distance. After this offset, critically refracted waves precede the direct wave. During processing, these first arrivals are marked for each geophone on a seismograph. They are associated with travel times and plotted on a time-distance graph. The gradient of this graph changes at the crossover distance from the slope of direct wave arrivals (characterized by the velocity of direct wave) to the slope for refracted signals. The time–distance graphs are then used to calculate the velocity of the interpreted layers and the depth of the interfaces. Several different interpretational methods for seismic refraction have been published. In *Reynolds (1997)*, two methods emerge as the most commonly used are the 'plus-minus' method (*Hagedoorn, 1959*) and the generalized reciprocal method (*Palmer, 1980*).

Seismic refraction tomography is an alternative to conventional seismic refraction analysis methods (*Sheehan et al., 2005*). Conventional refraction methods assume that seismic velocity structures are simple and primarily attempt to map a refractor. Tomography methods calculate travel times and raypaths in a regular grid model and use an inversion technique to reconstruct seismic velocities (*Zhang and Toksöz, 1998*). In the case of 2D refraction vertical tomography, the starting model must first be generated. Ray tracing is used for the calculation of travel times for this model. The synthetic data obtained by ray tracing are compared with the field data and the initial model is modified until the best fit between the model and field data is achieved.

Acquisition and processing

The data for seismic refraction tomography at the Katarínka archaeological site was obtained by a 24-channel DMT equipment with 10 Hz geophones and a hammer with 5 stacks as the source served for better resolution. In the other cases, a 36-channel M.A.E. A6000-S equipment with 4.5 Hz geophones and a hammer as a source was used.

The measured data were processed in Reflexw Version 8.0 software (developed by *Sandmeier, 2016*) for the processing of seismic, acoustic or electromagnetic reflection, refraction and transmission data. At first, the SEG-2 data were imported to the software background for refraction processing and the first arrivals were picked (see Fig. 6b). Then the time-distance curves were created from the picked travel times, and the slopes of primary wave

curves and refracted curves from various interfaces were marked for each shot (see Fig. 5a and Fig. 6c). After this analysis and interpretation of first arrivals, the velocity model of the subsurface environment was created. This served as the initial model for seismic refraction tomography. The result of tomography is a velocity model with a continuous velocity gradient across a subsurface which is interpreted depending on the specific case study.

Some examples also show the influence of various factors, such as the changing humidity of the rock environment or its consolidation, to obtained velocity values in the shallow survey. Interpreted velocity interfaces have been verified by other geophysical measurements (mainly ERT) in the Katarínka and Bystrička areas.

3. Case studies

3.1. Mapping the bottom of Monastery Pond at the Katarínka site

Katarínka is a famous archaeological site around the ruins of Saint Catherine's Abbey (founded in 1618) on the hills of the Malé Karpaty Mts. near the village of Dechtice (Figs. 1 and 2). Intensive geophysical research was conducted in this area in 2009 (*INCA, 2009* – International Course on ArchaeoGeophysics) to help find buried ruins of buildings near the monastery, surrounding chapels, a cavern under the presbytery and others. As a continuation of this research, seismic refraction measurements and ERT were applied to identify the bottom of Monastery Pond.

From a geological point of view, the entire archaeological site is located in the territory of the Brezovské Karpaty Mts., which belong to the Malé Karpaty Mts. The Brezovské Karpaty Mts. are mostly comprised of Mesozoic rocks. Triassic sediments are dominant, while Jurassic and Cretaceous sediments are less preserved. The Triassic sediments belong to the Nedzov Nappe Jablonica Group (*Salaj et al., 1987*). In area of abbey ruins bloom out light-grey bedded Wetterstein Dolomite (Ladinian-Kordevolian) (*Geological map of Slovakia, 2013*). Neogene and Quaternary deposits extend to the edge of the mountain range. Quartery deposits are represented by fluvial sediments of alluvial flats (deluvial and eolic sediments, loesses). Neogene sediments, in the prospecting area are represented by Lakšárska Nová Ves Formation – Jablonica Conglomerates (polymict conglomerates,

Karpatian) (*Salaj et al., 1987; Geological map of Slovakia, 2013*).

The seismic profile is situated southwest of the Abbey ruins, in the area where the pond was assumed on the basis of historical documents. According to documents in the State Archives in Bratislava, *Matulová (2003)* states that the pond dimensions are about 49 × 31.36 m. Remnants of the pond barrier are still visible in the terrain. Two 46 m long profiles in the SW–NE direction with 12 overlapping geophones for seismic refraction data acquisition were used for this survey (Fig. 3a). Geophone spacing at both profiles was 2 m. Shot points were placed along each profile at a distance of 2 m, with a beginning of excitation −2 m from the first geophone and the final shot being 2 m beyond the last geophone. The ERT was measured at a 94 m long profile with 1-m electrode spacing. The Schlumberger and dipole-dipole resistance methods were used. The Seismic and ERT profile began at the same point and had the same course. Measurements were made

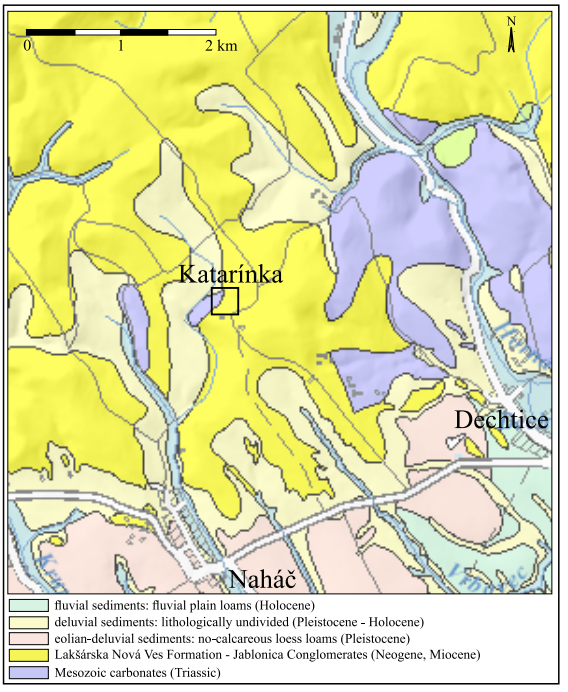

Fig. 2: Location of the Katarinka monastery area on a detailed geological map (after *Salaj et al., 1987* and *Geological map of Slovakia, 2013*).

on different days. If both methods can be measured together, the parallel profiles sufficiently distanced from each other should be used because of the degradation of the signal-to-noise ratio at geophones due to ERT measurement.

The sought after pond floor was interpreted by the velocity refraction profile, ERT profile, and seismic reflection profile (Fig. 3). Based on the

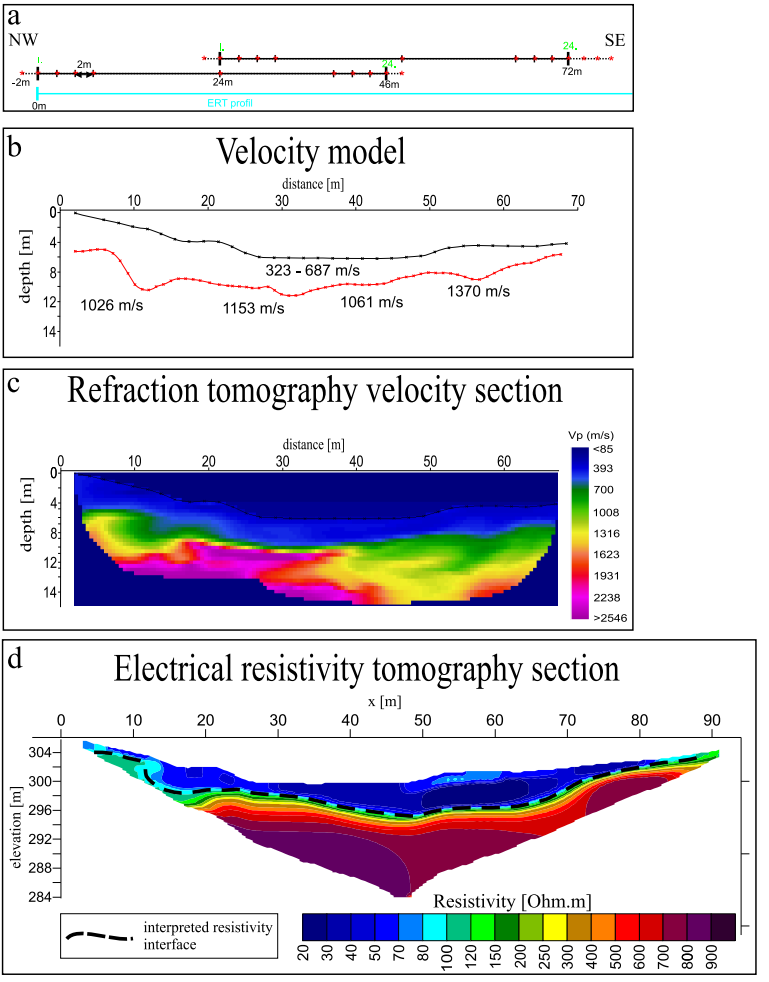

Fig. 3: Results along the seismic and ERT profile at the Katarinka case study locality. a) velocity model, b) SRT and c) ERT.

measured P-wave velocity ($V_p < 700$ m/s) and the resistance ($< 100\,\Omega$.m), the thickness of the surface sediments (scree, vegetal soil), that probably filled the pond space after the collapse of the monastery was determined. The bottom of the pond is anticipated to be at a depth of 2–3 m below the surface. At the bottom of the low velocity layer the conglomerate or dolomite rock bottom should be interpreted. In the upper part next to the surface sediment layer, the disturbed and wetted rocks are assumed due to a relatively low V_p and resistance values. The velocities m/s measured mainly in the NW section of the profile at a depth of 7–8 m correspond with standard Vp values for dolomites or conglomerates (dolomites and conglomerates have mostly the same standard velocity and resistivity range). In the case of dolomites, this can be a continuation of the occurrence of a Wetterstein dolomite rising to the surface at the church ruins. The same result can be interpreted on the ERT profile.

3.2. Estimation of the thickness of coal ash and the run of the bottom at the thermal power station ash storage area

This seismic profile passes through the thermal power station waste storage area. The area of interest consists of a hill of coal ash stored on loam cover on a surface of approx. 0.67 km^2. The area surrounding the dump is mostly formed by Quarternary fluvial sediments (Fig. 4), mainly fluvial plain fine-sandy loam to fine-grained sands or lithofacially undivided loam (*Geological map of Slovakia, 2013*).

The acquisition for seismic refraction tomography was performed on nine overlapping lines each of 175 m in length. The geophones were distributed at 5 m intervals, the acquisition lines lap was comprised of 12 geophones. The source position moved at 20 m intervals. The first shot was acquired at a distance of 20 m in front of the first geophone on the first seismic line. The entire length of the geophone line was 1135 m across the waste storage area (Fig. 4, Fig. 1). There was no ERT measurement because of unsatisfactory findings from the past.

The velocity model of the seismic refraction tomography section clearly shows the thickness and geometry of the ash storage area (Figs. 5b,c). A pronounced change in lithology is indicated by an increase in V_p from ~ 500 m/s to about 1600 m/s. P-wave velocities in several parts of the ash

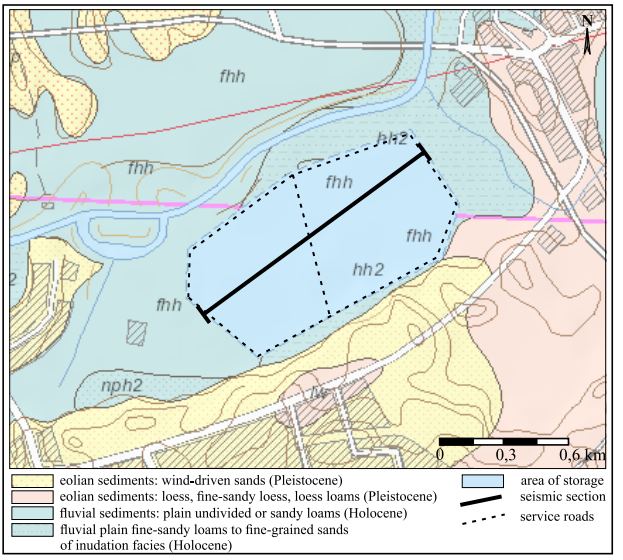

Fig. 4: Location of the thermal power ash storage area and investigated profile on a detailed geological map (after *Geological map of Slovakia, 2013*).

storage area vary from 200 m/s to 560 m/s depending on the consolidation of material, and ultimately to a variation of material moisture (as seen in Figs. 5b,c). At a length of 520–560 m the storage area is divided into two parts. The partition is shown on the velocity model as a zone of higher velocities (450–500 m/s). In the left part of the storage area the velocities are approx. 350 m/s. The velocities in the right part are very similar, but there is a depression on the surface and in area of depression slopes the velocities are lower ($\leq$ 300 m/s, 200–300 m/s). The surface water drains from the slopes and remains at the depression bottom. The velocities are then slightly higher at the bottom of the depression ($\sim$ 380 m/s) than in other flat parts. There is also an increase in V_p to values of about 380–400 m/s at the edges of ash storage area. This should also indicate high ash humidity, but it is likely caused by a consolidation of storage slopes. The storage area base runs at a depth of about 20 m under the measured profile. The velocity on the ground is about 1600 m/s. Higher values are recorded in the right part of the section. These values correspond to ambient Quarternary fluvial sediments.

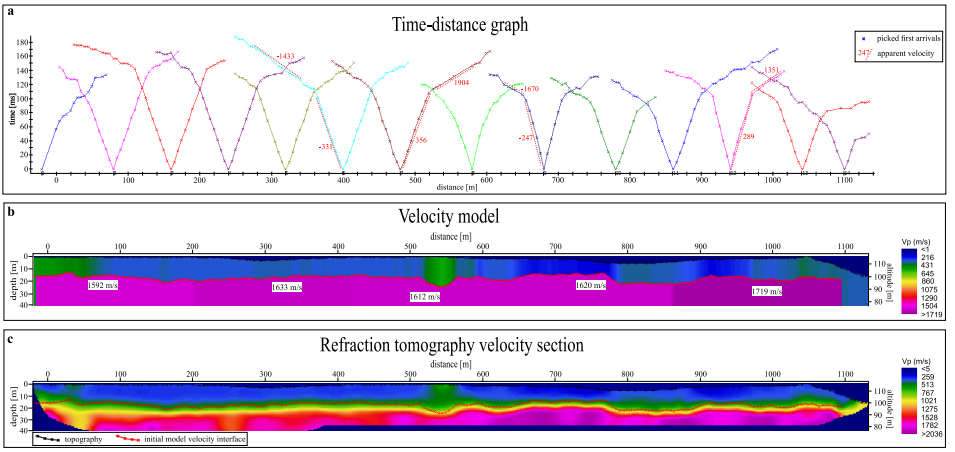

Fig. 5: Results along the seismic profile through the ash storage area. a) selection of time-distance graphs of some shots along the profile and pointing of some account apparent velocities, b) velocity model with velocity interface interpreted as a storage basement and c) SRT.

3.3. Determination of groundwater level

The survey was located in the western part of Slovakia near a village in the area of Borská nížina (Fig. 1). Since there was a shallow borehole with available data close to the measured profile, the velocity output could be directly correlated with geological information (Fig. 6a).

The thirty-six geophones were spaced at 3 m intervals along a straight profile with a length of 105 m, and 12 shots were measured 12 m from each other. The first shot point was at 24 m in front of the geophone line, while the shallow borehole was in the middle of the geophone line length (Fig. 6d,e). According to the borehole data, the groundwater level was expected at a depth of 3.35 m below the surface, while an interface of wet sand and Neogene clay was anticipated at a depth of 8 m.

Results and some examples of processing steps are shown in Fig. 6. The distribution of velocity values in the seismic section correlates with borehole data. Both records, the standard refraction model (Fig. 6d) and the tomography model (Fig. 6e), clearly reveal the level of groundwater. The low velocity layer (< 1000 m/s) is interpreted as dry sand. There is an increase in speed at a depth of 3 m (> 1500 m/s). This indicates the onset of wet

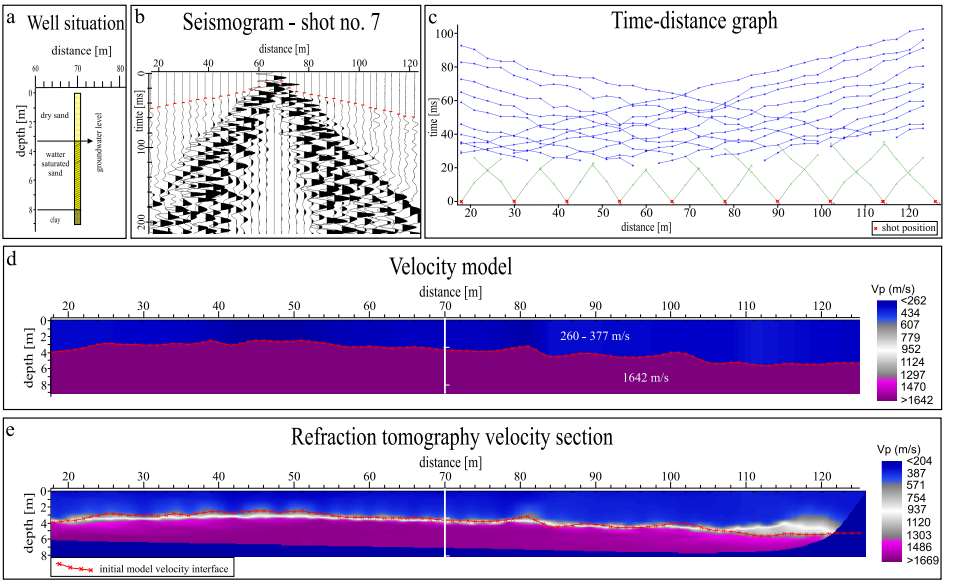

Fig. 6: Results and data along the seismic profile to determine ground water level. a) Well situation, b) example of seismogram with picked first arrivals, c) time-distance graphs of some shots along the profile, d) velocity model and e) SRT.

sand. The next interface – wet sand/Neogene clay, is not recorded at the velocity sections. We expected such result given the assumed low velocity contrast between these two layers.

3.4. Mapping of border fault between the Turiec Basin and the Malá Fatra Mts.

This case study is focused on the development of the tectonic contact of the Turiec Basin with the Malá Fatra Mts. specifically, the determination of the position of the Hradište fault zone.

The Malá Fatra Mts. is part of the Western Carpathians situated in the westernmost part of Slovakia. It is a typical core mountain range with a crystalline core, while its northern side and slopes are overlaid by a Mesozoic cover (*Földvary, 1988*). The Malá Fatra Mts. is divided into two parts – Lúčanská Malá Fatra Mts. (the southern part) and Krivánska Malá Fatra Mts. (the northern part). The crystalline core in the Lúčanská Malá Fatra

Mts. part (*Földvary, 1988*) consists of granitoids (granite-gneiss, biotite-oligoclase granite, granodiorite, quartz-diorite, Magura type granite) and metamorphics (mica schists of Jaraba Group and migmatites).

The south-east Lúčanská Malá Fatra Mts. region is adjacent to the Turiec basin. The Turiec basin is an approximately 40 km long and 10 km wide located between the Malá Fatra Mts. and Veľká Fatra Mts. (*Földvary, 1988*). The pre-Neogene basement consists of the paleo-Alpine alochthonous Mesozoic complexes, and Paleogene post-nappe sedimentary cover in its northern part (*Fusán et al., 1987; Kováč et al., 2011; Bielik et al., 2013*). The remaining part of the basin (*Földvary, 1988*) is filled by Neogene (Pliocene lacustrine and fluviatile deposits, Miocene sandstone and grit) and Quaternary sediments (Holocene alluvium, Pleistocene loess and fluvial gravel).

The eastern and western edges of the Turiec Basin are sharply delimited by fault planes (*Földvary, 1988*). The north-eastern corner is fragmented by SW–NE oriented faults considered to be pre-Quaternary in origin (*Földvary, 1988*). The Hradište fault zone is one of the basinal faults. Its course is not striking on the surface. We attempted to determine its location on a measured shallow seismic profile.

The NW–SE seismic profile of a total length of 440 meters was located SW of the city of Martin above the village of Bystrička (Fig. 7, Fig. 1). Data were measured by three overlapping lines, each 175 meters long with 12 geophones at the cover. The geophone interval for each line was 5 m and the source points were spaced 10 m along the geophone line starting at 2.5 m in front of the first geophone. For better resolution, 7 to 12 stacks were used for each shot.

At first, the typical signatures that the fault impacts on first arrivals as described by *Yan et al. (2005)* were observed on the time–distance graph. The reverse branch which exists far from the fault on the footwall on all shots and an unusual velocity variation pattern for the shot on the hanging wall can be seen (Fig. 8a).

The lateral change in velocities in the refraction velocity profile indicates significantly the Hradište fault (Fig. 8b and also Fig. 8c). A layer with low velocities is found at the top along the entire profile. It can be interpreted as soil and unconsolidated sediments. However, we are interested in the vertical contact of two velocity zones at a depth of approximately 10 m below the surface. A zone with velocities up to 3000 m/s appears on the left part of

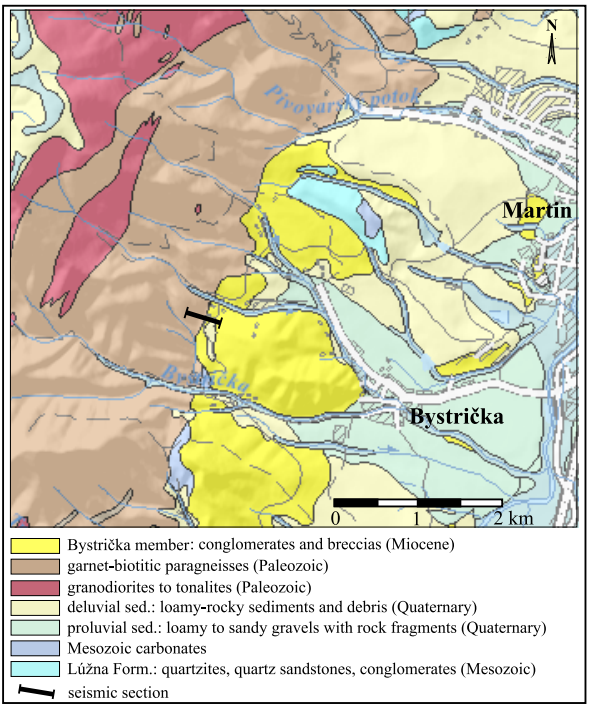

Fig. 7: Location of seismic profile up to the mapped Hradište fault on a detailed geological map (after *Geological map of Slovakia, 2013*).

the profile and can be interpreted as the granitoid rocks which are common in this area. The lateral change in velocity of about 160 m to the right along the measured profile and the zone of lower velocities (2000–2500 m/s) are interpreted as Neogene sediments.

4. Discussion

It is well known that the geophysical results, if possible, would be verified by complex different geophysical methods. Because of the high sensitivity of geophones to any noise, doing seismic measurements with other geophysical measurements on the same profile at the same time can be problematic. ERT is a frequently used method in combination with seismic measurements in shallow geophysical research (*Riddle et al., 2010; Leucci et al.,*

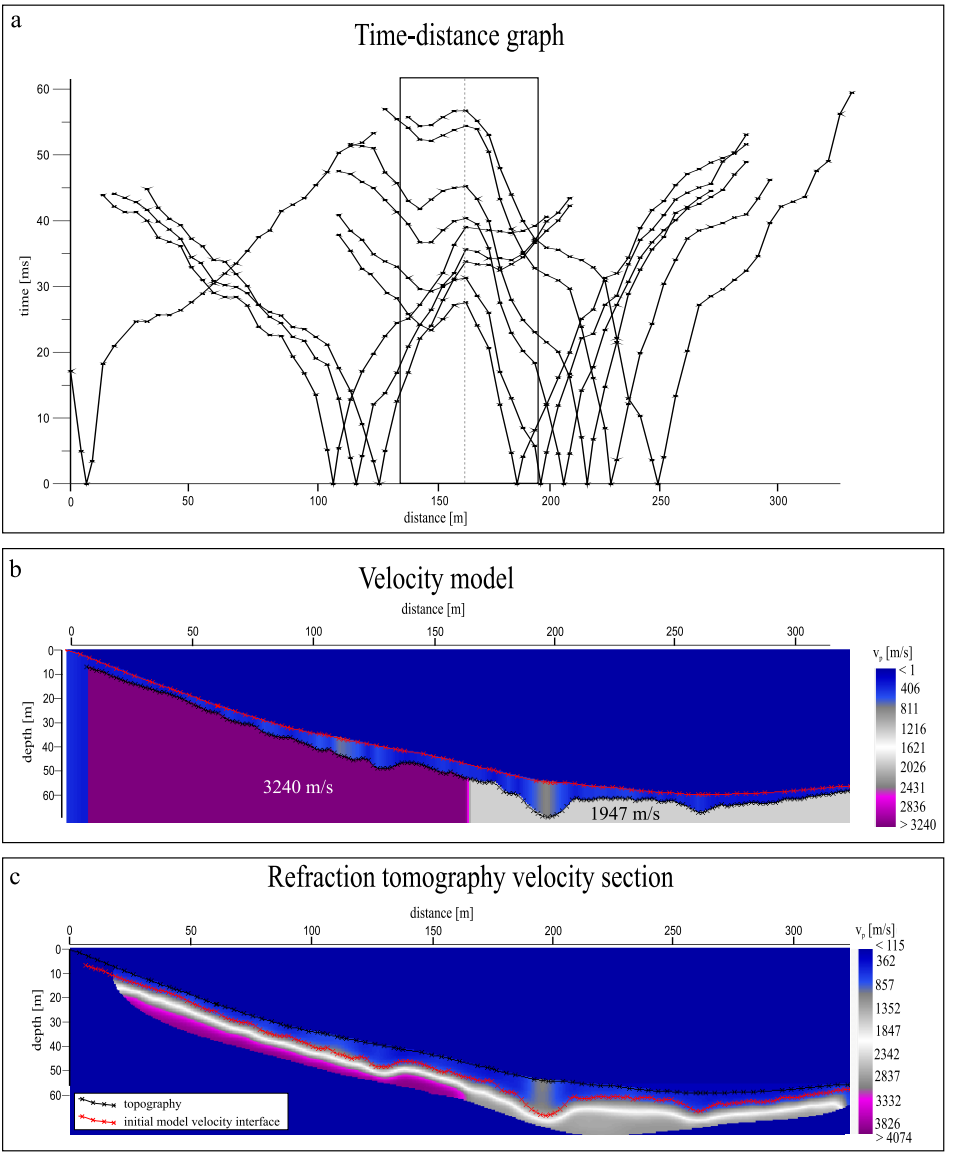

Fig. 8: Results along the seismic profile through the Hradište fault. a) selection of time-distance graphs of some shots along the profile (the dashed line and framed zone highlights fault impact on first arrivals), b) velocity model and c) SRT profile.

2007; Gabr et al., 2012; Shahrukh et al., 2012; Basheer et al., 2012; Hellman et al., 2017). These two methods can be measured together at the same time, but parallel profiles at a sufficient distance from each other should be used to avoid the degradation of signal-to-noise ratio at the geophones due to ERT measurement.

In the case of mapping the Hradište fault, well preserved outcrops, boreholes and geophysical data were available (*Kováč et al., 2011; Kušnirák et al., 2018*). The course of this fault was mapped by several geophysical methods. The data and results presented in this article were re-measured as another device with different equipment and acquisition geometry. It featured the use of 4.5 Hz vertical geophones which are often used for MASW. Geophones of 10–12 Hz are generally used for such a survey. However, the use of low frequency geophones and the larger step of geophones and shots (compared to older measurements during the multimethod geophysical study), did not have a major effect on the results of measurements in this case. Seismic refraction tomography and the effects on time-distance graphs map the fault successfully.

There is not always complete agreement between results obtained by different geophysical methods. In shallow measurements, interpretation may be influenced by various surface factors such as elevated humidity in the surface areas in a rainy season or by the disturbance and weathering of the rock bottom. The shallow zones are also often influenced by human activity. All of these affect the detected velocity values. In the case of the Katarínka measurements, there is no complete match over the interpreted pond bottom in the ERT profile and the seismic profile along the area which is about 50–70 meters of measured profile. The low resistance values recorded in this area in the surface layer on the ERT profile are apparently associated with increased humidity. The measurement was made after the rainy season, and water appears to flow in these places. It also influenced the detected V_p. There are higher values in this zone, which influences the continuance of the interpreted interface (it is interpreted at a slightly smaller depth than ERT).

In the case of the thermal power station, the ERT measurements were made first for the detection of the bottom of the ash storage area in the past, but it did not yield the desired results. The entire environment was too conductive and no interface was recorded. As shown by the results of

seismic measurements in this paper, seismic refraction tomography was an excellent alternative to achieving the desired findings.

5. Conclusion

These case studies demonstrate clearly that even shallow seismic refraction methods are valuable tools for research in several areas. Shallow seismic refraction tomography is an ideal method for areas characterized by strong lateral velocity gradients, and thus an effective tool for vertical fault exploration and mapping. It also can play an important role in ground water level estimation, environmental studies of waste storage and archaeological studies. By performing shallow refraction methods (especially SRT), a detailed view of velocity distribution and thus the geological structure of a subsurface can be obtained. It is a cost effective, non-destructive method which also reduces the cost of surveys that use it. However, as in the case of other geophysical methods, it requires input geological and geomorphological information. It is also suitable to verify the seismic interpretation by other geophysical methods. The SRT and ERT represent an appropriate combination which brings satisfactory results and can be measured together by a parallel profile sufficiently distant from each other.

Acknowledgements. This work was supported by the Slovak Grant Agency VEGA, grants No. 1/0559/17, 1/0462/16 and 2/0098/18, and by the Slovak Research and Development Agency under grants No. APVV-0129-12 and APVV-16-0146. We thank the Comenius University Science Park for providing the equipment.

References

Basheer A. A., Atya M. A., Shokri M., Abu shady M. M., 2012: Application of ERT and SSR to detect the subsurface cave at 15th May City, Helwan, Egypt. NRIAG Journal of Astronomy and Geophysics, **1**, 1, 23–32.

Beng T. S., Seng Y. K., Choo L. W., 1982: A seismic refraction survey for an expressway project in Singapore. Bulletin of the International Association of Engineering Geology – Bulletin de l'Association Internationale de Géologie de l'Ingénieur, **26**, 1, 321–326.

Bielik M., Krajňák M., Makarenko I., Legostaeva O., Starostenko V., Bošanský M., Grinč M., Hók J., 2013: 3D gravity interpretation of the pre-Tertiary basement in the intramontane depressions of the Western Carpathians: a case study from the Turiec Basin. Geologica Carpathica, **64**, 5, 399–408.

Bielik M., 1998: Analysis of the gravity field in the Western and Eastern carpathian junction area: density modeling. Geologica Carpathica, **49**, 2, 75–83.

Cardarelli E., Cercato M., De Donno G., 2014: Characterization of an earth-filled dam through the combined use of electrical resistivity tomography, P- and SH-wave seismic tomography and surface wave data. Journal of Applied Geophysics, **106**, 87–95.

Coulouma G., Samyn K., Grandjean G., Follain S., Lagacherie P., 2012: Combining seismic and electric methods for predicting bedrock depth along a Mediterranean soil toposequence. Geoderma, Elsevier, **170**, 39–47.

Enviroscan, 2018: Seismic refraction versus reflection [on line]. ©Enviroscan, Inc. [cit. 2018-01-04]. Available on: `http://www.enviroscan.com/home/seismic-refraction-versus-reflection`.

Földvary G. Z., 1988: Geology of the Carpathian region. World Science Publishing Co Pte Ltd., Singapore, 124–135.

Fusán O., Biely A., Ibrmajer J., Plančár J., Rozložník L., 1987: Basement of tertiary of the Inner West Carpathians. Geol. Úst. D. Štúra, Bratislava, 103.

Gabr A., Murad A., Baker H., Bloushi K., Arman H., Mahmoud S., 2012: The use of sesmic refraction and electrical techniques to investigate groundwater Aquifer, Wadi Al-Ain, United Arab emirates (UAE). Conference Proceedings, 14-16 September 2012, Tulcea – Romania.

Geological map of Slovakia M 1:50 000, 2013. [online] Bratislava: Štátny geologický ústav Dionýza Štúra, Available online: `http://mapservergeology.sk/gm50js`.

Gordon M. A., 1997: Application of field seismic geophysics to the measurement of geotechnical stiffness parameters. Thesis submitted for the degree of Doctor of Philosophy [on line]. Department of Civil Engineering, University of Surrey, UK. Available on: `http://epubs.surrey.ac.uk/862/1/fulltext.pdf`.

Hack R., 2000: Geophysics for slope stability. Surveys in Geophysics 21: 423–448 [on line]. ©2001 Kluwer Academic Publishers. Netherlands [cit. 2018-01-04]. Available on: `https://link.springer.com/article/10.1023/A:1006797126800`.

Haeni F. P., 1986: Application of seismic refraction methods in groundwater modeling studies in New England. Geophysics, **51**, 2, 236–249.

Hagedoorn J. G., 1959: The plus-minus method of interpreting seismic refraction section. Geophysical Prospecting, **7**, 2, 158–182.

Hellman K., Ronczka M., Günter T., Wennermark M., Rücker C., Dahlin T., 2017: Structurally coupled inversion of ERT and refraction seismic data combined with cluster-based model integration. Journal of Applied Geophysics, **143**, 169–181.

Henley D. C., 2003: Indiana Jones and the Seismic Anomaly: The Potential of Seismic Methods in Archaeology. CSEG Recorder, **28**, 1.

INCA – International Course on ArchaeoGeophysics, 2009: [online] In Beres J., Dogan D., Sanchez J., Wohmann R.: Geophysical research of Katarinka Abbey. ©2001–2018

OZ Katarínka [cit. 2018-01-04]. Available on: http://www.katarinka.sk/dokumenty/vyskum/poster_katarinka_results_28.7.2009.pdf.

Kováč M., Hók J., Minár J., Vojtko R., Bielik M., Pipík R., Rakús M., Kráľ J., Šujan M., Králiková S., 2011: Neogene and Quaternary development of the Turiec Basin and landscape in its catchment: a tentative mass balance model. Geologica Carphatica, **62**, 4, 361–379.

Kušnirák D., Zeyen H., Bielik M., Putiška R., Pašteka R., Dostál I., Mojzeš A., Zahorec P., Bošanský M., Krajňák M., Papčo J., Hók J., Brixová B., 2018: Multimethod geophysical study of a border fault: a case study from the Turiec Basin (Western Carpathians, Slovakia). Near Surface Geophysics (submitted).

Leucci G., Greco F., De Giorgi L., Mauceri R., 2007: Three-dimensional image of seismic refraction tomography and electrical resistivity tomography survey in the castle of Occhiolà (Sicily, Italy). Journal of Archaeological Science, **34**, 2, 233–242.

Lillie R. J., 1999: Whole Earth Geophysics. Prentice Hall. New Jersey, 1–361.

Matulová M., 2003: Monastery os St. Catherine near Dechtice (Kláštor Sv. Kataríny pri Dechticiach). Thesis, Department of Slovak history, Faculty of Arts, Comenius University, Bratislava [on line]. ©2001-2018 OZ Katarínka [cit. 2018-01-04]. Available on: http://www.katarinka.sk/dokumenty/prace/diplomova_praca_martinamatulova_klastorsvkatarinypridechticiach2003.pdf (in Slovak).

McClymont A., Bauman P., Johnson E., Pankratow L., 2016: Geophysical Applications to Construction Engineering Projects. CSEG Recorder, **41**, 4.

Nanda N. C., 2016: Seismic Reflection Principles: Basics. Chapter 2. In Seismic Data Interpretation and Evaluation for Hydrocarbon Exploration and Production. Springer International Publishing Switzerland, 19–35.

Nazarian S., Stokoe II K. H., Hudson W. R., 1983: Use of spectral analysis of surface waves method for determination of moduli and thicknesses of pavement systems. Transportation Research Record, **930**, 38–45.

Osumneje J. O., Kudamnya E. A., 2014: Hydro-geophysical Investigation Using Seismic Refraction tomography to Study the Groundwater potential of Ahmadu Bello University main campus, within basement Complex of Northern Nigeria. Journal of environment and Earth Science, **4**, 2, 16–22.

Palmer D., 1980: The Generalised Reciprocal Method of Seismic Refraction Interpretation. Tulsa: Society of Exploration Geophysicists, 113 pp.

Pandula B., 2000: Determination of degree of breakage and quality of airport ways by seismic methods (Určovanie stupňa porušenosti a kvality letiskových dráh seizmickými metódami). Acta Montanistica Slovaca, **5**, 2, 157–162 (in Slovak).

Park C. B., Miller R. D., Xia J., 1999: Multi channel analysis of Surface waves. Geophysics, **64**, 800–808.

Park C. B., Xia J., Miller R. D., 1998: Groundroll as a tool to image near surface anomaly. 68th Ann. Internal. Mtg, Soc. Expl. Geophys., Expanded Abstracts, 874–877.

Prekopová M., Janočko J., Budinský V., Friedmanová M., 2016: Integration of seismic and sedimentological methods for analysis of Quaternary alluvial depositional systems. Environ. Earth Sci. 2017) 76:25, Springer, https://doi.org/10.1007/s12665-016-6345-3.

Reynolds J. M., 1997: An Introduction to Applied and Environmental Geophysics, John Wiley and Sons Ltd, Chichester, first edition, 796 pp.

Riddle G. I., Riddle C. J., Schmitt D. R., 2010: ERT and Seismic Tomography in Identifying Subsurface Cavities [on line]. ©2010 GeoCanada CSEG [cit. 2018-01-04].

Salaj J., Began A., Hanáček J., Mello J., Kullman E., Čechová A., Šucha, P., 1987: Explanatory text of the Geological map of Myjavská Pahorkatina Upland, Brezovské and Čachtické Karpaty Mts., scale 1:50 000 (Vysvetlivky ku geologickej mape Myjavskej pahorkatiny, Brezovských a Čachtických Karpát 1:50 000). GÚDŠ, Bratislava.

Sander J. E., 1978: The blind zone in seismic ground-water exploration. Ground Water, **165**, 394–397. In Haeni (1986).

Sandmeier K. J., 2016: Reflexw – GPR and seismic processing software. ©Sandmeier geophysical research 2017 [cit. 2018-01-04]. Available on: `http://www.sandmeier-geo.de/reflexw.html`.

Shahrukh M., Soupios P., Papadopoulos N., Sarris A., 2012: Geophysical investigations at the Istron archaeological site, eastern Crete, Greece using seismic refraction and electrical resistivity tomography. Journal of Geophysics and Engineering, **9**, 6, 749–760.

Sheehan J. R., Doll W. E., Mandell W. A., 2005: An Evaluation of Methods and Available Software for Seismic Refraction Tomography Analysis. Journal of Environmental and Engineering, **10**, 1, 21–34.

Shtivelman V., 2003: Application of shallow seismic methods to engineering, environmental and groundwater investigations. Bolletino di Geofisica Teorica e Applicata. An international journal of Earth Science. Trieste, Italy, **44**, 3-4, 209–222.

Soske J. L., 1954: The blind zone problem in engineering geophysics. Geophysics, **24**, 359–365. In Haeni (1986).

Steeples D. W., 1998: Shallow seismic reflection section—Introduction. Special Issue. Geophysics, **63**, 4, 1210–1212.

Steeples D. W., 2000: A review of shallow seismic methods. Annali di Geofisica, Published by Istituto Nazionale di Geofisica e Vulcanologia, Bologna, Italy, **43**, 6, 1021–1044.

Steeples D. W., Miller R. D., 1990: Seismic reflection methods applied to engineering, environmental and groundwater problems. In: Ward S. H., Editor, Geotechnical and engineering geophysics, volume 1: Society of Exploration Geophysicists, 389 p.

Tsokas G. N., Papazachos C. B., Vafidis A., Loukoyiannakis M. Z., Vargemezis G., Tzimeas K., 1995: The detection of monumental tombs buried in tumuli by seismic refraction. Geophysics, **60**, 6, 1735–1742.

Widess M. B., 1973: How thin is a thin bed? Geophysics, **38**, 1176–1180. In Nanda, 2016.

Xia J., Miller R. D., Park C. B., 1999: Estimation of near surface shear wave velocity by inversion of Rayleigh waves. Geophysics, **64**, 3, 691–700.

Xia J., Miller R. D, Park C. B., 2000: Advantages of calculating shearwave velocity from surface waves with higher modes. SEG Technical Program Expanded Abstracts 2000, 1295–1298.

Yan Z., Clayton R. W., Saleeby J., 2005: Seismic refraction evidence for steep fault cutting higly attenuated continental basement in the central Transverse ranges, California. Geophys. J. Int., **160**, 651–666.

Zhang J., Toksöz M. N., 1998: Nonlinear refraction traveltime tomography. Geophysics, **63**, 5, 1726–1737. Available on: http://cseg.ca/assets/files/resources/abstracts/2010/1010_GC2010_ERT_and_Seismic_Tomography_in_Identifying_Subsurface_Cavities.pdf.

DE GRUYTER
OPEN

Contributions to Geophysics and Geodesy Vol. 48/1, 2018 (23–74)

Interplanetary external driven quasidynamo as the origin of geomagnetic jerks correlated with length of day and gravity anomaly

[The origin of 5.9-years and 11-years and semi-annual periodic geophysical signals and Jovian planets alignments as the origin of the abrupt geomagnetic jerks]

Mohsen LUTEPHY

Chemistry engineer and independent researcher
Islamic Azad University Tehran Science and Research Branch,
Hwy Haggi St., Ahang, Iran; e-mail: lutephy@gmail.com, tel.: 00989354444405

Abstract: We report phenomenological inevitable correlation between the Sun's magnetic field oscillation through the Earth and the Jupiter, with sinusoidal geomagnetic jerks observed at the Earth, additionally aligned with the gravity and length of day sinusoidal variations and we observe too that the Sun and Jovian planets alignments with Jupiter are origin of the observable abrupt geomagnetic jerks whether historical or new, and experimental results demonstrate a possible explanation on the base of the planetary induced currents upon the metallic liquid cores of the planets upon the varying external magnetic fields as the source of heat flows continued by frictional turbulent and convectional fluid fluxes, amplified and expanding by the Earth magnetic field and observations are showing too that it should be an electric coupling effect between metallic cores of the planets, under the magnetic field oscillation so that Jupiter conductive metallic region interacts with Earth metallic core while the Sun's magnetic field is oscillating through the Jupiter and we see a relation between secular variation of the Earth's magnetic field and long term trend of 5.9-years signals as a new method to measure geomagnetic secular variation by LOD signals.

Key words: geological and geophysical evidences of deep processes, core dynamics, heat flow, magnetic and electrical methods, gravity variations, dynamo theory, geomagnetic field variations, solar-terrestrial interaction, planets alignment, geomagnetic jerks, LOD variations

1. Introduction

A geomagnetic jerk or secular geomagnetic variation impulse is a relatively sudden change in the second derivative of the Earth's magnetic field with respect to time. These events were noted initially by *Courtillot et al. (1978),*

doi: 10.2478/congeo-2018-0002

Malin and Hodder (1982), Courtillot and Le Mouël (1984). The clearest ones, observed all over the world, happened in 1969, 1978, 1991, and 1999. Data before 1969 is scarce, but there is evidence of other global jerks in 1901, 1913, and 1925. Other events at 1932, 1949, 1958, 1986 and 2003 were detected only in some parts of the world and new analyzing has detected some next jerks. We do not want to introduce here a technical version of the geomagnetic jerk features in detail for example the exact geographical map of the magnetic field variations or exact inverse engineering of the secular variations to shape the core flows dynamics because that our paper is not on the detection of the geomagnetic jerks. But we want to explain here the origin of the detected geomagnetic jerks in addition with detection of the LOD variations and relevant gravity changes all on the base of experimental results and solar system phenomenology and Maxwell equations and hydrodynamics, and in reality we want to show here that the reported geomagnetic jerks aligned with LOD variations and relevant gravity changes are not appeared randomly suppose originated externally out of the Earth's atmosphere. But the introduction of geomagnetic jerks features in detail is visible at multitude of the papers published before and for an excellent general definition of the geomagnetic jerk features we may refer to the paper *Tozzi et al. (2009)* and many next papers are included to the relevant introductions not needed to repeat here.

By the way, measurements are showing the abrupt changes of the secular magnetic field in some dates (*De Michelis et al., 2005; Brown et al., 2013; Alexandrescu et al., 1996*) assumed to be connected to the core flows (*Bloxham and Jackson, 1991; Mandea et al., 2010; Holme, 2007*) and at the paper "The origin of the geomagnetic jerks" (*Bloxham et al., 2002*), we see a general explanation of process as noted that:
"The fact that they represent a reorganization of the secular variation implies that they are of internal origin, and their short timescale implies that they are due to a change in the fluid flow at the surface of the Earth's core (as has also been established through mapping the time-varying flow at the core surface). However, little is understood of their physical origin. Here we show that geomagnetic jerks can be explained by the combination of a steady flow and a simple time-varying, axisymmetric, equatorially symmetric, toroidal zonal flow. Such a flow is consistent with torsional oscillations in the Earth's core, which are simple oscillatory flows in the core that are

expected on theoretical grounds, and observed in both core flow models and numerical dynamo models."

An analysis on the measurements data is showing a background oscillating geomagnetic jerk as 5.9 years' periodic oscillation of the geomagnetic jerks (*Silva et al., 2012; Brown et al., 2013*) and as noted at *Silva et al. (2012)* paper:
"The first time derivative of residual length-of-day observations is known to contain a distinctive 6-year periodic oscillation. Here we theorize that through the flow accelerations at the top of the core the same periodicity should arise in the geomagnetic secular acceleration. We use the secular acceleration of the CHAOS-3 and CM4 geomagnetic field models to recover frequency spectra through both a traditional Fourier analysis and empirical mode decomposition. We identify the 6-year periodic signal in the geomagnetic secular acceleration and characterize its spatial behaviour."

The analysis by scientists on the LOD observations show that the length of day is changing periodically almost 5.9 years (*Vondrák and Burša, 1977; Liao and Greiner-Mai, 1999; Abarca del Rio et al., 2000; Mound and Buffett, 2003; 2006; Olsen and Mandea, 2007; Holme and de Viron, 2013*) as a verification for oscillation of the Earth's rotation aligned with geomagnetic jerk 5.9 years oscillation and not only the 5.9 years periodic signals are confirmed for times above 1960 suppose as noted at *Holme and de Viron (2013)*, the 5.9 years signals have been confirmed for times before 1960 as:
"Also plotted (vertically shifted for clarity) are the decadal varying signal alone and the data with the 5.9-year oscillation subtracted, demonstrating the separation of the oscillation from the background trend. Inference from spectral studies suggests that the 5.9-year oscillation is also present prior to 1960."

We have shown here phenomenological evidences for link of the interplanetary external sources and internal core flows, and new reported geomagnetic jerks and historical geomagnetic jerks (*Korte et al., 2009; Qamili et al., 2013; Matzka et al., 2010*) are being detected all in agreement with Jovian planets alignments and observations show the 11-year periodic signals too and strongly this is correlated to the solar activity and we have shown here the origin of the planetary semi-annual signals too. On the other hand, recently it was published an article by *Anderson et al. (2015)* on the gravitational constant G measurements data, reported in these decades and their

analysis in the data shows the Earth's gravity is oscillating at the same period the Earth rotation is oscillating and *Mandea et al. (2012)* has analyzed the data from continuous satellite measurements made from 1999 to 2010 so that oscillation of the Earth's magnetic jerk aligns with Earth's gravity oscillation and for exact analysis on data we may refer to *Schlamminger et al. (2015)*.

We need to notice that the main reason of jerks is outside of the Earth. In the paper it is considered as the interplanetary driven partial quasidynamo which, of course, is not the self consistent hydromagnetic dynamo, mechanism operating in the Earth‘s outer core. This partial quasidynamo is an of external origin perturbation of flows and magnetic fields on the CMB.

In the section 1 – in the introduction we have described the annals of the Geomagnetic jerks and LOD variations and gravity anomalies in relevant together and we have shown some examples of the occurrences and a simple definition of the parameters and data and in the section 2. We have discussed purely the possible mechanism and probable methods and we have resulted the equations and formulas on the base of the Maxwell equations and hydrodynamics and in section 3. We have shown the observational data and experimental results referenced to the published papers and reported data by scientists to set with pure results aligned with description of the compatibles included to the relevant figures and tables and this section, we have referred to the solar system simulators to evaluate the parameters and ultimately in the conclusions it has been described the most important motes of the paper in simplest and shortest sentences.

2. Method and theory

For explanation of the observations and experimental reports we put forward a logical mechanism on the base of the Maxwell equations and hydrodynamics, in addition with some experimental results, actually accepted and we refer to the scientific references and we have verified the mechanism in result by reported data and observed phenomena. Generally, the proposed mechanism is a quasidynamo, initiated externally by the Sun and Jovian planets affecting at the Earth's conductive outer core. But it should be noticed

that this quasidynamo is not the self consistent hydromagnetic dynamo in dynamo region of the cosmic body. But in the Earth‘s core it is a partial dynamo as a perturbation on the CMB.

2.1. Interplanetary induced currents as the origin of the partial core flows

The geomagnetic jerks reveal presence of the core flows (*Bullard, 1948*) as quoted by Bullard that:
“It may be subject to turbulent currents due to thermal convection or to the shearing forces associated with the secular deceleration of the Earth. Such motions would cause the conducting material of the core to move across the Earth’s magnetic field and would produce electric currents. These electric currents would produce a further magnetic field, and it is the purpose of this paper to consider the hypothesis that the changes in this field constitute the secular change. We do not consider the origin of the main field itself, but merely use the observed fact of its existence as part of the mechanism required to produce the secular change.”

It has been theorized to exist secular change of the magnetic field, relevant to the chaotic occurrences of the core flows as mentioned in some papers, for example *Qamili et al. (2013)*. But observations are showing that partial geomagnetic jerks over time scale of a year or more, almost all are not random suppose random processes probably are atmospheric (ionosphere and magnetosphere) tiny effects and some long time secular variations might dependent too to convectional heat processes in the mantle (*Biggin et al., 2012*) and then based on the Bullard suggested mechanism, it remains turbulent currents due to the thermal convection as a possible internal origin of the geomagnetic jerks whereas that we may refer to newer papers, for example *Bloxham et al. (2002), Dumberry and Bloxham (2006)*. For geomagnetic jerk extraction from core flows and dynamo driven core currents, we may refer to a scientific technical report (*Wardinski, 2004*) “Core Surface Flow Models from Decadal and Sub decadal Secular Variation of the Main Geomagnetic Field”.

At all papers the geomagnetic jerks are completely on the Maxwell equations and hydrodynamics related to the core fluxes and the fluid fluxes cause to oscillate the gravity and Earth’s spin because of asymmetric change in the

moment of inertia for change of gravity (*Dumberry, 2010*) and the exchange of angular momentum between the outer core and solid mantle (*Mound and Buffett, 2006*). For Earth's spin change and in addition to periodic geomagnetic jerks we observe, abrupt geomagnetic jerks, reported in some dates, and these abrupt geomagnetic jerks are aligned with gravity and LOD anomalies too (*Holme and de Viron, 2005; Nakada, 2009*).

The cores of the planets are liquid conductors and then a possible explanation is on the base of the eddy currents or generally geomagnetic induced currents (GIC) (*Fink and Christiansen, 1989*). Eddy currents are loops of the electric currents, induced within conductors by a changing magnetic field in the conductor due to the Faraday law of induction.

A conductor object in a varying magnetic field or upon an AC voltage will experience dissipation of kinetic energy and braking effect. This mechanism does generate an external driven fluid fluxes as a partial quasidynamo which might be defined as a perturbation in the whole Earth's dynamo and versus a theory published newly on the whole generation of the Earth's dynamo by lunar tidal effect (*Andrault et al., 2016*) which is so far to accept, the mechanism of interplanetary external driven dynamo here is a secondary partial dynamo and ultimately, the drag forces are created by induced currents and electrical resistance within conductors cause a dragging effect analogous to friction which dissipates the kinetic energy as a source for convectional hydrodynamic flows. In both externally driven and internally driven secular variations of the magnetic field, the cause are induced currents and relevant heat convection and core fluid fluxes, based on the Maxwell electromagnetism and hydrodynamics. However, the braking effect of the eddy currents too may result, the variation in the length of day.

We should notice that the Earth has internal driven fluid fluxes too and some of the core flows which they cause to appear secular variation of the geomagnetic field are relevant to the internal sources as the secondary dynamos. But external driven partial dynamos have own relevant induced currents, penetrative in the Earth's metallic core and some partial induced currents are generated by external sources and continued by relevant core flows. Motion of these external driven core flows through the Earth's magnetic field will generate again, secondary induced currents by dynamo shape mechanism. The Earth's magnetic field will expand and amplify the externally driven heat processes. Thus, the Earth's magnetic field is reason to

continue and expand occurrences of the fluid fluxes and then the retardation of the visible events, and ultimately neutralized in an equilibrium point by Magnetohydrodynamics as a mechanism initially developed by *Alfvén (1942)* which causes to set fluids along the magnetic field lines or returning to ever stable motions in equilibrium points with those relevant secular change.

On the other hand against the internally driven core flows which moving at whole inside of the core, on the base of the externally driven quasidynamo we understand that the external driven core flows will be generated near the core mantle boundary (CMB) for that, in a perfect conductor with no resistance, the surface eddy currents, exactly cancel the field inside the conductor, so no external magnetic field penetrates inside the conductor and then, eddy currents will be generated on the core mantle boundary. Recent investigations of the secular acceleration pulses in the Earth's magnetic field have concluded that these events, observed at the Earth's surface, are resulted at the core mantle boundary (*Bloxham, 1988; Buffett et al., 2016; Chulliat et al., 2010; Mandea et al., 2000; Gire et al., 1986*) or, (*Voorhies, 1986, 1993, 1995, 2004*). Then the core mantle boundary (CMB) is dominant area for external driven fluxes originated by induced currents with hundreds kilometer diameter to generate geomagnetic jerks as reported and mentioned by scientists in references. Of course penetration of the externally driven quasidynamo to the core inside concerns to conductivity of the metallic core and by decrease of the conductivity, the penetration depth of external driven quasidynamo will increase proportionally.

In reality, the core flows models are scientific predictions from observations of the geomagnetic secular variations (with jerks included), accompanied with LOD variations and gravity anomalies, as an inverse engineering of the geomagnetic jerks' observations and for a mathematical analysis on the inverse theory, schematically we may refer in some sections to the paper *Aubert (2013)*.

Fluid fluxes are not ended after end of the initial generation of induced currents, but continued by the Earth's magnetic field. Because of the absorption and generation of the heat, they do not occur simultaneously and not in a constant position. They can't neutralize themselves suppose continued in the core as the hydrodynamic flows to develop induced currents upon the Earth's magnetic field. While it exits several number of the fluid

fluxes, the event is visible as global. But since there is alone one fluid flux it seems local event (*Bloxham et al., 2002; De Michelis et al., 2005; Duka et al., 2012*).

Mathematical solutions on the base of the Maxwell equations and hydrodynamics have been developed for such an inverse theory and the problem of electromagnetic induction in thin sheets was first formulated by *Price (1949)* in terms of the scalar magnetic potentials of the inducing and induced magnetic fields and developed by *Ashour (1950)* to investigate the problem of induction of electric currents in a uniformly conducting circular disk.

But we have a schematic comparable similarity between planetary driven induced currents and ionosphere induced currents by geomagnetic field oscillations (*Ashour and Price, 1948*). Strong reason of this schematic correlation is conductivity of both ionosphere and liquid cores and the reality that the penetration of the Solar magnetic fields into the planetary interiors is possible and similar to this penetration into their ionospheres.

It has long been known that the compass needle daily executes small regular oscillations and *Stewart (1882)* concluded that the daily magnetic variations were due to electric currents in the upper atmosphere and Stewart also suggested that convective currents established by the Sun's heating influence are to be regarded as "conductors moving across lines of magnetic force, and are thus the vehicle of electric currents which act upon the magnet". It is convenient to call this hypothesis of Stewart's the "dynamo theory".

The theory received early support from *Schuster (1889)*, who proved that the greater part of the field of the Geomagnetic variations has its origin outside the Earth, and that the remainder may reasonably be attributed to the Earth's currents induced by the varying external field and *Schuster (1908)* developed a dynamo theory for such an external effect. Improved the theory further, giving special attention to the magnetic variations due to tides caused by Moon, which are more amenable to theoretical treatment of externally driven induced currents. *Martyn (1949)* showed that the oscillation of the ionospheric E region was likely to be due to the electrodynamic forces associated with the currents responsible for the lunar magnetic variations.

The current induction in an anisotropic ionosphere by external fields has been studied by *Ashour and Ferraro (1962; 1964)* so that certain distribu-

tions of freely decaying currents in a spherical shell model of the ionosphere of non-isotropic electric conductivity would rotate about the geomagnetic axis. We may refer to the paper *Ferris and Price (1965)* as the currents induced by periodic and aperiodic magnetic fields in a uniformly ionized spherical shell rendered anisotropic by a permanent dipole field. Schematically here we consider spherical shell of the Earth's core, rendered anisotropic by the permanent dipole field of the Earth, situated to generate induced currents by initial effect of interplanetary external magnetic fields and the generation of the eddy currents in the ionosphere by oscillation of the geomagnetic field, mechanically is the same generation of the eddy currents in the core of the Earth by oscillation of the external magnetic fields and for motion of the induced currents in the core of the planets by external magnetic fields, we may refer to the paper *Price and Ferris (1962).* We can generalize mathematical equations of the electromagnetic induction in an infinite plane sheet with a circular hole by an external magnetic field (*Ferris, 1973*), with a spherical conductor with a hole in the centre to show the mathematical equations for induced currents in the conductive cores of the planets and it needs no to repeat equations again here.

2.2. Jupiter intermediate electric coupling effect upon terrestrial planets metallic cores

The flows at the top of the core, affect to generate LOD variations as noted by *Holme and Buffett (2015)* that:
"We also consider the implications for the connection between core-surface flow and length-of day variation – a stably stratified layer has implications for interpretation of core flow and the Earth's angular momentum budget."

And we may refer to *Holme and de Viron (2013)* as noted that:
"Interdecadal periods have been less clear, and have been characterised by signals with a wide range of periods and varying amplitudes, including a peak at around 6 years. Here, by working in the time domain, rather than the frequency domain, we demonstrate a clear partition of non-atmospheric component into only three components: a decadally varying trend, 5.9-year period oscillation and jumps at times contemporaneous with geomagnetic jerks."

The observations of 5.9 years periodic signals are showing we have geo-

magnetic jerks in the Earth by varying the Sun's magnetic field through the Jupiter and this phenomenology shows that the Jupiter with big metallic region has an intermediate effect electromagnetically on the Earth's conductive core and thus, we have the Jupiter driven partial core flows on the terrestrial planets conductive cores and Jupiter effect is much larger than that of other Jovian planets for its giant metallic region and nearness to the Sun and nearness to the terrestrial planets and then mainly we detect Jupiter-driven core flows at the Earth by the Sun's magnetic field oscillation through the Jupiter.

The Jovian magnetic field amplitude at the Earth's position is very smaller than that of the Sun and this means that the Jupiter's magnetic field is not directly affecting to generate eddy currents at the core of the Earth and in reality, the period of signals in LOD variations and geomagnetic jerks, don't verify such a direct effect suppose the periodicities are showing that the Jupiter has an intermediate effect on the Earth's core to generate geomagnetic jerks and relevant LOD variations and probable gravity anomalies.

Observations are showing that the Sun should be affecting on the Jupiter electrically conducting region and this Jupiter metallic Hydrogen region is influencing on the Earth's metallic core as an indirect intermediate effect. But what is the mechanism of this interaction between metallic electrically conducting regions?

It is almost impossible for such an interacting effect of the metallic cores under the magnetic field variations by Hall effect and then we may refer to Nipher experiments as a possible explanation. In the Nipher experiments (*Nipher, 1916; 1917; 1918*) two metallic spheres were used so that a small metallic core was in the Faraday cage and a next big metallic core was outstanding and when Nipher used a AC voltage into the outstanding big metallic core, it was observed a difference in the atomic level electric field as a reason to generate electric interaction between these metallic spheres.

As noted in the *New York Times* (19 September 1917):

"It will be shown that gravitational attraction between masses of matter not only has been diminished into zero, but has been converted into repulsion which is more than twice as great as normal attraction."

In further experiments (1918), Nipher decided to check his results. To do this he replaced the large solid lead spheres with two metal boxes, each filled

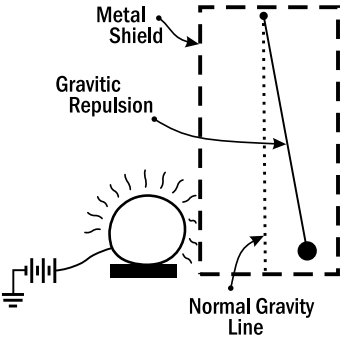

Fig. 1. Gravitational repulsion caused between large & small masses. Current on.

with loose cotton batting. These hollow boxes (having practically no mass) rested upon insulators. They were separated from the protective screen by sheets of glass and were grounded to it by heavy copper wires. The metal boxes were then charged in every way that the solid lead spheres had been, but not the slightest change in the position of the lead balls could be detected. This would seem to prove conclusively that the "repulsion" and "gravitational nullification" effects that he had produced when the solid balls were electrically charged were genuine and based undoubtedly on a true inter-atomic electrical reaction, and not upon any form of electrostatic or electromagnetic effects between the large and small masses. In Nipher experiments (*Nipher, 1920*) it was noted that:

"Results obtained on December 12 last are alone sufficient to establish the fact that enormous local changes in the earth's potential are constantly occurring and these changes produce variations in gravitational attraction between large masses and suspended masses."

In addition, it was noted by *Very (1919)* that:

"Nipher has shown that electric charges slowly penetrate into the substance of the leaden spheres of the Cavendish apparatus, producing a repulsion which is of the same order as their gravitational attraction, and this is no matter whether the electricity be positive or negative. After equilibrium is attained, and exhibition of the opposite sort of electricity penetrates most rapidly into the substance of the smaller spheres and reverses their electric sign first, when, for a time, there may be electric attraction, or at least a progressively diminishing repulsion between the large and small spheres; but

when saturation is reached, the spheres repel each other as before... It is a misnomer, however, to call the effect as Nipher does, a "gravitational" repulsion."

Then we can generalize such a phenomenon to the solar system and if we consider the Jupiter's metallic core as the same big outstanding metallic sphere in the Nipher experiments and Earth's metallic core as the same small metallic sphere in the Nipher experiments, then schematically we can wait for a very small electric interaction between Jupiter's and Earth's metallic cores, while the Sun's magnetic field is oscillating through the Jupiter as the same that Nipher used AC voltage into big outstanding metallic sphere.

From Nipher experiments, the metallic atoms show infinitesimal small electric interaction under the influence of the vibrational magnetic field and then, when the Sun's magnetic field is oscillating through the Jupiter metallic region, it appears an infinitesimal small electric interaction as an electric coupling effect between Jupiter metallic region and other planets electrically conducting regions.

The electric coupling effect of planets electrically conducting regions however, is infinitesimal small but in the planetary scales we may see for Jupiter very big metallic Hydrogen region, a small measurable effect reasoning to vary the atomic potential energy of other planets metallic regions and too an electric force between metallic regions to appear braking effect and too shearing forces between metallic region and surrounding shell (e.g. mantle in the Earth).

Such a similar mechanism has been revealed newly for super conductors and we may refer to the famous experiments by Eugene Podkletnov (*Podkletnov and Nieminen, 1992; Podkletnov and Vuorinen, 1996; Podkletnov, 1997*), known for his claims made in the 1990 of designing devices consisting of rotating discs constructed from ceramic superconducting materials. Podkletnov used a superconducting ceramic disc by rotating it above powerful electromagnets and he noticed something extremely strange. Small objects above the disc seemed to lose weight.

By the way, strongly the metallic bodies on the influence of the magnetic field variation will generate an electric interaction, however not easy to detect in small scales but we may observe a very small size of electric interaction between the large scale metallic bodies, for example the cores of the planets and it has been false idea to consider just the pure gravity

between planets and we may accept ultimately that there is a partial electric interaction while the planets are upon the Sun's magnetic field oscillation.

Then Sun's magnetic field oscillation through the Jupiter will generate shearing forces at the CMB as a turbulent flows generated by frictional forces between solid mantle and molten core, and mechanism of this frictional core flows is the same initially proposed by *Bullard (1948)* and the change of atomic level potential energy is creating too, convectional heat flows.

The primordial heat generation of the planets may be too relevant to the change of the atomic level potential energy in the metallic cores and this change of the potential energy possibly may reason to generate heat flows in the core and their relevant convectional flows and then all geomagnetic jerks may not be relevant to the shearing forces but directly may be relevant to convectional flows.

The interaction of the planets cores is visible in the phenomena and here, we will see that LOD variations and geomagnetic jerk reports and relevant gravity anomalies are verifying external driven quasidynamo included systematically to the metallic cores electric coupling effect and this is a proposed mechanism here as a theory on the base of the phenomenological reports and physical sciences. But scientists may refer to their theories however experimental reports show that the Jupiter metallic region has an influence on the Earth's core as a coupling effect and Jovian planets alignments with Jupiter are verifying such a process and this is verified by analysis of the data here.

2.3. Jovian planets alignments as the amplifier effect

It was understood above that the Jupiter metallic region is active to interact on the terrestrial planets metallic cores, of course since it be upon the Sun's magnetic field oscillation. But at the alignment dates which the Jupiter is aligned with other Jovian planets or the Sun is in the middle of Jovian alignment, the empirical results are showing that the Sun and Jovian planets alignments with Jupiter are reason to enhance the electric activity of the Jupiter to interact upon the terrestrial planets metallic cores. The mechanism of this amplification phenomenon is not exactly clear yet but as we will show it in the next sections, the reported data of geomagnetic jerks

are verifying completely it and we will see that analysis of the scientific reported data shows exactly that the alignment effect is not a direct magnetic effect suppose it works as an amplification for electric coupling effect and the size of the planetary magnetic fields is tiny to generate such a direct effect.

At the alignments, the Jupiter metallic region has the more tendency to interact with terrestrial planets metallic cores means that the alignment of active conductive cores cause the electric coupling effect between metallic cores to be amplified as an electric resonance and such a phenomenon requires to be followed by scientists in detail whereas here on the base of the jerks data and LOD variations, it is visible that the alignment effect amplifies the electric coupling effect between metallic cores of planets means that the Sun's magnetic field oscillation upon the electrically conducting regions of planets activates the planets electric interaction and Jovian planets alignments enhances it.

It was noted above that there exist a schematic similarity between the ionosphere induced currents by external magnetic field variations and interplanetary externally driven quasidynamo and then it is probable to observe the enhancement effect of geomagnetic variations in the ionosphere too. In a theoretical discussion of the solar atmosphere, *Cowling (1932)* considered the consequences, for the electron conductivity, of the inhibition of the Hall current by polarization of the medium; he found this conductivity thereby increased from the Pedersen value to that which obtained in the absence of a magnetic field. *Martyn (1948)* suggested that this effect might be responsible for the high conductivity necessary in the ionosphere to meet the requirements of the dynamo theory.

As noted *Egedal (1947)*, the daily magnetic variations are considerably enhanced in a narrow zone near the magnetic equators. *Martyn (1949)* examined the data accumulating regarding this equatorial enhancement, with a view to testing the applicability of the enhanced conductivity to this region. He found evidence consistent with the existence of a narrow belt of high conductivity encircling the Earth in a region lying near the equators and for Hall current polarization on ionosphere at all latitudes we may refer to *Baker and Martyn (1953)*.

Then it is very probable that Jovian planetary alignments which cause to enhance the Jovian driven quasidynamo, to be dependent to the induced

current polarization at Jupiter by Jovian planets alignments with Jupiter and such a mechanism may be discussed by scientists in detail for that here, inverse engineering of phenomena shows existence of enhancing effect by Jovian planets alignments.

3. Results

3.1. Solar magnetic field oscillation and planetary core flows

Schematically referring to the paper *Ferris and Price (1965)*, the idea that the ionosphere shields the Earth from magnetic field fluctuation outside it is not entirely valid and then, for induced current driven by variation of the external magnetic field and the reality that the magnitude of the current in a given loop is proportional to the strength of the magnetic field, it is resulted that the magnetic jerks O_M in each planet M, it corresponds to the first time derivative of the external magnetic fields B_{iM} through the planet which $i$is *i-th* magnetic field and M is *M-th* planet which the magnetic field passes through in so that:

$$O_M = k_M \left|\partial B_{iM}/\partial t\right|. \tag{1}$$

The influence of the external magnetic fields to the conductive core of the planets is not equal for different planets suppose coefficient k_M seems to be small for terrestrial planets, probably for those with solid mantle and thus we should wait for record of the geomagnetic jerks in the Jovian planets highly, directly by the Sun's magnetic field variation through them however this realization is very hard and in this time some scientists are analyzing large scale variations in Jupiter (*Ridley and Holme, 2016*). For the Earth by consideration of the Sun's inverse cube force of magnetic field and Earth's equation of its elliptical orbit we deduce the Sun's effect on the Earth's core by Eq. (1) that:

$$O_3 = K_{30}\, r_{30}^{-4} \times \left|\sin\left(\frac{2\pi}{T_3}t + \theta_3\right)\right|. \tag{2}$$

So that K_{30} is a coefficient for penetration of the Sun's magnetic field into the Earth's core and r_{30} is Sun-Earth distance and T_3 is the Earth orbital period and t is date and θ_3 is time phase relevant to the considered

date however θ_3 is almost near to zero for Earth because that year beginning is at the date that the Earth is almost at the major axis however θ is not zero for other planets clearly.

By equation (2) we expect relevant geomagnetic jerk and LOD variations and this equation is showing semi-annual signal for geomagnetic jerk and LOD variation in the planets relevant to oscillation of the θ's magnetic field through the planets, of course actually included to those relevant retardations. By Eq. (2) we should expect minimum amplitudes for signals when the Earth is on the major axis because, the sinus function at Eq. (2) is zero at major axis and for points of the orbit that first time derivative of the Sun's magnetic field through the Earth is maximum we should expect peaks for geomagnetic jerk and LOD variation diagrams and, for orbits near to circle, these maximum values of the magnetic field time derivative should lie on the minor axis.

This semi-annual oscillation is just match with first time derivative of the Sun's magnetic field through the planets because that the Sun's features similar to the solar wind and heat and radiation are not oscillating at the planets position in such a oscillation phase which peaks be happened just at the major axis and minor axis of the orbits and then if the measurements at the Earth are verifying semi-annual signals which the peaks be happened at the major and minor axes then such an experimental results will verify completely the reality that the Sun's magnetic field oscillation at the planets does generate relevant semi-annual signals.

Now question is that is visible such a sinusoidal semi-annual signals at the LOD variation and geomagnetic jerk and gravity anomalies?

For such a semi-annual signals we may refer to many papers for example *Le Mouël et al. (2010)* or in the paper *Höpfner (1998)* we observe clear semi-annual oscillations of the LOD, relevant to reality that the core flows are dependent on the Sun as a complete phenomenological evidence for externally driven quasidynamo and we observe in the Fig. 2, complete agreement of LOD variation semi-annual signals with Sun's magnetic field sinusoidal oscillation at the Earth position as a wonderful inevitable paradigm.

As it is visible the sinusoidal functions are completely in agreement and such a symmetry is impossible to be occurred accidentally and similar semi-annual variations should be appeared in the other planets too, of course planetary semi-annual sinusoids in that planets.

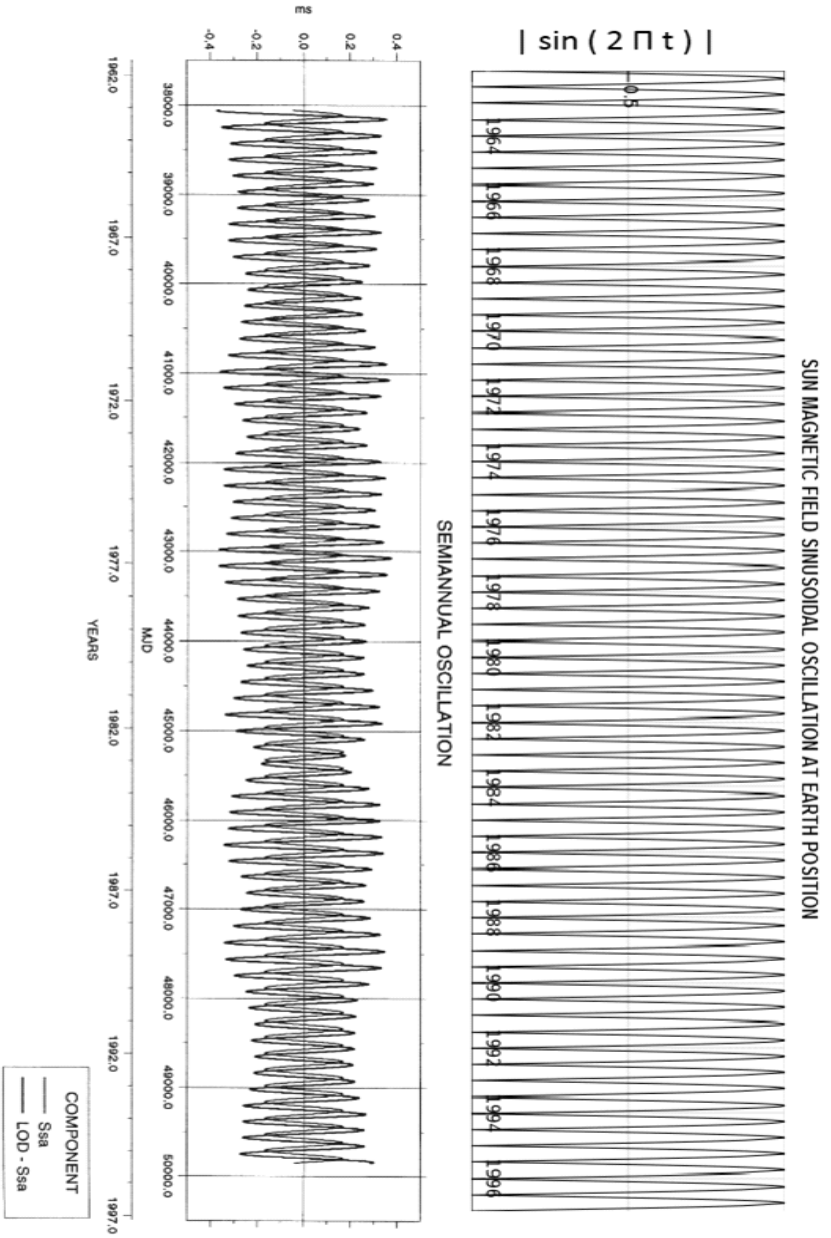

Fig. 2. The comparison of semi-annual LOD signals (*Höpfner, 1998*) versus the Sun's magnetic field oscillation through the Earth's orbit.

3.2. The 5.9-years geophysical signals

Jupiter metallic region is able not only to induct flows to the core of the terrestrial planets suppose even, the induction is being amplified and expanded by planets magnetic field and for Earth we have below equation so that u_{53} is showing Jupiter penetration coefficient as the fifth planet on the Earth as the third planet in the solar system and i is *i-th* external magnetic field indices so that:

$$O_3 = \sum_{i=0}^{N} u_{53} \left| \partial B_{i5} / \partial t \right| . \tag{3}$$

Of course the Sun's magnetic field B_{05} through the Jupiter is much greater than that of the other external magnetic fields at the Jupiter position and then this equation is transferred to a simpler equation that:

$$O_3 = u_{53} \left| \partial B_{05} / \partial t \right| . \tag{4}$$

Then geomagnetic jerks in terrestrial planets are mainly relevant to the first time derivative of the external magnetic fields through the Jupiter with partial effect dependent to the Jupiter distance from the Earth so that by inverse cube force of magnetic field and the equation of Jupiter elliptical orbit we deduce for Sun's effect on Jupiter and Jupiter secondary interaction effect on Earth that:

$$O_3 = K_{50} r_{50}^{-4} \times \left| \sin\left(\frac{2\pi}{T_5} t - 0.9 \right) \right| . \tag{5}$$

And K is additional coefficient different for each planet and r_{50} is distance of the Sun from the Jupiter and geomagnetic jerk O_3 is relevant just to the value of the external magnetic fields allowing us to compare the Sun and planets in their effect to the Jupiter and -0.9 is phase of the Jupiter in its orbit around the Sun relevant to the considered date. The Eq. (5) has period as half of the Jupiter orbital period means $T_5/2 = 5.93\, yr$ for that, the magnetic field changing through the Jupiter is relevant to radial distance varying.

Observations confirm tightly both the period and phase of the signals with partially Jovian driven quasidynamo and such a complete agreement never could be appeared randomly and for geomagnetic jerk confirmation

with Eq. (5), we may refer to paper *Silva et al. (2012)* and as noted by (*Brown et al., 2013*), the jerk amplitudes suggest possible periodic trends which may related to the 6-year periods detected independently in the geomagnetic secular variation and length-of-day. Length of day and secular variation of the magnetic field are dependent on the core flows (*Holme and de Viron, 2005*) as noted in this paper for a time-series that:
"By subtracting computed atmospheric angular momentum from a time-series for length-of-day variations, we obtain a high-resolution time-series that is useful for studying the effects of core on length-of-day variations. Features in time-series are closely correlated with time at which geomagnetic jerks have been observed, suggesting a role for core in angular momentum exchange within Earth system on timescales as short as one year, and that jerks are directly related to processes responsible for changes in core angular momentum."

At Fig. 3 we observe correlation between sinusoid of LOD variations and Jupiter driven geomagnetic sinusoid at Eq. (5) so that the left side diagram contributes to the analysis at *Duan (2015)* and we may refer to other databases too.

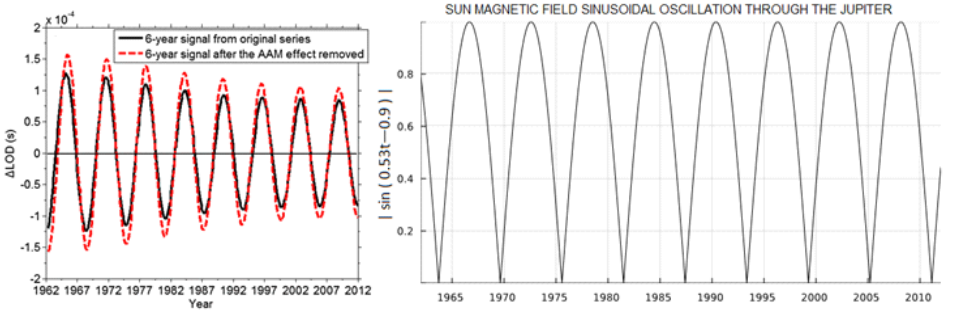

Fig. 3. Comparison of the LOD variations signals and the Sun's magnetic field sinusoid through the Jupiter.

For gravity changes, referring to *Schlamminger et al. (2015)* as noted by *Anderson et al. (2015)*, fit shows the period is almost 5.91 years and agreement of oscillation of the Sun's magnetic field through the Jupiter and gravity oscillation is visible at Fig. 4.

Coefficient u_{53} in Eq. (3) corresponds to Jupiter-Earth distance because that the electric coupling effect of the cores is relevant partially to the

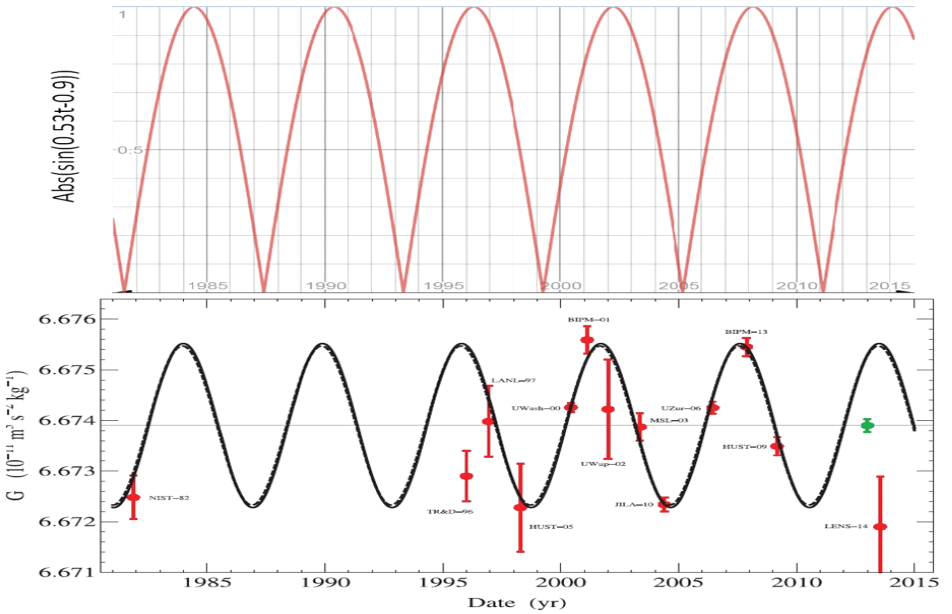

Fig. 4. A set of 13 measurements of G exhibit a 5.9-year periodic oscillation (solid curve) (Credit: *Anderson et al. (2015)* EPLA) that closely matches the 5.9-year oscillation in the Sun's magnetic field through the Jupiter.

Jupiter-Earth distance. but we should notice that the sinusoid of geomagnetic jerk is not dependent on the parameter u_{53} for that, peaks are relevant to the first time derivative of the Sun's magnetic field through the Jupiter. Coefficient u_{53} is almost constant for small changes of distance like the Jupiter-Earth distance as a factor between 1–1.5 however probably detectable in very accurate analysis and it was detected a near period 1.023 yr in revised G measurement (*Schlamminger et al., 2015*) as noted in *Anderson et al. (2015)*.

3.3 Jovian planets alignments as the source of abrupt geomagnetic jerks

Then the Jovian planets alignments with Jupiter is reason to amplify the electromagnetic activity of the Jupiter which is the source of 5.93 years periodic signal. This amplification is a source to generate abrupt geomag-

netic jerks visible at the Earth surface. It means that the Jovian planets alignments with Jupiter are reason to enhance the Jupiter metallic region electromagnetic activity to influence on the Earth's core so that Jovian driven geomagnetic jerk is enhanced by an alignment amplifier factor λ as:

$$O_3^* = \lambda O_3 \,. \tag{6}$$

So that $O_3$is geomagnetic jerk at Eq. (4) and O^* is relevant total geomagnetic jerk amplified by jovian planets alignments.

We show here in the tables, the correlation of the alignments with observed geomagnetic jerks O^*. The line arc is the angle between Jupiter's major axis and Sun-Jupiter line and the geomagnetic jerks are proportional with sinusoid of line arc of the Jupiter according to the Eq. (5) and correlation of Jovian planets alignments with amplification of the geomagnetic jerks is an inevitable confirmation.

The geomagnetic jerks are not simultaneous because spatial distribution of the core flows occur with retardation and usually the event begins from northern hemisphere and ends to the south (*De Michelis et al., 2005*). This may concern to the migration of the flows, and the alignment date should be almost the beginning time of occurrence. This is an evidence that the core flows are expanding by Earth's magnetic field after generation at alignment epoch. The research of all alignments between 1890 to 2020 is presented in the next Tables 1–9.

In these tables for alignments dates we have referred to NASA's solar system simulator (NASA'S EYES: Jet Propulsion Laboratory). Line arc is angle between Jupiter's major axis and Sun-Jupiter line in that orbit around the Sun and L as the length of the alignment defined as the distance between left and right planets in the alignment and reports are data for occurrences of the geomagnetic jerks referring to the published papers and each mentioned amplitude for an especial geomagnetic jerk in the tables it is relevant to the detected amplitude referenced in the relevant report in that table.

Saturn-Jupiter-Uranus is very strong alignment so that it is visible the reports in the fewer line arcs too and we observe agreement between the alignments line arcs and amplitudes of the reported geomagnetic jerks as a verification for Eqs. (5, 6).

For Jupiter-Saturn-Uranus in comparison with Saturn-Jupiter-Uranus we

Table 1. Saturn-Jupiter-Uranus

Line date	Reported jerks epoch	Line arc	L (AU)	Reports
1915.08.30	for event 1915	∼ 25	∼ 29	*Brown et al., 2013; Qamili et al., 2013*
1922.08.02	Less marked event	∼ 8	∼ 28	–
1925.02.04	for event 1925	∼ 77	∼ 27	*Alexandrescu et al., 1996*
1958.03.16–1959.08.12	Tangential event 1958	∼ 9 – 45	∼ 28	*Golovkov et al., 1989*
1968.07.09	Related to 1969 event	∼ 37	∼ 29	*Le Mouël et al., 1982; Malin et al., 1983*
2010.07.10	For event 2011	∼ 25	∼ 30	*Chulliat and Maus, 2014*

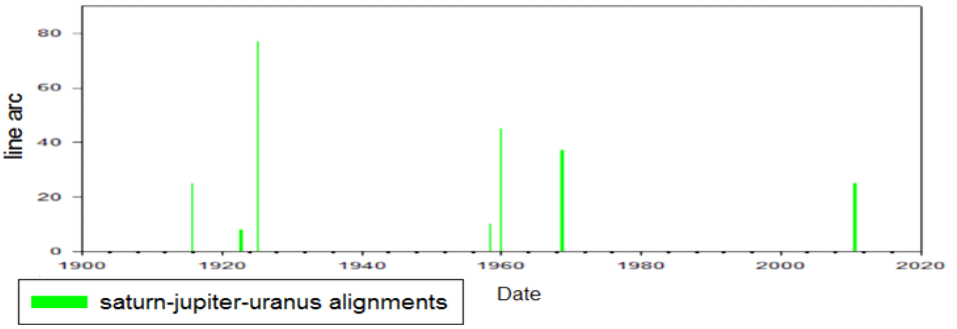

Fig. 5. The Saturn-Jupiter-Uranus alignments and relevant line arcs.

see that when Jupiter is between the Jovian planets, the generated effect is almost two times stronger and it is wonder that recorded jerk at 1896 is exactly for lining up at 1895.08.11.

Again we see that the alignments of Saturn-Jupiter-Neptune with much less line arcs, have no any jerk reports and generally all relevant geomagnetic jerks are less marked as a relation between alignment arm length and amplitude of the geomagnetic jerk.

Jupiter-Saturn-Neptune average arm length is almost equal to Saturn-Jupiter-Neptune arm length but Jupiter is not in the middle and then the amplitude is almost half and there is no any reported geomagnetic jerks relevant to these alignments else a less marked event for 1989.11.11 if it be possible to discriminate between other geomagnetic jerks occurred almost simultaneously.

It is visible that the relevant geomagnetic jerks are less marked and this is completely in agreement with size of the alignments arm length and value

Table 2. Jupiter-Saturn-Uranus

Line date	Reported jerks epoch	Line arc	L (AU)	Reports
1895.08.11	Observed at 1896–1898	∼ 86	∼ 24.5	*Balasis et al., 2016*
1944.05.15	From 1945, a strong field spreads until 1949	∼ 51	∼ 19.5	*Duka et al., 2012*
1989.02.04	for a group of events centred at 1990.1	∼ 49	∼ 24.5	*Cafarella and Meloni, 1995; Macmillian, 1996; De Michelis et al., 2005*

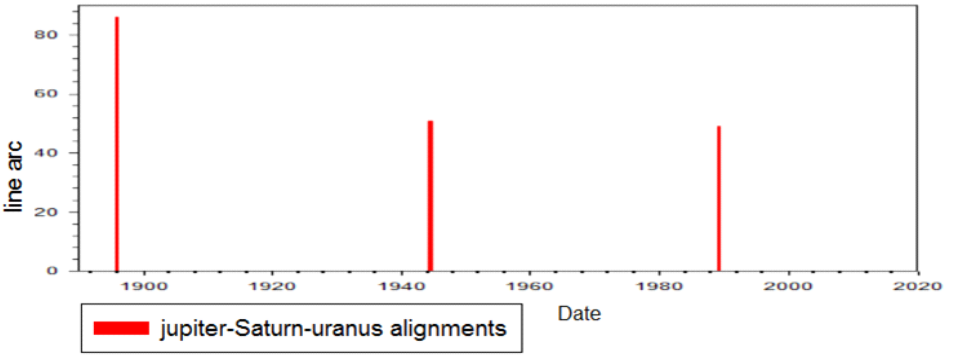

Fig. 6. The Jupiter-Saturn-Uranus alignments and relevant line arcs.

of the line arcs in the Uranus-Jupiter-Neptune alignment.

Jupiter-Uranus-Neptune alignment is once happened in considered interval and in this alignment, the Jupiter is not in the middle but alignment length is lesser than that of Uranus-Jupiter-Neptune and then probably less marked report at 1992 is caused by this alignment.

At the date 1998.06.20, the Jupiter has no any alignment but Saturn is almost in MOID (Minimum Orbit Intersection Distance) with Jupiter and Saturn plays the role of Jupiter here so that we have an alignment Neptune-Uranus-Saturn to activate highly the Saturn, and Saturn influence on the Jupiter is in the same manner that Jupiter is influencing Earth and thus, consequently the Jupiter is influencing on the Earth by Saturn alignment effect and Saturn should be in its active zone of influence and solar system simulators are verifying this and the report of geomagnetic jerk at epoch 1999 (*Brown et al., 2013; Mandea et al., 2000*) is revealing this. Such an event is being occurred at the date 1936.06.15 for alignment Saturn-

Table 3. Saturn-Jupiter-Neptune.

Line date	Description	Line arc	L (AU)	Report
1896.01.05	Less marked event	∼ 73	∼ 39	*Balasis et al., 2016*
1902.10.26	Less marked event 1902–1903 1902–1903	∼ 58	∼ 39	*Alexandrescu et al., 1996; Duka et al., 2012*
1904.05.01	–	∼ 6	∼ 39	–
1933.11.30	–	∼ 10	∼ 39	–
1971.07.10	For event 1972.1	∼ 47	∼ 40	*Chambodut et al., 2007; Duka et al., 2012*
2008.11.11	for 2009 (–18.6 nT/yr^2)	∼ 80	∼ 40	*Chulliat and Maus, 2014; Kotzé and Korte, 2016*

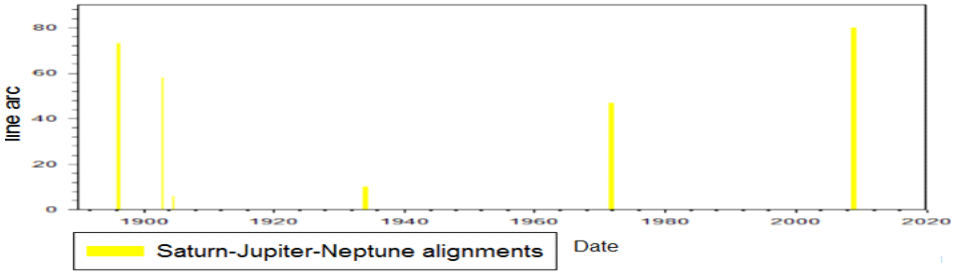

Fig. 7. The Saturn-Jupiter-Neptune alignments and relevant line arcs.

Table 4. Jupiter-Saturn-Neptune.

Line date	Reported jerks epoch	Line angle	L (AU)	Report
1915.12.18	–	∼ 15	∼ 34	–
1952.08.06	–	∼ 19	∼ 35	–
1989.11.11	For event centred at 1990.1	∼ 74	∼ 35	*Cafarella and Meloni, 1995; De Michelis et al., 2000)*

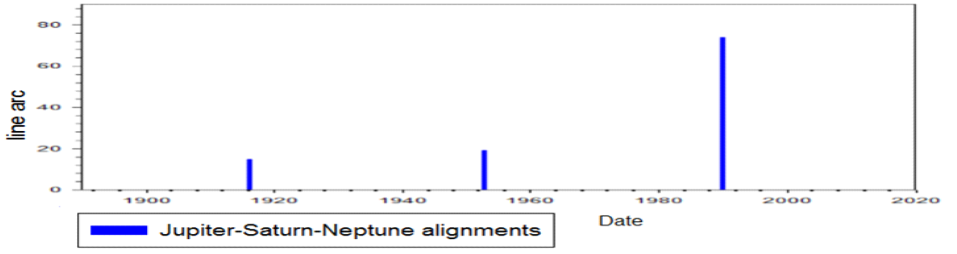

Fig. 8. The Jupiter-Saturn-Neptune alignments and relevant line arcs.

Table 5. Uranus-Jupiter-Neptune

Line date	Reported jerks epoch	Line arc	L (AU)	Jerk reports
1896.06.17	CLF and NGK Y-component	~ 61	~ 49	*Balasis et al., 2016*
1899.04.10	Much less marked event	~ 45	~ 49	–
1907.05.04	Less marked event observed 1908 observed 1908	~ 87	~ 50	*Qamili et al., 2013; Balasis et al., 2016*
1915.03.14	Less marked event at 1915	~ 43	~ 49	*Balasis et al., 2016*
1918.06.08	Less marked observed event 1919	~ 66	~ 49	*Alexandrescu et al., 1996*

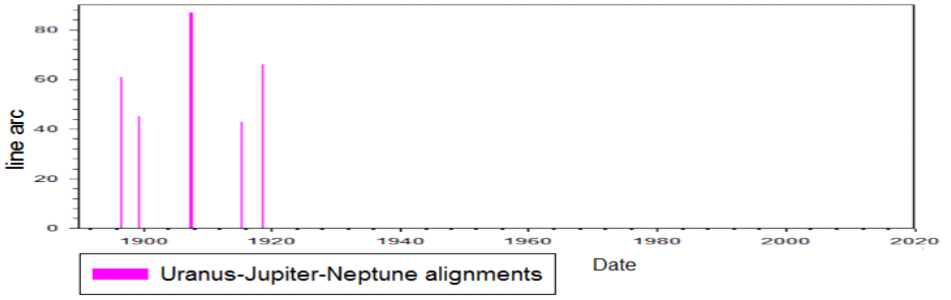

Fig. 9. The Uranus-Jupiter-Neptune alignments and relevant line arcs.

Table 6. Jupiter-Uranus-Neptune

Line date	Description	Line arc	L (AU)	Jerk reports
1991.09.05	Report around 1992	~ 52	~ 34	*Le Huy et al., 1998; Brown et al., 2013*

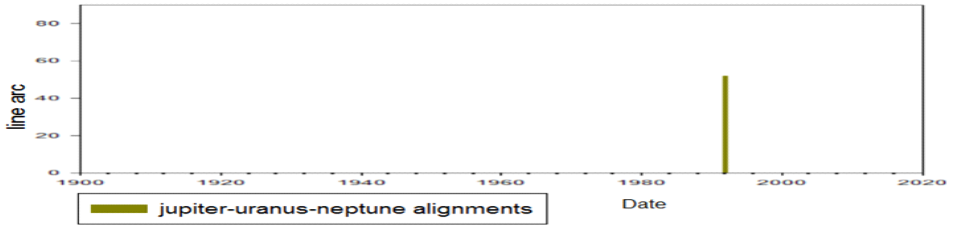

Fig. 10. The Jupiter-Uranus-Neptune alignments and relevant line arcs.

Sun-Neptune which the Saturn is almost in minimum distance with Jupiter and it is observable a less marked geomagnetic jerk for that at epoch 1937 (*Golovkov et al., 1989*).

Table 7. Jupiter-Sun-Saturn

Line date	Reported jerks epoch	Line arc (deg)	Jerk reports
1892.01.16	observed event at 1983	∼ 22	*Nevanlinna, 2004; Balasis et al., 2016*
1911.05.14	observed event at 1912–1913	∼ 25	*Alexandrescu et al., 1996; Ducruix et al., 1983*
1930.12.23	observed event at 1932	∼ 87	*Alexandrescu et al., 1996*
1951.08.04	observed event at 1952	∼ 14	*Duka et al., 2012*
1971.01.12	observed event at 1972	∼ 36	*Chambodut and Mandea, 2005; Qamili et al., 2013*
1990.07.22	observed event at 1991	∼ 84	*De Michelis et al., 2005*
2011.02.18	–	∼ 2	–

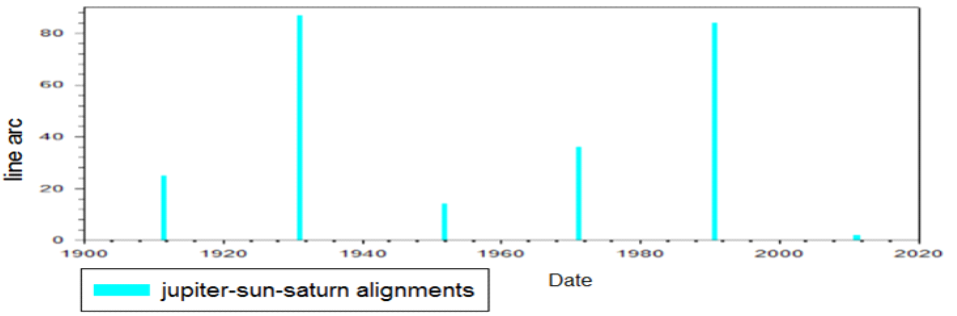

Fig. 11. The Jupiter-Sun-Saturn alignments and relevant line arcs.

By the way, the Jovian alignments generate geomagnetic jerks proportional with sinus of the line arcs and some very strong alignments are possible to occur in much less line arcs and null results are in weak influence zone of the Jupiter and this phenomenology is verifying that Jupiter alignments with Jovian planets enhance the Jupiter activity on the Earth's core and Jupiter-Sun-Jove alignments are affecting on the Jupiter activity and while the Sun is not in the middle of alignment we have no noticeable effect whereas that while the Sun is in the middle of the alignment, the effect is strong and for Jupiter-Sun-Jove alignments we refer to the below tables and those relevant figures.

It is manifest that null result is relevant to the much less line arc and all alignments are relevant to the reported geomagnetic jerks and we see that jerks of 1913 and 1991 and 1932, are iteration of a unit event.

Table 8. Jupiter-Sun-Uranus

Date	Reported jerks epoch	Line arc	Jerk reports
1893.05.10	observed event at epoch 1894	∼ 21	*Nevanlinna, 2004; Balasis et al., 2016*
1907.02.15	observed event at epoch 1908	∼ 85	*Qamili et al., 2013; Balasis et al., 2016*
1920.10.20	observed event at epoch 1921	∼ 43	*Duka et al., 2012; Pinheiro and Travassos, 2010*
1934.08.24	–	∼ 12	–
1948.07.11	Jerk observed in pacific area and American regions at epoch 1949	∼ 71	*Alexandrescu et al., 1996*
1962.06.04	this event is similar to 1920.11.02 event and observed at epoch 1963	∼ 48	*Duka et al., 2012; Qamili et al., 2013*
1976.03.30	observed event in the field 1978	∼ 17	*Alexandrescu et al., 1996*
1989.12.10	observed event at epoch 1990	∼ 76	*De Michelis et al., 2005; Balasis et al., 2016*
2003.09.06	Much less marked jerk	∼ 49	–
2017.07.07	–	∼ 12	–

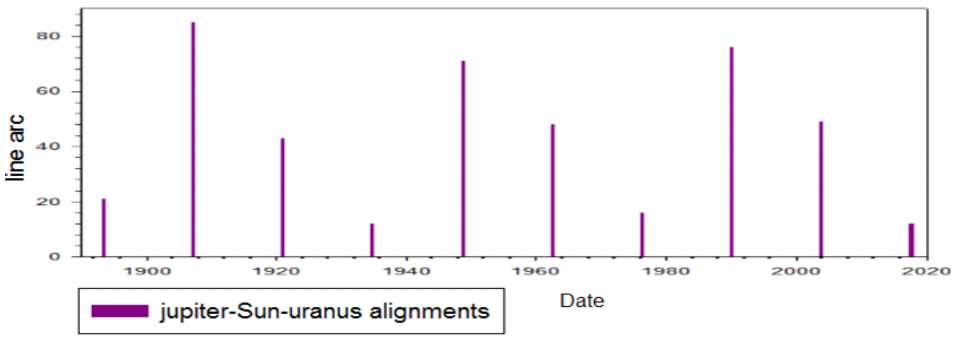

Fig. 12. The Jupiter-Sun-Uranus alignments and relevant line arcs.

Reports amplitudes fit with inverse square of the arm length and this is possible to observe for other Jovian planets alignments with Jupiter too as a verification for such a correlation between arm length of the alignments and geomagnetic jerks amplitudes.

The average arm length of the Jupiter-Sun-Neptune alignment is 1.4 times longer than that of Jupiter-Sun-Uranus and then, relevant alignments to the Jupiter-Sun-Neptune should be almost 2 times weaker and then, all

Table 9. Jupiter-Sun-Neptune.

Line date	Reported jerks epoch	Line arc	Jerk reports
1901.02.27	Saturn-Jupiter-Sun-Neptune Event at epoch 1901–1902	∼ 71	*Alexandrescu et al., 1996*
1913.12.18	Less marked event reported 1913–1914	∼ 80	*Balasis et al., 2016; Alexandrescu et al., 1996*
1926.09.15	–	∼ 52	–
1939.05.12	–	∼ 26	–
1952.02.01	–	∼ 0	–
1964.10.13	Revealed by Moscow observatory	∼ 30	–
1977.06.18	Observable in the field 1978	∼ 57	*Alexandrescu et al., 1996*
1990.04.19	Much less marked event between next events	∼ 85	–
2002.12.15	Less marked event observed at epoch 2003 detected by a new high resolution technique	∼ 65	*Olsen and Mandea, 2007; Balasis et al., 2016; Silva and Hulot, 2012*
2015.11.03	–	∼ 39	–

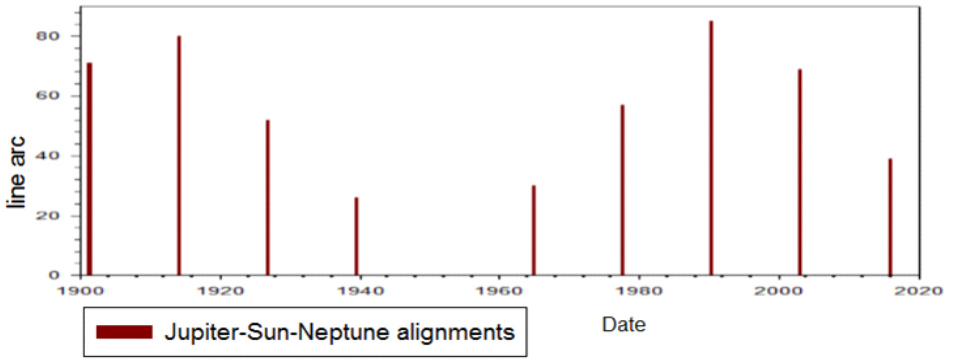

Fig. 13. The Jupiter-Sun-Neptune alignments and relevant line arcs.

alignments of Jupiter-Sun-Neptune should be less marked events and this is agreement else at 1901 that the alignment is enhanced by Saturn near lining with Jupiter-Sun-Neptune.

Ultimately we observe that all reported geomagnetic jerks occur at the alignment dates and too, inversely while we have a Jovian alignment, it exist a relevant geomagnetic jerk in reports as a very strong confirmation for one by one correlation between geomagnetic jerks and Jovian alignments. Solar system simulators are verifying exactly all the correlations between reports

and alignments, but for shortening the paper we show at Fig. 14, some of the famous geomagnetic jerks relevant to their Jovian planets alignments.

Of course when the Sun is not in the middle of the Jovian planets alignments it is visible that the amplitude of the effect is weak as the same manner for Jupiter when Jupiter is not in the middle. But for alignments of Sun-Jupiter-Saturn it seems to exist some relevant Much less marked events in reports for example for epochs 1901, 1981, 2000 (*Balasis et al., 2016*) and 1921, 1941 (*Duka, 2012; Pinheiro and Travassos, 2010*) and 1961 because of the reality that arm length of Sun-Jupiter-Saturn is short proportionally and Sun-Jupiter-Saturn effect might be relevant to the Saturn which the Sun's magnetic field is rapidly varying at alignment time through the Saturn and this is in agreement with quick succession of geomagnetic jerks at these epochs.

We observe that there are several consequanet noticeable events as Jupiter-Saturn-Uranus at epoch 1989.02.04, Jupiter-Sun-Uranus at epoch 1989.

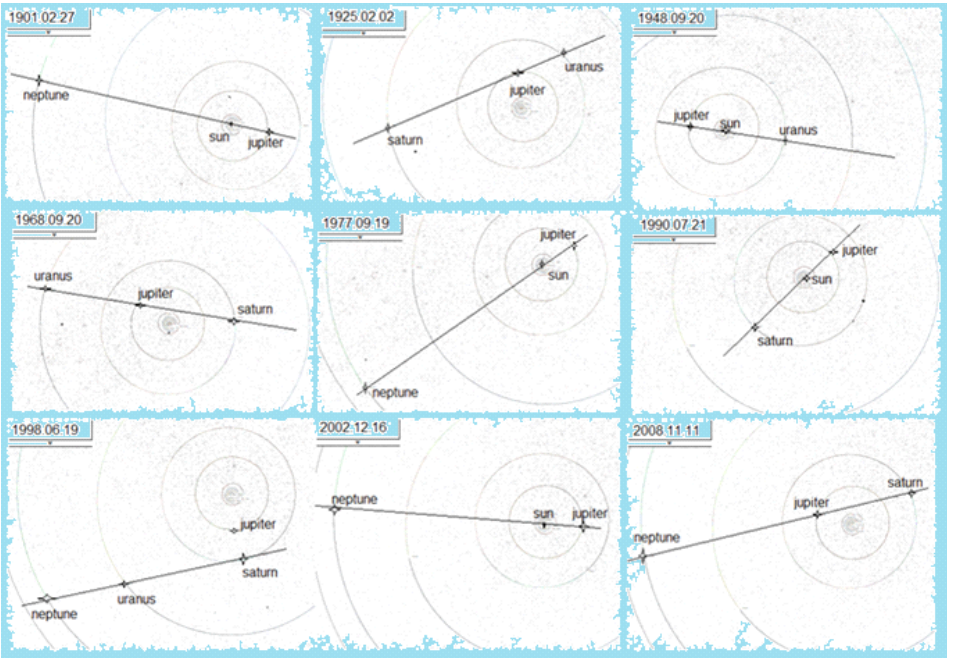

Fig. 14. Several alignments concern to relevant geomagnetic jerk dates.

12.10, Jupiter-Sun-Saturn at epoch 1990.07.22 and these alignments are very near in time, visible as a unified event centered at 1990.1 (*De Michelis et al., 1998; 2000*) and as noted at *Chambodut and Mandea (2005)* that: *"For the so-called 1969 event a first group of dates is centered on 1969.5 ±0.5 and another one 1972.1 ±0.5; their merging date being around 1971."*

Whereas, here we observe that the reported jerk about 1972 is different from reported jerk at 1969. Suppose we have a clear event at 1972. We should notice that the Saturn and Uranus and Neptune metallic cores have almost equal sizes and then the amplitude of the geomagnetic jerks generated at Jovian alignment ideally should be proportional with inverse square of arm lengths and too according to the Eq. (5), the amplitude of the geomagnetic jerks in the alignments should be proportional with sinus of the line arcs and too we should consider a coefficient for realization between different alignments structurally and then, almost we have a simple formula for ideal geomagnetic jerks generated by Jovian planets alignments that:

$$O_3 \propto \frac{1}{L^2}\beta \sin(\alpha). \tag{7}$$

So that β is structure coefficient of the alignments and α is line arc and L is arm length.

We can't find an accurate formula for geomagnetic jerks for that the geomagnetic jerks are relevant to the planets interiors and probably declined by number of the core flows so that we observe greater amplitudes in quasi-local events and probably there is a conservation law of geomagnetic jerk's amplitudes in an event divided to several number of the events in a global event.

New exact analysis (*Kotzé and Korte, 2016*) shows for epoch 2009 we have a jerk with mean amplitude $18.6\,\mathrm{nT/yr^2}$ and we can consider Saturn-Jupiter-Neptune alignment occurred at epoch 2009 as a standard reference for other occurences and line arc in this alignment is 80 degree and arm length is 40 AU and by Eq. (7) for pure Jovian planets alignment we have:

$$O_3^*[J - Jup - J]/18.6 = \sin(\alpha)/\sin(80) \times 1600/L^2, \tag{8}$$

$$O_3^*[J - Jup - J] \approx 30000 \sin(\alpha)/L^2. \tag{9}$$

Now referring to the reported geomagnetic jerk at epoch 2003 with amplitude $25\,\mathrm{nT/yr^2}$ we can calculate structures' coefficient β. At epoch 2003 we

have Jupiter-Sun-Neptune with line arc 65 degree and arm length, 35 AU. But 2003 event is almost at middle of the solar maximum activity and then by consideration of calculations in the next section we find that the Sun's alignment effect while the Sun is in the middle, is 1.2 times stronger than Jovian planets alignments while Jupiter is middle and so, structure coefficient is deduced as:

$$\beta_{Jup-Sun-J} = 1.2\beta_{J-Jup-J} = 2.4\beta_{Jup-J-J}. \tag{10}$$

Then not only here we can show the correlation of geomagnetic jerks with Jovian planets alignments suppose we have an almost simple approximate formula for ideal amplitude of the geomagnetic jerks and by this formula we get amplitudes for jerks at Fig. 15. For existing alignments in the considered interval 1980–2020 which confirms again the agreement of the correlations included to the arm length inverse square and, correlation of the geomagnetic jerk's amplitudes to the sinus of the line arcs as the angle between the Jupiter's major axis and Jupiter-Sun line and ultimately, inevitable verification for essential relation of the Sun's magnetic field oscillation through the Jupiter and Earth's CMB core flows as the sources for the reported geomagnetic jerks in these decades. It is wonder that there is a complete one by one correlation between geomagnetic jerks and Jovian planets alignments means that for each observable Jovian alignment in the solar system we have a report for geomagnetic jerk at that time and inversely for each reported geomagnetic jerk in the data, we have a relevant Jovian alignment and this confirmation is arguing inevitable correlation of the Jovian planets alignments and geomagnetic jerks and at Fig. 15. It is visible correlation of equations with observations carefully.

We need to notice that however the Jovian planets alignments with Jupiter are to some extent strong that it is possible to measure their relevant geomagnetic jerks at the Earth. But it is possible to observe such a phenomenon about the Saturn instead Jupiter by improvement of the precise of the measurements and data analysis. For example, we may detect a much less marked event for Saturn-Uranus-Neptun, when the Saturn is at the active zone of its line arc and probably it is possible to detect a very weak periodic 14.5-years signals, half of the Saturn orbital period. However, detection of the Saturn dependent effect is easier at its alignment dates.

We see strong agreement between amplitudes of the observed geomag-

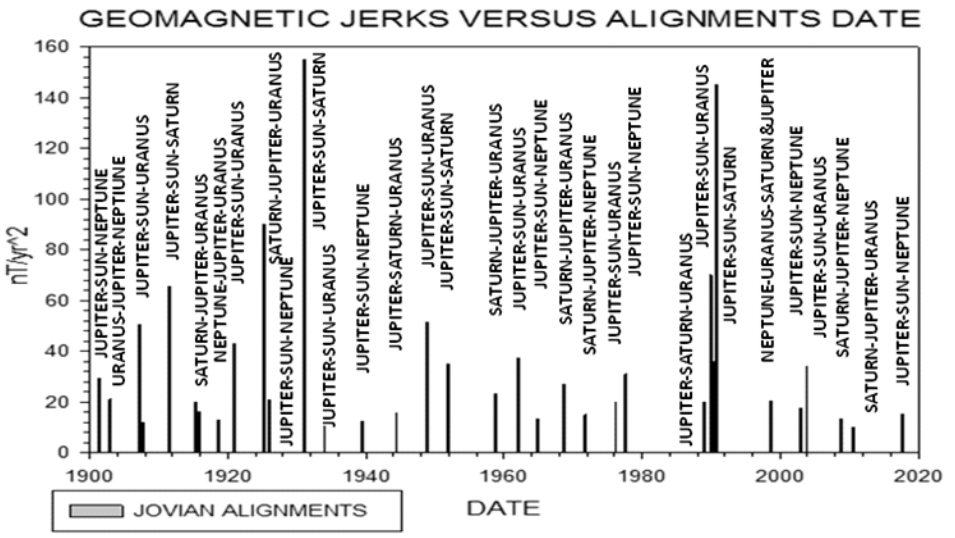

Fig. 15. Geomagnetic jerks reported dates correlated to the Jovian planets alignments.

netic jerks and ideal formula at Eq. (7) above and for alignment at 2017.07.07, the ideal formula shows $11\,\mathrm{nT/yr^2}$ and because that this is a much less marked event, the visibility of such an event is rare for distribution of geomagnetic jerk's power and because of entopic reasons.

3.4. Historical jerks reports and inevitable agreement with Jupiter alignments

We refer here to historical reports however unfortunately analysed dates have been approximate for that there is no magnetic three components time series of data and we have listed alignments accordance to NASA's solar system simulator versus the dates of geomagnetic jerk's reports (*Korte et al., 2009*) and everybody may refer to every accurate solar system simulator arbitrary.

In the Fig. 16, we see the Table 10 in a diagram to easy visibility of the correlations between the historical alignments and reported jerks date for amplitudes of these historical geomagnetic jerks we refr to the ideal formula at Eq. (7) above.

And for another data base of historical geomagnetic jerks, reported in the

Table 10. Geomagnetic jerks from 1410 to 1990 in comparison with alignments.

Line date	Alignments	Arm (AU)	Line arc	Report date
1409.10.07	JUP-SUN-URA	∼ 25	∼ 72	1410
1447.01.01	JUP-SAT-URA	∼ 17	∼ 60	1448
1506.07.02	JUP-SUN-URA	∼ 25	∼ 53	1508
1597.05.01	SAT-JUP-URA	∼ 27	∼ 40	1598
1603.02.10	JUP-SUN-URA	∼ 25	∼ 40	1603
1658.11.15	JUP-SUN-NEP	∼ 35	∼ 73	1661
1692.10.01	JUP-SUN-SAT	∼ 15	∼ 55	1693
1706.02.19	JUP-SAT-NEP	∼ 32	∼ 79	1708
1741.05.05	JUP-SUN-URA	∼ 25	∼ 90	1741
1764.07.01	JUP-SAT-URA	∼ 19	∼ 74	1763
1860.10.17	SAT-JUP-NEP	∼ 37	∼ 65	1861
1888.04.14	JUP-SUN-NEP	∼ 35	∼ 43	1889

Source: (*Korte et al., 2009*).

measurements (*Qamili et al., 2013; Matzka et al., 2010*), we see strong confirmations between dates of Jovian planets alignments and reported dates for geomagnetic jerk as visible at Table 11.

However, the measurements have not generated precise dates but again correlations are very strong between assumed parameters and we observe,

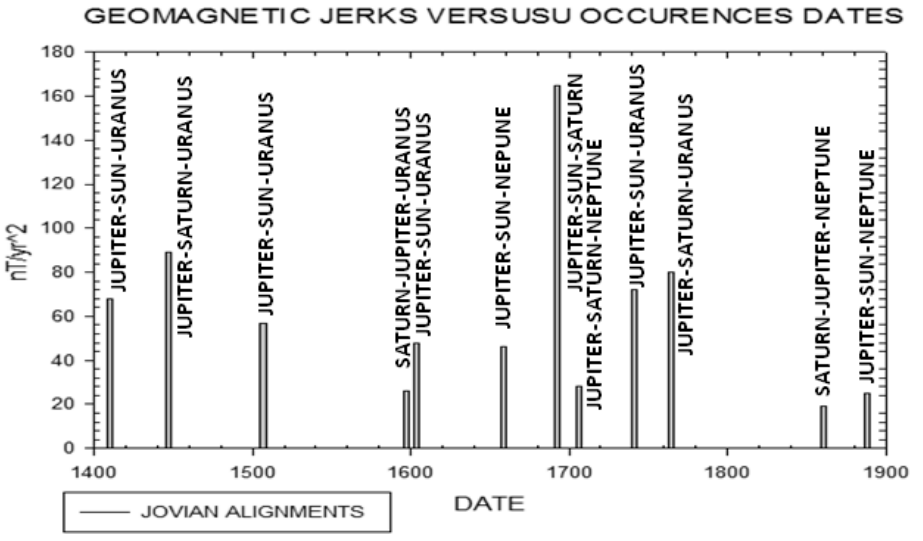

Fig. 16. The alignments in agreement with reported geomagnetic jerks.

Table 11. Geomagnetic jerks reported in the interval 1600–1900.

Line date	Alignments	Arm (AU)	Line arc	Report date
1603.12.10	JUP-SUN-URA	∼ 25	∼ 40	1603
1633.10.07	JUP-SUN-SAT	∼ 15	∼ 64	1635
1659.02.09	JUP-SUN-URA	∼ 25	∼ 65	1663
1672.09.01	JUP-SUN-SAT	∼ 15	∼ 21	1672
1700.01.05	JUP-SUN-URA	∼ 25	∼ 79	1703
1718.01.14	SAT-JUP-NEP	∼ 38	∼ 90	1719
1733.10.08	JUP-SUN-SAT	∼ 15	∼ 39	1733
1752.10.16	JUP-SUN-SAT	∼ 15	∼ 83	1751
1762.12.09	JUP-SAT-URA	∼ 15	∼ 24	1763
1769.06.05	JUP-SUN-URA	∼ 25	∼ 37	1770
1778.01.03	SAT-JUP-URA	∼ 28	∼ 70	1779
1788.09.27	SAT-JUP-URA	∼ 29	∼ 80	1789
1808.09.09	JUP-SAT-URA	∼ 20	∼ 33	1810
1824.09.01	JUP-SUN-URA	∼ 25	∼ 90	1826
1838.02.28	JUP-SUN-URA	∼ 25	∼ 35	1838
	UNKOWN			1844
1852.03.07	JUP-SUN-SAT	∼ 15	∼ 25	1853
1866 (1868)	JUP-SUN-URA (SAT-JUP-NEP)	∼ 25(38)	∼ 87(30)	1868–1870
1879.11.10	JUP-SUN-URA	∼ 25	∼ 40	1882
1888.05.13	JUP-SUN-NEP	∼ 35	∼ 43	1888

Source: (*Qamili et al., 2013; Matzka et al., 2010*).

the data as a diagram at Fig. 17 to see easier the correlations between events dates and Jovian planets alignments.

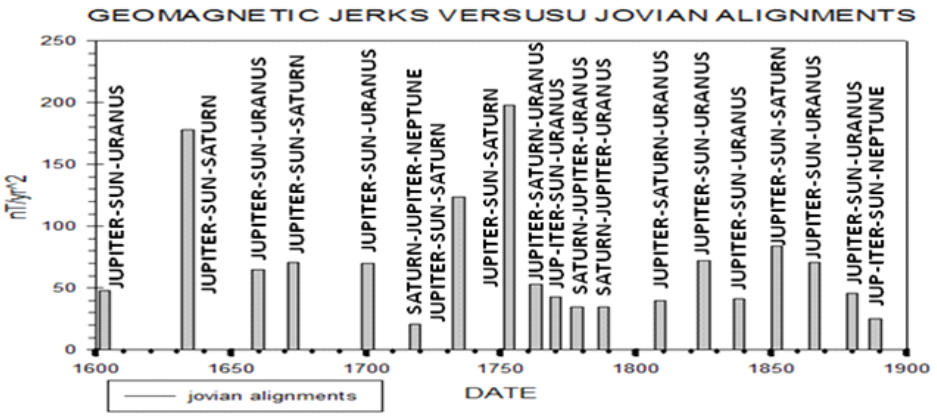

Fig. 17. The alignments in agreement with reported geomagnetic jerks.

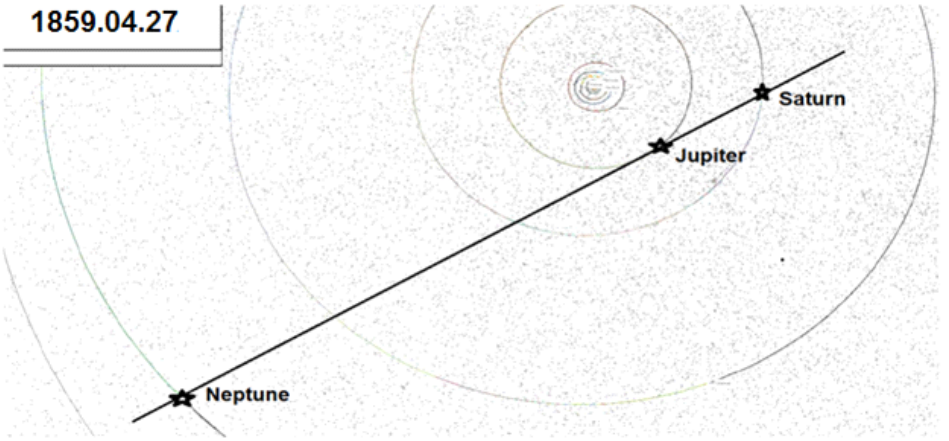

Fig. 18. The alignment completely in agreement with reported geomagnetic jerk at epoch 1860 (*Newitt and Dawson, 1984*).

The iteration of an alignment is iteration of the jerk as a strong confirmation and we see the similar events with event at epoch 1901.

It is wonder that all the alignments are a bit occurred before of reports dates as a verification for ever existing retardation and a verification for Jovian driven quasidynamo at the Earth because that Jovian driven quasidynamo is in agreement ever with the reality that the alignments should be prior to the reports date. For example, there is evidence of a jerk around 1860 (*Newitt and Dawson, 1984*) and when we refer to the solar system simulators we observe that we have an alignment Saturn-Jupiter-Neptune at 1859.04.27 with almost 37 AU arm length which is proportionally short and too, Jupiter is at the middle of the alignment as a feature of stronger effect.

3.5. Solar activity effect on the geomagnetic jerks and LOD variations

In addition to semi-annual signals generated by oscillation of the Sun's magnetic field at the Earth orbiting around the Sun, clearly we should wait for 11 years' periodic oscillation of the geomagnetic jerk and LOD, relevant to the solar cyclical activity which concerns to the absolute oscillation of the Sun's magnetic field as noted at *Vukcevic (2014)* that:

"Sunspots are associated with rise and fall of the soar toroidal magnetic field, and normally appear in pairs. Direction of the magnetic field vector $\boldsymbol{B}$ *in the northern hemisphere coincides with the direction of solar rotation (positive orientation,* $B > 0$*) during even-numbered cycles, it is opposite for the southern hemisphere. Relationship between direction of rotation and the magnetic field vector orientation is reversed during odd-numbered cycles (for the northern hemisphere* $B < 0$*)."*

Then solar cyclical activity will result two shapes of the 11-years periodic signals in the LOD and geomagnetic jerks as:

1. Direct effect by the Sun's magnetic field absolute oscillation through the Earth,
2. Jupiter driven external effect dependent on the absolute variation of the Sun's magnetic field through the Jupiter.

Both direct absolute effect and Jupiter driven absolute effect of the solar cyclical activity will clearly imply 11-years periodic signals on the LOD and geomagnetic jerks and probably on the gravity too.

This 11 years' periodic signals have been detected before in several analyzings (for example *Gu, 1990; Abarca del Rio et al., 2003; Wardinski and Holme, 2003; Alexandrescu et al., 1995*) and as noted at *Le Mouël et al. (2010)*:
"We study the evolution of the amplitude A of the semi-annual variation of the length-of-day (lod) from 1962 to 2009. We show that A is strongly modulated (up to 30%) by the 11-yr cycle monitored by the Sunspot number WN."

Dependency to the solar activity has been detected well in the LOD variation as mentioned by *Ma (2007)* that:
"In this present paper, wavelet technique is applied to analyse the time series of the Earth's length-of-day series during 1832–1997 and the Sunspot relative numbers during 1700–2006, with emphasis on investigating external excitation source of the Earth's variable rotation. The results show modulation action from solar activity plays an important role in decadal change of the Earth rotation, and this strengthens the conclusion that the Earth's rotation is modulated by the solar activity."

Or we may refer to work "Possible influence of the 11-year solar cycle on length-of-day change" (*Ma, 2015*).

Up to here in this paper, we have considered constant, the Sun's absolute magnetic field but solar activity indexes are showing that the solar magnetic field is changing by time cyclical as the famous 11 years' oscillation of the solar activity and then not only, the Jupiter orbiting causes, the change of the Sun's magnetic field through the Jupiter relatively suppose absolutely, the Sun's magnetic field is too changing through the Jupiter and through the other planets too. Then, the change of the Sun's magnetic field through the Jupiter is divided to the two realizable origins so that by generalization of the Eq. (1) we have:

$$O_3 = k_{53} \left| \left(\partial B_{05}/\partial t\right)_{orbital} + \left(\partial B_{05}/\partial t\right)_{absolute} \right| \tag{11}$$

In some dates for example at epochs 1948.07.11 and 1958 and 1968.07.09 we observe that the reported amplitudes of the geomagnetic jerks are stronger than that of calculated by ideal Eqs. (7, 10) for geomagnetic jerk. According to Eq. (11), the geomagnetic jerks relevant to these three dates are amplified by solar activity because that these events are in maximum solar activity occurred at solar active cycle period, referring to the NASA reports for solar activity as visible at Fig. 19. These three events have been compared together before by *Golovkov et al. (1989)* titled as "Common features and differences between jerks of 1949, 1958 and 1969".

Ultimately we see a total equation for external driven interplanetary signals at the Earth so that:

$$\begin{aligned} O_3 = {} & k_{53} \left| \left(\partial B_{05}/\partial t\right)_{orbit} + \left(\partial B_{05}/\partial t\right)_{absolute} \right| + \\ & + k_{03} \left| \left(\partial B_{03}/\partial t\right)_{orbit} + \left(\partial B_{03}/\partial t\right)_{absolute} \right| . \end{aligned} \tag{12}$$

This equation results four kinds of the signal at the Earth as:

1. Direct absolute effect of the Sun at the Earth interior resulting 11-years signal,
2. Direct orbital effect of the Sun at the Earth interior resulting semi-annual signal,
3. Indirect absolute effect of the Sun's magnetic field through the Jupiter resulting 11-years signal,
4. Indirect orbital effect of the Sun's magnetic field through the Jupiter resulting 5.9-years signal.

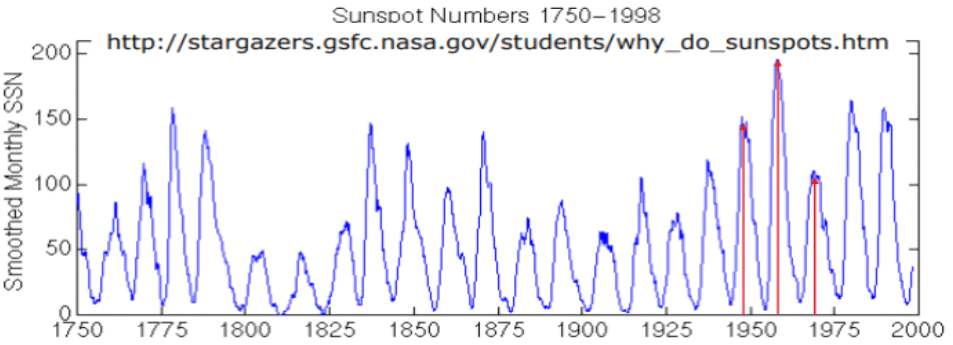

Fig. 19. Strengthening of geomagnetic jerks while those are in maximum activities of solar.

Such a mix of signals with different origins can generate apparent phase shift in tiny intervals and such a phase shift at the 11-years and 5.9-years signals is visible some times in the measurements. However, ultimately the signals return to the pure 11-years and pure 5.9-years signals and now by understanding of the real sources of the signals it is easier to discriminate signals at observed data.

The 5.9-years period of LOD signal has been detected accurately in experiments for example at *Duan (2015)* as quantitatively the 6-years signal, from $1962 \sim 2012$, using normal Morlet wavelet (NMWT) method combining wavelet packet and Fourier analysis technique, for the first time in both time and frequency domains. But in some experiments it is possible to appear phase shift in some time intervals as a deviation in the signals, however the signals trend return to full strength in the next cycles.

While solar activity peak is adequately large, the absolute variation of the Sun's magnetic field is prevailing factor and apparently may be reason to cancel 5.9-years signal as noted by *Duan (2015)* that:
"Gorshkov (2010) indicated that the $6 \sim 7$-year oscillation signals decreased abruptly in the 1990s and speculates it is due to the stronger signals in a $2 \sim 3$-year band cancelling out the $6 \sim 7$-year signals; while, Holme and de Viron (2013) further indicated that the "6-year oscillation" shows an apparent drop in amplitude in the 1990s (but this amplitude returns to full strength in the next cycle), and they interpreted it as the consequence."

And at epoch 1990, the solar activity is in its maximum and then the

solar activity is possible to cancel apparently the six-year signal. However, this phenomenon is possible too to be appeared by occurrence of the abrupt geomagnetic jerks related to Jovian planets alignments to cancel apparently 6-year signal from measurements and it is wonder that we observe Jupiter-Sun-Saturn lining up at epoch 1990.07.02 as the same 2–3 years stronger signal band covering smaller six years signal.

We have an increase in the additional activity of the Sun between 1830 and 1900 and in this interval we may discriminate easier the geomagnetic jerks dependent to the solar activity.

Nevanlinna (2004) shows secular variation of the Earth magnetic field in the interval 1830–1900 dependent to the solar activity oscillation and we see correlation between the solar activity and reported geomagnetic jerks in the considered interval in Fig. 20.

The alignment effect can't amplify direct absolute effect of the Sun's magnetic field oscillation through the Earth whereas that indirect absolute effect through the Jupiter can be amplified by Jovian alignment and then, such a difference is allowing us to discriminate between indirect absolute effect and direct absolute effect of the Sun's magnetic field which both have 11-years signals. On the other hand, observations verify that the indirect absolute and indirect orbital effect of the Sun's magnetic field are near together in size at the Earth measurements because that they are prevailing each other by small changes. For example, by equality of the indirect absolute and indirect orbital effects at epoch 1969, the reported geomagnetic jerk at epoch 1969 based on the Eq. (11) is almost 2 times stronger than our

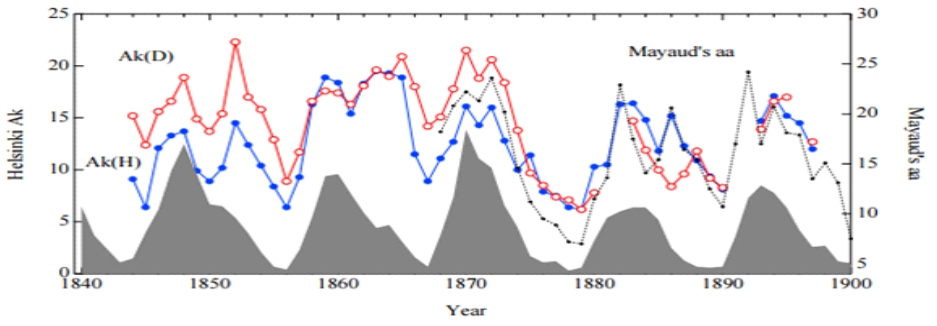

Fig. 20. Annual values of activity indices. Ak(H) (blue) and Ak(D) (red) are derived from the H- and D-components, respectively, using the Helsinki data reported by H. Nevanlinna.

calculated amplitude by Eqs. (7, 10) and then by Eq. (11) at epoch 1969 we have almost that:

$$(\partial B_{sun}/\partial t)_{orbit} \simeq (\partial B_{sun}/\partial t)_{absolute} \ . \tag{13}$$

And then every theory claiming to explain the solar cyclical activity is limited to this condition at Eq. (13) that averagely, the first time derivative of the Sun's absolute magnetic field through the Jupiter is near to its orbital variation at Jupiter position and this equality at Eq. (13) is showing that Sun's magnetic field absolute variation is a noticeable effect, not a partial change. For example, according to the Eq. (13) on the base of the orbital variation of the Sun's magnetic field at Jupiter position we deduce that the Sun's absolute magnetic field could to vary 25% at three years, when Jupiter moves from perihelion to the aphelion. By this noticeable variation of the Sun's absolute magnetic field we find that solar cyclical activity should be a large scale phenomenon at the Sun and such a great change in the magnetic field amplitude is almost impossible by planetary sources. Of course yet, the partial effect of the external sources is possible to influence on the generation of some sunspots at the Sun surface (*Ferris, 1969*). It is arresting that the Ferris is who he has discussed the electric current induction in the ionosphere and metallic sheets (*Ferris and Price, 1965; Ferris, 1973*).

On the other hand, when we see that the yearly change of the Sun's magnetic field is noticeable, then we can deduce a direct relation between the solar cyclical activity and cosmic radiation. Of course, the correlation of the solar activity and cosmic ray has been revealed by scientists before and we may refer to the *Balasubrahmanyan (1969)* and a newly analysis by *Barlyaeva et al. (2014)*. Strongly, emissions of the matter and electromagnetic fields from the Sun increase during high solar activity, making it harder for Galactic cosmic rays to reach Earth. Cosmic ray intensity is lower when the solar activity is high.

By the way, we have revealed here again that the Sun activity relevant to Sunspots number, approximately is proportional with first time derivative of the Sun's absolute magnetic field. But we can consider an accurate factor for solar activity with Aso that with assuming a constant C we have:

$$A = C\partial B_{sun}/\partial t. \tag{14}$$

We should notice that A is a pure factor for the solar activity value on the base of the solar magnetic field absolute variation and this parameter A

is in relation with the sunspots number approximately, because that *SSN* is not a regular parameter. The generation of the sunspots under the change of the Sun's magnetic field is an approximate phenomenon might be relevant to many conditions. It seems that when sunspots number is not small, the correlation of the *SSN* to the solar activity factor A is linear too. However, the scientist can calculate a phenomenological formula as a good approximation for such a correlation between parameter A and *SSN*.

Then on the base of the observations ("Extreme Space Weather Events". National Geophysical Data Center) we see that the solar activity oscillation peaks are conformal with peaks of the cosmic ray entrance amplitude. This phenomenon is showing us that solar activity may be reasonable by cosmic ray because that cosmic ray is relevant to the Sun's magnetic field amplitude, not its first time derivative. If Sun's magnetic field variation was reason of the oscillation of the cosmic ray, then cosmic ray oscillation phase should be conformal with Sun's magnetic field amplitude, not its time derivative.

The cosmic ray entrance oscillation phase is conformal with first time derivative of the Sun's magnetic field leading us to the side that the cosmic ray may be a wave with its wave period as the same period of solar activity and this is remembering us the theory of the sea of the electrons (*Dirac, 1930*) as a theoretical model of the vacuum as an infinite sea of particles with negative charges.

Such a correlation is so far possible to accept. But if the cosmic ray is not naturally a wave shape radiation then why the cosmic ray and solar activity are conformal in both period and phase?

The phase shift is possible to be tiny accidentally, but about the period of cosmic ray entrance and solar activity, conformal period is not accidental suppose if we consider Sun's magnetic field as a mathematical function then unity of the period means that the solar activity is not a partial change in the Sun's magnetic field suppose it should be the change of the whole Sun's magnetic field as a strong verification again for Eq. (14). In this shape the correlation of the solar activity to the cosmic ray amplitude is not a direct relation suppose direct relation is between the Sun's magnetic field and cosmic ray. But solar activity is conformal with magnetic field and magnetic field is conformal with cosmic way. Then solar activity is conformal with cosmic ray as a charming correlation. Then solar activity is whole change of the Sun's magnetic field and this shows that the Sun's magnetic field

reversal is a real phenomenon and Sun's magnetic field is really changing totally and it is not far to see that such a mechanism is impossible else by self consistent dynamo, in agreement with the Sun.

3.6. Long term decreasing trend of lod signals and geomagnetic secular variation

On the other hand, referring to the paper *Duan (2015)* we see the long term decreasing trend of LOD signals about 0.05 ms during the past 50 years and this decreasing trend should be relevant to the Earth magnetic field strength's decreasing trend during past 50 years and reason is that LOD signals are relevant to turbulent frictional CMB flows which their development amplitude is affected by the Earth's magnetic field amplitude. Inverse mechanism too is possible to do so that core flows are reason to explain the variation of the axial dipole as noted by *Holme and Buffett (2015)* that:
"Buffett (2014) has recently provided a model in which zonal toroidal motions are associated with the excitation of a zonal poloidal instability. This model is able to explain the broad variation of the axial dipole over the past 100 years, and also to explain feature of geomagnetic jerks that cannot be explained by purely torsional motions."

By comparison of the two different measurements for LOD signals and secular variation of the geomagnetic field we obtain a relation between secular variation of 5.9 years periodic LOD signal and geomagnetic field secular variation as visible at Fig. 21.

We see that the total intensity at Toronto has decreased 14%, from approximately 64 000 nT to 55 000 nT, during the last 160 years and long term trend amplitude of LOD signals decreases 0.05 ms during past 50 years which is near to 14% and too, we may refer to the axial dipole measurement of geomagnetic field in comparison with 5.9 years LOD signals secular variation visible at Fig. 22.

Schematically we see that it should be a relation between LOD variation and geomantic field and at (*Whaler and Holme, 2011*) it has been discussed before correlation between the axial dipole strength and flows in the outer core.

The geomagnetic field is an amplifier of external driven 5.9-years signal and this concerns to the reality that the currents are amplified and expanded

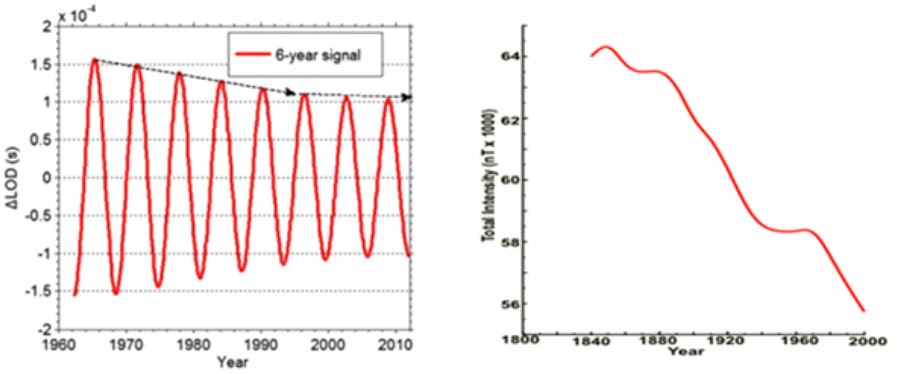

Fig. 21. Long term trend variation of the LOD signals versus Earth secular variation of magnetic field in Toronto.

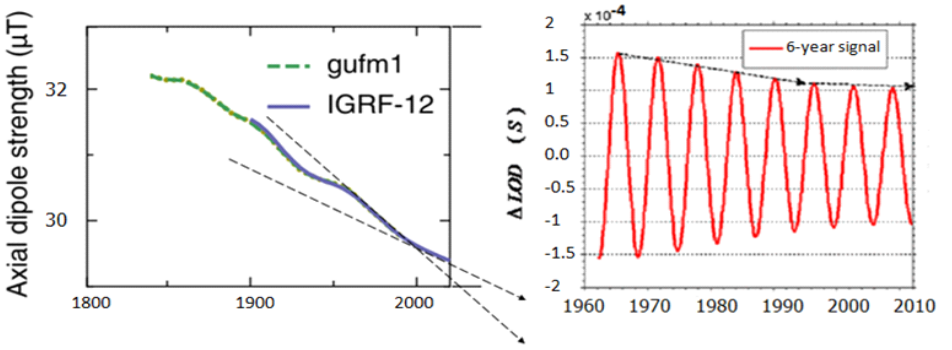

Fig. 22. Long-term damping trend of LOD signals versus strength of the axial dipole component of Earth's magnetic field from 1600 to 2020 (*McElhinny and McFadden, 1998*).

by Earth's magnetic field as a dynamo and similar to the alignments amplification effect at Eq. (6), here the geomagnetic field is too amplifier of the external driven LOD variation to generate observed amplified LOD variation as:

$$\Delta^* LOD = \eta B_{earth} \times \Delta LOD\,. \tag{15}$$

So that observed LOD variation is total amplitude of LOD variation, possible to observe and η is scale coefficient and now in a limited interval of time, possible to consider constant, the peak of external driven LOD variation, we result:

$$\Delta^* LOD = \mu B_{earth} \,. \tag{16}$$

So that μ is assumed as a constant and by this relation we obtain that:

$$\mu \frac{\partial B_{earth}}{\partial t} = \frac{\Delta^* LOD}{\Delta t} \,. \tag{17}$$

And this is visible at Fig. 22 and it is wonderful that LOD variation gradient is changed at the epoch 1992, exactly at the same date that geomagnetic field gradient is changed and in reality, the long term trend variation of 5.9-years LOD signal is unrelated to the AAM effect (*Duan, 2015*), Atmospheric Angular Momentum effect. Then it should exist an internal effect as a variation in generation of LOD signals by core flows.

In addition, at *Wilson et al. (2008)*, we see a spin-orbit coupling between the Sun and the Jovian planets to generate solar cycle and it seems that we are now near to resolve the question of the solar cyclical activity and ultimately we should remember the correlation between geomagnetic jerks and increase of the earthquakes number detected by *Gokhberg et al. (2016)* as a correlation between liquid motion of the Earth and earthquakes and variations in the Earth's length of day as a verification for core flows effecting on the Earth's spin.

4. Conclusions

It is visible that some of the Earth's interior partial core flows are external origin phenomena as the interplanetary driven partial quasidynamo. We have verified it on the base of the physics and experimental reports and we see that the oscillation of the external magnetic fields affect the planets interior too to generate partial effects similar to the geomagnetic jerks and LOD variations and gravity anomalies. We are seeing inevitably that the Jovian planets alignments are affecting on the amplification of these effects and effects are dependent too to the solar activity. The quasidynamo is not the self consistent hydromagnetic dynamo in dynamo region of the cosmic body. In the Earth‘s core it is a partial dynamo as a perturbation on the CMB. The Geodynamo in the Earth ‘s outer core is not of an external origin, but some variations, for example jerks, have external causes.

References

Abarca del Rio R., Gambis D., Salstein D. A., 2000: Interannual signals in length of day and atmospheric angular momentum. Ann. Geophys., **18**, 347–364, doi: 10.1007/s00585-000-0347-9.

Abarca del Rio R., Gambis D., Salstein D., Nelson P., Dai A., 2003: Solar activity and earth rotation variability. Journal of Geodynamics, **36**, 423–443, doi: 10.1016/S0264-3707(03)00060-7.

Alexandrescu M., Gibert D., Hulot G., Le Mouël J.-L., Saracco G., 1995: Detection of geomagnetic jerks using wavelet analysis. J. Geophys. Res., **100**, B7, 12557–12572, https://doi.org/10.1029/95JB00314.

Alexandrescu M., Gibert D., Hulot G., Le Mouël J.-L., Saracco G., 1996: Worldwide analysis of geomagnetic jerks. J. Geophys. Res., **101**, B10, 21975–21994, https://doi.org/10.1029/96JB01648.

Alfvén H., 1942: Existence of electromagnetic-hydrodynamic waves. Nature, **150**, 3805, 405–406, doi: 10.1038/150405d0.

Anderson J. D., Schubert G., Trimble V., Feldman M. R., 2015: Measurements of Newton's gravitational constant and the length of day. EPL (Europhysics Letters), **110**, 1, 10002, doi: 10.1209/0295-5075/110/10002.

Andrault D., Monteux J., Le Bars M., Samuel H., 2016: The deep Earth may not be cooling down. Earth and Planetary Science Letters, **443**, 195–203, doi: 10.1016/j.epsl.2016.03.020.

Ashour A. A., 1950: The induction of electric currents in a uniform circular disk. Quart. J. Mech. Appl. Math., **3**, 1, 119–128, https://doi.org/10.1093/qjmam/3.1.119.

Ashour A. A., Ferraro V. C. A., 1962: Induction of electric currents in a uniform anisotropie ionosphere. Nature, **196**, 4851, 260, doi: 10.1038/196260a0.

Ashour A. A., Ferraro V. C. A., 1964: The induction of electric currents in an anisotropic ionosphere with a belt of high conductivity running along the equator. J. Atmosph. Terrest. Phys., **26**, 4, 509–523, https://doi.org/10.1016/0021-9169(64)90030-3.

Ashour A. A., Price A. T., 1948: The induction of electric currents in a non-uniform ionosphere. Proc. Roy. Soc. A, **195**, 1041, 198–224, doi: 10.1098/rspa.1948.0114.

Aubert J., 2013: Flow throughout the Earth's core inverted from geomagnetic observations and numerical dynamo models. Geophysical Journal International, **192**, 2, 537–556, https://doi.org/10.1093/gji/ggs051.

Baker W. G., Martyn D. F., 1953: Electric currents in the Ionosphere. I. The Conductivity. Phil. Trans. R. Soc. A, **246**, 913, 281–294, doi: 10.1098/rsta.1953.0016.

Balasis G., Stelios M., Potirakis, Mandea M., 2016: Investigating Dynamical Complexity of Geomagnetic Jerks Using Various Entropy Measures. Frontiers in Earth Science, **4**, 71, doi: 10.3389/feart.2016.00071.

Balasubrahmanyan V. K., 1969: Solar activity and 11-year modulation of the cosmic rays. Solar physics, **7**, 1, 39–45.

Barlyaeva T., Bard E., Abarca-del-Rio R., 2014: Rotation of the Earth, solar activity and cosmic ray intensity. Ann. Geophys., **32**, 761–771, https://doi.org/10.5194/angeo-32-761-2014.

Biggin A. J., Steinberger B., Aubert J., Suttie N., Holme R., Torsvik T. H., van der Meer D. G., van Hinsbergen D. J. J., 2012: Possible links between long-term geomagnetic variations and whole-mantle convection processes. Nature Geoscience, **5**, 8, 526–533, http://dx.doi.org/10.1038/ngeo1521.

Bloxham J., Jackson A., 1991: Fluid flow near the surface of Earth's outer core. Rev. Geophys., **29**, 1, 97–120, https://doi.org/10.1029/90RG02470.

Bloxham J., Zatman S., Dumberry M., 2002: The origin of geomagnetic jerks. Nature, **420**, 6911, 65–68, https://doi.org/10.1038/nature01134.

Bloxham J., 1988: The determination of fluid flow at the core surface from geomagnetic observations. In: Mathematical Geophysics: A Survey of Recent Developments in Seismology and Geodynamics, edited by Vlaar N. J., Nolet G., Wortel M., Cloetingh S. A. P. L., chapter 9, 189–208, doi: 10.1007/978-94-009-2857-2_9.

Brown W. J., Mound J. E., Livermore P. W., 2013: Jerks abound: an analysis of geomagnetic observatory data from 1957 to 2008. Phys. Earth Planet. Inter., **223**, 62–76, https://doi.org/10.1016/j.pepi.2013.06.001.

Buffett B., 2014: Geomagnetic fluctuations reveal stable stratification at the top of the Earth's core. Nature, **507**, 7493, 484–487, doi: 10.1038/nature13122.

Buffett B., Knezek N., Holme R., 2016: Evidence for MAC waves at the top of Earth's core and implications for variations in length of day. Geophysical Journal International, **204**, 3, 1789–1800, https://doi.org/10.1093/gji/ggv552.

Bullard E. C., 1948: The secular change in the Earth's magnetic field. Geophysical supplements to the Monthly Notices of the Royal Astronomical Society, **5**, 7, 248-257, https://doi.org/10.1111/j.1365-246X.1948.tb02940.x.

Cafarella L., Meloni A., 1995: Evidence for geomagnetic jerk 1990 across Europe. Annals of Geophysics, **38**, 3-4, 451–455, https://doi.org/10.4401/ag-4106.

Chambodut A., Mandea M., 2005: Evidence for geomagnetic jerks in comprehensive models. Earth Planets Space, **57**, 2, 139–149, https://doi.org/10.1186/BF03352558.

Chambodut A., Eymin C., Mandea M., 2007: Geomagnetic jerks from Earth surface to the top of the core. Earth Planets Space, **59**, 7, 675–684, https://doi.org/10.1186/BF03352730.

Chulliat A., Maus S., 2014: Geomagnetic secular acceleration, jerks, and a localized standing wave at the core surface from 2000 to 2010. J. Geophys. Res. Solid Earth, **119**, 3, 1531–1543, doi: 10.1002/2013JB010604.

Chulliat A., Thébault E., Hulot G., 2010: Core field acceleration pulse as a common cause of the 2003 and 2007 geomagnetic jerks. Geophys. Res. Lett., **37**, 7, L07301, https://doi.org/10.1029/2009GL042019.

Courtillot V., Ducruix J., Le Mouël J.-L., 1978: Sur une accélération récente de la variation séculaire du champ magnétique terrestre. C. r. Acad. Sci. Paris, Série D, **287**, 1095–1098 (in French).

Courtillot V., Le Mouël J.-L., 1984: Geomagnetic secular variation impulses. Nature, **311**, 709–716, doi: 10.1038/311709a0.

Cowling T. G., 1932: The electrical conductivity of an ionized gas in the presence of a magnetic field. Mon. Not. R. Astron. Soc., **93**, 1, 90–97, https://doi.org/10.1093/mnras/93.1.90.

De Michelis P., Cafarella L., Meloni A., 1998: Worldwide character of the 1991 geomagnetic jerk. Geophysical Research Letters, **25**, 3, 377–380, https://doi.org/10.1029/98GL00001.

De Michelis P., Cafarella L., Meloni A., 2000: A global analysis of the 1991 geomagnetic jerk. Geophys. J. Int., **143**, 3, 545–556, https://doi.org/10.1046/j.1365-246X.2000.00208.x.

De Michelis P., Tozzi R., Meloni A., 2005: Geomagnetic jerks: observation and theoretical modeling. Memorie della Società Astronomica Italiana, **76**, 957–960.

Dirac P. A. M., 1930: A theory of electrons and protons. Proc. R. Soc. Lond. A. Royal Society Publishing, **126**, 801, 360–365, doi: 10.1098/rspa.1930.0013.

Duan P., Liu G., Liu L., Hu X., Hao X., Huang Y., Zhang Z., Wang B., 2015: Recovery of the 6-year signal in length of day and its long-term decreasing trend. Earth, Planets and Space, **67**, 161, https://doi.org/10.1186/s40623-015-0328-6.

Ducruix J., Gire C., Le Mouël J. L., 1983: Existence et caractère planétarie de la secousse de la variation séculaire en 1912–1913. C. r. Acad. Sci. Paris, **296**, Ser. II, 1419–1424, (in French).

Duka B., De Santis A., Mandea M., Isac A., Qamili, 2012: Geomagnetic jerks characterization via spectal analysis. Solid Earth, **3**, 1, 131–148, https://doi.org/10.5194/se-3-131-2012.

Dumberry M., 2010: Gravity variations induced by core flows. Geophys. J. Int., **180**, 2, 635–650, doi: 10.1111/j.1365-246X.2009.04437.x.

Dumberry M., Bloxham J., 2006: Azimuthal flows in the Earth's core and changes in length of day at millennial timescales. Geophys. J. Int., **165**, 1, 32–46, https://doi.org/10.1111/j.1365-246X.2006.02903.x.

Egedal J., 1947: The magnetic diurnal variation of the horizontal force near the magnetic equator. Terr. Magn. Atmos. Electr., **52**, 4, 449–451, https://doi.org/10.1029/TE052i004p00449.

Ferris G. A. J., Price A. T., 1965: Electric currents induced in an anisotropic ionosphere. Geophys. J. Roy. Astorn. Soc., **9**, 4, 285–308, https://doi.org/10.1111/j.1365-246X.1965.tb03888.x.

Ferris G. A. J., 1969: Planetary influences on sunspots. Journal of the British Astronomical Association, **79**, 385–388.

Ferris G. A. J., 1973: A note on electromagnetic induction in an infinite plane sheet with a circular hole. Q. J. Mechanics Appl. Math., **26**, 1, 19–21, https://doi.org/10.1093/qjmam/26.1.19.

Fink D. G., Christiansen D., 1989: Electronics engineers' handbook. McGraw-Hill, ISBN 9780070209824.

Gire C., Le Mouël J. L., Madden T., 1986: Motions at the core surface derived from SV data. Geophys. J. Royal Astr. Soc., **84**, 1, 1–29, https://doi.org/10.1111/j.1365-246X.1986.tb04342.x.

Gokhberg M. B., Olshanskaya E. V., Chkhetiani O. G., 2016: Correlation between large-scale motions in the liquid core of the earth and geomagnetic jerks, and variations in the earth's length of day. Dokl. Earth Sci., **467**, 1, 280–283, doi: 10.1134/S1028334X1603003X.

Golovkov V. P., Zvereva T. I., Simonyan A. O., 1989: Common features and differences between "jerks" of 1947, 1958 and 1969. Geophys. Astrophys. Fluid Dyn., **49**, 81–96, https://doi.org/10.1080/03091928908243465.

Gorshkov V. L., 2010: Study of the interannual variations of the Earths rotation. Sol. Syst. Res., **44**, 6, 487–497.

Gu Z. N., 1990: A relation between solar activity and the earth rotation. Earth, Moon, and Planets, **48**, 3, 189–195, https://doi.org/10.1007/BF00113856.

Holme R., 2007: Large-scale flow in the core. In: Treatise on Geophysics, **8**, 4, 107–130, Eds. Schubert G., Olson P., Elsevier, Amsterdam, doi: 10.1016/B978-044452748-6.00127-9.

Holme R., Buffett B., 2015: Secular variation and core-flow modelling with stable stratification at the top of the core. EGU General assembly 2015, held 12–17 April, 2015 in Vienna, Austria. Id.4897.

Holme R., de Viron O., 2005: Geomagnetic jerks and a high-resolution length-of-day profile for core studies. Geophys. J. Int., **160**, 2, 435–439, https://doi.org/10.1111/j.1365-246X.2004.02510.x.

Holme R., de Viron O., 2013: Characterization and implications of intradecadal variations in length of day. Nature, **499**, 7457, 202–204, doi: 10.1038/nature12282.

Höpfner J., 1998: Seasonal variations in length of day and atmospheric angular momentum. Geophys. J. Int., **135**, 2, 407–437, https://doi.org/10.1046/j.1365-246X.1998.00648.x.

Korte M., Mandea M., Matzka J., 2009: A historical declination curve for Munich from different data sources. Phys. Earth Planet. Inter., **177**, 3-4, 161–172, https://doi.org/10.1016/j.pepi.2009.08.005.

Kotzé P. B., Korte M., 2016: Morphology of the southern African geomagnetic field derived from observatory and repeat station survey observations: 2005–2014. Earth Planets Space, **68**, 23, https://doi.org/10.1186/s40623-016-0403-7.

Le Huy M., Alexandrescu M., Hulot G., Le Mouël J.-L., 1998: On the characteristics of successive geomagnetic jerks. Earth, Planets and Space, **50**, 9, 723–732, doi: 10.1186/BF03352165.

Le Mouël J.-L., Ducruix J., Duyen C., 1982: The world wide character of the 1969–1970 impulse of the secular acceleration rate. Phys. Earth Planet. Inter., **28**, 4, 337–350, https://doi.org/10.1016/0031-9201(82)90090-5.

Le Mouël J.-L., Blanter E., Shnirman M., Courtillot V., 2010: Solar forcing of the semi-annual variation of length-of-day. Geophys. Res. Lett., **37**, 15, L15307, https://doi.org/10.1029/2010GL043185.

Liao D. C., Greiner-Mai H., 1999: A new ΔLOD series in monthly intervals (1892.0–1997.0) and its comparison with other geophysical results. J. Geodesy, **73**, 9, 466–477, doi: 10.1007/PL00004002.

Ma L. H., 2007: Decadal modulation in length-of-day variations from solar activity: a wavelet approach. International Conference on Wavelet Analysis and Pattern Recognition Year: 2007, **4**, 1679–1682.

Ma L. H., 2015: Possible influence of the 11-year solar cycle on length-of-day change. Stud. Geophys. Geod., **59**, 3, 477–488, https://doi.org/10.1007/s11200-014-1040-x.

Macmillan S., 1996: A geomagnetic jerk for the early 1990s. Earth Planet. Sci. Lett., **137**, 1-4, 189–192, https://doi.org/10.1016/0012-821X(95)00214-W.

Malin S. R. C., Hodder B. M., 1982: Was the 1970 geomagnetic jerk of internal or external origin? Nature, **296**, 726–728, doi: 10.1038/296726a0.

Malin S. R. C., Hodder B. M., Barraclough D. R., 1983: Geomagnetic secular variation: A jerk in 1970. In: Cardús, J. O. (Ed.), Contribuciones Científicas para Conmemorar et 75 Aniversario del Observatorio del Ebro. Publ. Obs. Ebro, Memoria, **14**, 239–256.

Mandea M., Bellanger E., Le Mouël J.-L., 2000: A geomagnetic jerk for the end of the 20th century? Earth Planet. Sci. Lett., **183**, 3-4, 369–373, https://doi.org/10.1016/S0012-821X(00)00284-3.

Mandea M., Holme R., Pais A., Pinheiro K., Jackson A., Verbanac G., 2010: Geomagnetic Jerks: Rapid Core Field Variations and Core Dynamics. Space Science Reviews, **155**, 1-4, 147–175, doi: 10.1007/s11214-010-9663-x.

Mandea M., Panet I., Lesur V., de Viron O., Diament M., Le Mouël J.-L., 2012: Recent changes of the earth's core derived from satellite observations of magnetic and gravity fields. Proc. Natl. Acad. Sci. USA, **109**, 47, 19129–19133, https://doi.org/10.1073/pnas.1207346109.

Martyn D. F., 1948: Electric conductivity of the ionospheric D-region. Nature, **162**, 142–143, doi: 10.1038/162142a0.

Martyn D. F., 1949: Lunar variations in the principal ionospheric Regions. Nature, **163**, 685, doi: 10.1038/163034a0.

Matzka J., Chulliat A., Mandea M., Finlay Ch., Qamili E., 2010: Geomagnetic Observations for Main Field Studies: from Ground to Space. Space Sci. Reviews, **155**, 1–4, 29–64, doi: 10.1007/s11214-010-9693-4.

McElhinny M. W., McFadden P. L., 1998: Paleomagnetism: Continents and Oceans. Academic Press. ISBN 978-0124833555.

Mound J. E., Buffett B. A., 2003: Interannual oscillations in length of day: implications for the structure of the mantle and core. J. Geophys. Res., **108**, B7, 1–17, https://doi.org/10.1029/2002JB002054.

Mound J., Buffett B., 2006: Detection of a gravitational oscillation in length-of-day. Earth Planet. Sci. Lett., **243**, 3-4, 383–389, doi: 10.1016/j.epsl.2006.01.043.

Nakada M., 2009: Earth's rotational variations by electromagnetic coupling due to core surface flow on a timescale of ∼1 yr for geomagnetic jerk. Geophys. J. Int., **179**, 1, 521–535, https://doi.org/10.1111/j.1365-246X.2009.04256.x.

Nevanlinna H., 2004: Results of the Helsinki magnetic observatory 1844–1912. Annales Geophysicae, **22**, 5, 1691–1704, doi: 10.5194/angeo-22-1691-2004.

Newitt L. R., Dawson E., 1984: Secular variation in North America during historical times. Geoph. J. Int., **78**, 1, 277–289, https://doi.org/10.1111/j.1365-246X.1984.tb06484.x.

Nipher F. E., 1916: Gravitation and electrical action. Trans. Acad. Sci. St. Louis, 163–175.

Nipher F. E., 1917: Gravitational Repulsion. Trans. Acad. Sci., St. Louis, **XXIII**, 5.

Nipher F. E., 1918: Can Electricity Destroy Gravitation? Electric Experimenter.

Nipher F. E., 1920: New evidence of a relation between gravitation and electrical action and of local charges in the electrical potential of the Earth. Trans. Acad. Sci. of St. Louis, **XXVII**, 383–387.

Olsen N., Mandea M., 2007: Investigation of a secular variation impulse using satellite data: the 2003 geomagnetic jerk. Earth Planet. Sci. Lett., **255**, 1-2, 94–105, https://doi.org/10.1016/j.epsl.2006.12.008.

Pinheiro K., Travassos J. M., 2010: Impulses of the geomagnetic secular variation at Vassouras magnetic observatory detected by wavelet analysis. Revista Brasileira de Geofisica, **28**, 1, 37–46, http://dx.doi.org/10.1590/S0102-261X201000010000.

Podkletnov E., Nieminen R., 1992: A possibility of gravitational force shielding by bulk $YBa_2Cu_3O_{7-x}$ superconductor. Physica C, **203**, 3-4, 441–444, https://doi.org/10.1016/0921-4534(92)90055-H.

Podkletnov E. E., Vuorinen P. T., 1996: Gravitation shielding properties of composite bulk $YBa_2Cu_3O_{7-x}$ superconductor below 70 K under electromatic field. Journal of Applied Physics D. Retrieved April 29, 2014.

Podkletnov E., 1997: Weak gravitation shielding properties of composite bulk $YBa_2Cu_3O_{7-x}$ superconductor below 70 K under e.m. field. Retrieved April 29, 2014. This is believed to be substantially the same paper accepted for publication in 1996 by Journal of Physics D which was later withdrawn by the author.

Price A. T., 1949: The Induction of Electric Currents in Non-uniform Thin Sheets and Shells. Quart. J. Mech., **2**, 3, 283-310.

Price A. T., Ferris G. A. J., 1962: A resonance property of ionosphere duo to its anisotropic conductivity. Nature, **196**, 258–260, doi: 10.1038/196258b0.

Qamili E., De Santis A., Isac A., Mandea M., Duka B., Simonyan A., 2013: Geomagnetic jerks chaotic fluctuation of the earth's magnetic field. Geochem. Geophys. Geosyst., **14**, 4, 839–850, https://doi.org/10.1029/2012GC004398.

Ridley V. A., Holme R., 2016: Modeling the Jovian magnetic field and its secular variation using all available magnetic field observations. J. Geophys. Res. Planets, **121**, 3, 309–337, https://doi.org/10.1002/2015JE004951.

Schlamminger S., Gundlach J. H., Newman R. D., 2015: Recent measurements of the gravitational constant as a function of time. Phys. Rev. D, **91**, 121101.

Schuster A., 1889: The diurnal variation of terrestrial magnetism. Phil. Trans. Roy. Soc. London Ser. A., **180**, 467–518.

Schuster A., 1908: The diurnal variation of terrestrial magnetism. Phil. Trans. Roy. Soc. London Ser. A., **208**, 163–204.

Silva L., Hulot G., 2012: Investigating the 2003 geomagnetic jerk by simultaneous inversion of the secular variation and acceleration for both the core flow and its acceleration. Physics of the Earth and Planetary Interiors, **198–199**, 28–50.

Silva L., Jackson L., Mound J., 2012: Assessing the importance and expression of the 6 year geomagnetic oscillation. Journal of Geophysical Research: Solid Earth, **117**, B10, 2156–2202.

Stewart B., 1882: Terrestrial Magnetism. In: Baynes T. S. and Smith W. R., Eds., Encyclopedia Britannica, 9th Edition, **16**, A and C Black, Edinburgh, 159–184.

Tozzi R., De Michelis P., Meloni A., 2009: Geomagnetic jerks in the polar regions. Geophysical Research Letters, **36**, 15, L15304, doi: 10.1029/2009GL039359.

Very F. W., 1919: On Nipher gravitational experiment and anomalies of the Moon's motion. Popular Astronomy, **27**, 158.

Vondrák J., Burša M., 1977: The rotation of the earth between 1955.5 and 1976.5. Stud. Geophys. Geod., **21**, 2, 107–117.

Voorhies C. V., 1986: Steady flows at the top of Earth's core derived from geomagnetic field models. J. Geophys. Res., **91**, B12, 12444–12466, https://doi.org/10.1029/JB091iB12p12444.

Voorhies C. V., 1993: Geomagnetic estimates of steady surficial core flow and flux diffusion: unexpected geodynamo experiments. In: Dynamics of Earth's Deep Interior and Earth Rotation. Geophys. Monogr. Ser. AGU, Washington D. C., 113–125, https://doi.org/10.1029/GM072p0113.

Voorhies C. V., 1995: Time-varying fluid flow at the top of Earth's core derived from Definitive Geomagnetic Reference Field models. J. Geophys. Res., **100**, B6, 10029–10039, https://doi.org/10.1029/95JB00863.

Voorhies C. V., 2004: Narrow-scale flow and a weak field by the top of Earth's core: Evidence from Ørsted, Magsat, and secular variation. J. Geophys. Res., **109**, B03106, https://doi.org/10.1029/2003JB002833.

Vukcevic M. A., 2014: Evidence of length of day (LOD) bidecadal variability concurrent with the solar magnetic cycles. [Research Report] STAR, HAL Id: hal-01071375, https://hal.archives-ouvertes.fr/hal-01071375v2.

Wardinski I., 2014: Core surface flow models from decadal and subdecadal secular variation of the main geomagnetic field. Scientific Technical Report, http://www.diss.fu-berlin.de/diss/receive/FUDISS_thesis_000000001688.

Wardinski I., Holme R., 2003: Decadal and Subdecadal Secular Variation of Main Geomagnetic Field. In: Reigber C., Lühr H., Schwintzer P. (Eds.): First CHAMP Mission Results for Gravity, Magnetic and Atmospheric Studies. Springer, Berlin, Heidelberg.

Whaler K. A., Holme R., 2011: The axial dipole strength and flow in the outer core. Physics of the Earth and Planetary Interiors. **188**, 3-4, 235–246, doi: 10.1016/j.pepi.2011.07.006.

Wilson I. R., Carter B. D., Waite I. A., 2008: Does a spin-orbit coupling between the Sun and the Jovian planets govern the solar cycle? Publications of the Astronomical Society of Australia, **25**, 2, 85–93, doi: 10.1071/AS06018.

DE GRUYTER
OPEN

Contributions to Geophysics and Geodesy Vol. 48/1, 2018 (75–112)

A new original conception in rock magnetism, paleomagnetism and geomagnetism: An origin of the reversed magnetization of rocks on Earth

Oto ORLICKÝ

Private scientist, Damborského 6, 841 01 Bratislava, Slovakia, oto.orlicky@gmail.com

Abstract: So far the field-reversal theory has been accepted to account for the reversed remanent magnetization (RM) of rocks on the Earth. *Orlický (2014)* revealed a frequent occurrence of the antiferromagnetic (AFM) Fe-Ti oxides in the rocks. Now I have renamed these minerals as the Fe-Ti ferrimagnetic-antiferromagnetic chemical phases (Fe-Ti FriM-AFM ChPs). They may have either cubic spinel, or tetragonal spinel symmetry, respectively. They behave as the Fe-Ti polycrystalline materials. These Fe-Ti FriM-AFM ChPs are the two sublattice A and B ChPs, with some specific magnetic behaviour. The titanomagnetite (Ti-Mt, Curie temperature, $T_C = 230\,^{\circ}C$; FriM alignment) and the titanomaghemite (Ti-Mgh, Néel temperature, $T_N = 450\,^{\circ}C$; AFM alignment) containing rocks have been identified as the representants of the the Fe-Ti FriM-AFM cubic spinel ChPs. The interactions with the magnetizing field, with the Weis molecular fields (Weiss-Heisenberg forces) have generated the reversally oriented internal field. The reversally oriented spontaneous magnetization has arosen in the rock. This internal field has been identified as the most important phenomenon leading to the production of the reversally oriented magnetization in the Fe-Ti FriM-AFM ChPs containing rocks. The equations expressing the magnetic behaviour of the magnetic susceptibility (κ) of rocks versus temperature have been derived. The Fe-Ti FriM-AFM cubic spinel can undergone the transition in favour of the Fe-Ti FriM-AFM tetragonal spinel in the rocks, due to a change of the thermodynamic conditions in nature. The reversed RM has supposed been inparted from the Fe-Ti FriM-AFM cubic spinel during this alteration-transition processess. Such tetragonal spinel is more stable and it is able to survive in the rocks in nature. The results of laboratory magnetization of the selected groupings of rocks have been presented below. The basic laboratory methods for the detection of the magnetic behaviour of the Fe-Ti FriM-AFM ChPs containing rocks are described as well. The presented results have shown that we do not need to apply the field reversal theory, because I have revealed the realistic mechanism which is able to generate the reversed RM of rocks under a presence of the normal geomagnetic field.

Key words: The Fe-Ti FriM-AFM cubic and tetragonal spinels, exchange interactions, Weiss molecular field, the reversed magnetization of rocks

doi: 10.2478/congeo-2018-0003

1. Introduction

The most frequent magnetic minerals in the rocks are the Fe-Ti solid solutions, titanomagnetites (Ti-Mt-es, $Fe_{3-x}Ti_xO_4$) and titanohematites (Ti-hem-es, $Fe_{2-x}Ti_xO_3$). The Fe-Ti magnetic minerals have been largely studied by many authors as the carriers of magnetic and paleomagnetic properties of rocks. Many specialists have believed that these minerals are very stable and are able to survive from their origin up to the present in an unchanged state in nature. I have found that most of the magnetic minerals have undergone dramatic transformation not only in chemical composition but also structurally.

I revealed a very frequent occurrence of the Fe-Ti antiferromagnetic (AFM) phases in the rocks (*Orlický, 2014*). They could be now designated as the two sublattice containing polycrystalline chemical phases (ChPs). In such ChPs the ferrimagnetic-antiferromagnetic (FriM-AFM) alignment exists and they have produced a negative exchange interaction between the two sublattices (it was anticipated by *Néel (1948)*, in (*Goodenough, 1963*).

The Fe-Ti FriM-AFM phases originated nearly in each type of rock on the Earth. Some of them have been preserved, but most of them were either decayed or transformed to the other type of AFM phase, depending on thermodynamic conditions. I discovered the Fe-Ti FriM-AFM ChPs in about 288 samples from 78 localities of volcanic rocks and in about 346 samples of the sedimentary rocks (*Orlický, 2014*).

The two basic phenomena: the Fe-Ti FriM-AFM ChPs in the rock, the local molecular fields with so called Weiss-Heisenberg forces (*Néel, 1971*) are decisive for the acquirement of the reversed magnetization in the rock. It is a completely new field in paleomagneetic research, because such category of knowledge is missing completely in standard literature.

2. A review about the self-reversal origin of rocks

2.1. The results of rocks having the self-reversed origin of RM

I have completed my results with those of available works of other authors. A dominant topic is a solution of an of origin of the reversed RM of rocks.

2.2. The rocks containing the Hematite-Ilmenite solid solutions

Many scientific papers and books were devoted to the self-reversal origin of the reversed RM of the Haruna rhyodacite pumice, erupted in Japan about 1420 years ago (*Nagata, 1952; Ishikawa and Syono, 1963; Stacey and Banerjee, 1974; Orlický et al., 2000; Orlický and Funaki, 2000a; 2000b; 2001; Ozima and Funaki, 2001; Orlický, 2011*) and Late Brunhes dacite from Mt. Natib, from Philippines (*Kennedy, 1981*) and dacite and dacite pumice pyroclastics having ages between 9000–10000 years, from Mt. Shasta, California (*Lawson et al., 1987*), the pyroclastics and andesitic pumice from the disastrous 1985 eruption of the Nevado del Ruiz, Colombia (*Heller et al., 1986; Haag et al., 1990*), dacite pumice from the 1991 Pinatubo eruption from Philippines (*Ozima et al., 1992; Hoffmann and Fehr, 1996; Bina et al., 1999; Goguitchaichvili and Prévot, 2000*), and the dacite ash from the 1991 Pinatubo eruption from Philippines (*Orlický and Funaki, 2001*), the synthetic hematite – ilmenite solutions (*Carmichael, 1961; Hoffman, 1975; Lawson et al., 1981; Nord and Lawson, 1989; 1992; Westcot-Lewis and Parry, 1971*).

The rhyo-dacite pumice from Haruna volcano and from Pinatubo volcano contains the hem-ilm with a composition of ilm_{45} to ilm_{75}. Many petrographic types of acidic, intermediate and basic volcanic rocks contain the hem-ilm-es with ilm composition of ilm_5–ilm_{12} to ilm_{15}–ilm_{25}. According to *Nagata et al. (1951)* the reversed RM of Haruna rhyodacite pumice resulted from the hem-ilm phase acquiring a self-reversed thermoremanent magnetization (TRM). The magnetite-ulvöspinel (Mag-Usp) is also in these rocks. The ratio of the Mag-Usp to Hem-Ilm was approximately 100 to 1 in the Haruna rocks (*Nagata et al., 1951; Uyeda, 1958*). For these rocks it is typical that their magnetic properties differ from sample to sample. Some samples have shown only normal polarity, while other samples showed only reversed RM, due to the different state of Fe-Ti alterations. The authors ascribed the dominant remanence signal to the hem-ilm phase. *Uyeda (1958), Ishikawa and Syono (1963)* found that the acquisition of the self-reversed TRM requires that the bulk of the ferrimagnetic sample be ordered and that it needs to contain a second phase. They called it as the x phase. They proposed the antiphase-contact-two phase model to explain the self-reversal TRM of the rocks of Haruna volcano. The striking result is that the reverse TRM exists in the intermediate state and it is not found in either the fully

ordered or fully disordered state. I was very surprised that such negligable amount of the ilmenite-hematite grains – 1 grain among of 100 Ti-Mt grains is able to generate the relatively intense reversed RM in the rock.

I found the AFMP in these rhyodacites (*Orlický, 2011*). The Néel temperature of this phase is $T_N = 420\,^{\circ}C$ and there is also the hem-ilm of $T_C = 230\,^{\circ}C$, and Ti-Mt of $T_C = 520\,^{\circ}C$) in the rock. The AFM phase corresponds to the anonymous x phase, which was predicted by *Ishikawa and Syono (1963)* in the Haruna dacite.

2.3. The rocks containing the titanomaghemites

Havard and Lewis (1965) studied the basalt lava flows from India which showed self-reversed RM during laboratory magnetization of samples. *Ozima and Ozima (1967)* studied 8 samples of dredged submarine basalts. Three samples showed self-reversed TRM when they were heated to 300 °C during 30 minutes and cooled to room temperature in geomagnetic field. Similar results were achieved by *Ozima and Larson (1968).* Only normal TRM was induced after repeated magnetization in the sample. The authors suggested some models and mechanism of self-reversed magnetization of the rocks, based on either magnetostatic or exchange interactions of the two Fe-Ti phases, differing by Curie temperatures. *Krása et al. (2005)* studied the basalt samples from Olby (France) and Vogelsberg (Germany). During acquisition of a thermoremanence the two phases are magnetically coupled, leading to a remanent magnetization of the two Curie temperature phases which is antiparallel to the applied external magnetic field. They suggested coupling of the two phases by magnetostatic interaction which resulted in the self-reversal origin of RM in the rock. *Heller and Petersen (1982)* studied the self-reversal of young basalts from Olby and La Shamp area, from Massif Central, France. *Doubrovine and Tarduno (2004)* reported on partial and complete self-reversal due to N-type behaviour in some oceanic basalts. They suggested that this magnetization is carried by the Ti-Mgh Fe-Ti associations. They detected a normal PTRM until 250–275 °C, followed by a component antiparallel self-reversed to the normal applied magnetic field, between 275–350 °C. At higher temperatures they again observed the acquisition of a PTRM oriented parallel to the applied field. No self-reversal of the same sample was observed in repeated

runs. Hemoilmenite, if present, would retain its self-reversing properties after such thermal treatment. *Pan et al. (2006)* studied the Thellier-Coe paleointensity of Al-substituted Ti-Mt-es of the Neogene Hannuoba basalts from northern China. The laboratory experiments were done in argon gas to prevent oxidation of Fe-Ti oxides. The samples acquired the thermoremanence with the antiparallel direction to the external field, leading to intensity decreases. They explained the decrease of PTRM as being due to partially self-reversed thermoremanence carried by Al-substituted Ti-Mt and newly formed magnetite. *Schult (1971)* pointed out that the titanomaghemites undergo self-reversal by ionic reordering. According to *Schult (1968)* if one assumes that the vacancies are all on the B-site the magnetization of the B-sublattice becomes smaller with oxidation and it is possible that for a certain composition the spontaneous magnetization of B-sublattice equals that of the A-sublattice or becomes even less. *Carvallo et al. (2010)* studied the X-Ray Magnetic Circular Dichroism (XMCD) spectra of magnetite (Mt), maghemite (Mgh) and natural titanomaghemite (Ti-Mgh-te). For Ti-Mgh-te, all features of the XMCD spectrum reverse with temperature, indicating that the magnetization of each individual site is reversed. The intensities of the three peaks (A,B,C) remain almost in the same ratio for XMCD at high and low temperatures. This indicates that there are the antiferromagnetic magnetic interactions between octahedral and tetrahedral sites. In Ti-Mgh-te with a high Ti content, Fe^{2+} ions are present both in tetrahedral and octahedral sites, but at room temperature, the ratio of intensities of peak A and B is lower than at low temperature (20 K). One even observes that peak A is dominating the pre-edge XMCD signal. This can indicate that there is a high magnetic disorder of Fe^{2+} on octahedral sites at high temperatures, i.e. the magnetic moments are not aligned along the direction of external magnetic field. At low temperature, the magnetic moments from Fe^{2+} on tetrahedral sites are more ordered and the moments of Fe^{2+} on tetrahedral sites overcome the moments of Fe^{2+} on octahedral sites, probably causing the magnetization to reverse. The reversal of these two structures with temperature indicates that the dominant subnetworks are reversed at high temperature, the magnetic moment of the octahedral subnetwork is larger than that of the tetrahedral magnetic moment, and at low temperature the tetrahedral magnetic moment dominates.

A distinguished category of rocks are those having dominantly the mag-

netite. *Balsley and Buddington (1954)* discovered a correlation between magnetic Fe-Ti minerals and that of the polarity of RM of metamorphic rocks in the Adirondack Mountains. The rocks of reversed polarity invariably contained hematite-ilmenite, the rocks of normal polarity contained magnetite. These mineralogical differences indicate self-reversal and also indicate that the geomagnetic field was not reversing its polarity during the long interval when these rocks were acquiring their RM. *Orlický (2002b; 2006; 2010a; 2010b).* I revealed that, if there are dominantly Ti-rich quasi homogeneous titanomagnetites (Ti-Mt-es), or magnetites in the rocks, they have always normal polarity of RM, in continental and submarine volcanics (*Orlický, 2010a; 2010b*).

According to *Stacey and Banerjee (1974)* even in the 1950's the reality of field-reversal theory was not proven. The above presented ideas about the self-reversed magnetization of rocks have not fully solved the origin of the reversed magnetization of the rocks in general. Many authors have solved the problem of the decrease of magnetic characteristics in submarine basalts, but the origin of the reversed RM of rocks was not a subject of their interest. The transformation of titanomagnetite to titanomaghemite (maghemitization of Ti-Mt oxides) due to the low-temperature oxidation were solved e.g. (*Irving, 1970; Kelso et al., 1996; Kirkpatrick, 1979; Lowrie et al., 1973; Marshall and Cox, 1972; Petersen, 1979; Petersen et al., 1979; Zhou et al., 2001; Xu et al., 1997*).

3. Experimental part

3.1. A temperature oxidation of Fe-Ti spinels and ilmenite

Oxidation of titanomagnetite: Cubic Ti-Mt (Usp-Mt) can be oxidized by two mechanisms (*Lindsley, 1991*): (a) oxidation at low pressure and below 600 °C to yield cation-deficient spinels of the metastable titanomaghemite series (Usp-Mt-γ-Fe_2O_3, which in some cases may then subsequently convert to members of the Hem-Ilm series; (b) Oxidation at low to moderate pressures and above 600 °C with the direct formation of Ilm-Hem. Distinct textural stages of oxidation are recognized and have been classified as follows (the prefix C distinguished primary cubic phases from primary

ilmenite-rhombohedral): C1 stage: Optically homogeneous Usp-rich magnetite solid solutions; C2 stage: Magnetite enriched solid solutions with a small number of exsolved ilmenite lamellae parallel to 111; C3 stage: Ti-poor magnetite with densely crowded exsolved ilmenite lamellae parallel to 111 of the host. Typical reactions that apply to the C2 and C3 assemblages, with the partial and more complete oxidation ulvöspinel are as follows:

$$\mathrm{C2}: 6\mathrm{Fe_2TiO_4} + \mathrm{O_2} = 6\mathrm{FeTiO_3} + 2\mathrm{Fe_3O_4}; \tag{1}$$

$$\mathrm{C3}: 4\mathrm{Fe_2TiO_4} + \mathrm{O_2} = 4\mathrm{FeTiO_3} + 2\mathrm{Fe_2O_3}; \tag{2}$$

The previous mineralogical composition of rock has been enriched by higher content of magnetite (Fe_3O_4) after an oxidation of ulvöspinel and the rock became more ferrimagnetic. This process has taken place under the influence of the normally oriented geomagnetic field in the nature. The level of magnetic susceptibility of rock will be enhanced and the direction of RM of rock will be changed. If the RM was previously of a reversed nature, it will become more positive; (a mineral enriched with higher concentration of Fe_3O_4 in the rock would acquire the positive RM). Its intensity and the direction will depend on a portion of transformed Fe-Ti material during the above described oxidation.

3.2. An explanation of $1/\kappa$ curves presented in the article

According to *Néel (1971)* the magnetic susceptibility of magnetic minerals of rocks could reflect the effect of magnetic arrangement of active cations and the internal field in the minerals. The exchange interactions between their magnetic moments M_A and M_B will be actual. As an example, the author considered an alloy composed of two kinds of randomly distributed atoms A and B. *Néel (1971)* introduced local molecular field. Weiss' hypothesis amounts to writing that the energy E_c of the system of A and B atoms is expressed in the form:

$$E_c = -\frac{1}{2n}(J_A + J_B)^2 \tag{3}$$

where J_A and J_B denote the magnetizations of the A and B atoms respectively. Actually, since their energy is the sum of the contributions made by

pairs of close-neighbour atoms, three types of exchange interactions $A-A$, $A-B$, and $B-B$ are involved in the process, so we should rather write:

$$E_c = -\frac{1}{2}(n_{AA}J_A^2 + 2n_{AB}J_AJ_B + n_{BB}J_B^2) \tag{4}$$

Then will be actual the introduced local molecular fields, $h_A = n_{AA}J_A + n_{AB}J_B$, and $h_B = n_{AB}J_A + n_{BB}J_B$, acting on the A and B atoms respectively. The author has showed that the susceptibility χ of an alloy containing proportions P and Q of A and B atoms, with Curie constants C_A and C_B, was expressed by:

$$\chi = \frac{T(PC_A + QC_B) - PQC_AC_B(n_{AA} + n_{BB} - 2n_{AB})}{T^2 - T(Pn_{AA}C_A + Qn_{BB}C_B) + PQC_AC_B(n_{AA}n_{BB} - n_{AB^2})} \tag{5}$$

Instead of being represented by a straight line, the temperature dependence of the reciprocal susceptibility $1/\kappa$ was now represented by a hyperbola. It means that the shape of temperature dependence of the κ or $1/\kappa$ curves is in relation with the proportions of active atoms of A and B sublattices, their Curie constants C_A and C_B, portions of other quantities, and also with the forces of three types $n_{AA}J_A$, $n_{AB}J_AJ_B$ and $n_{BB}J_B$ exchange interactions in the two sublattice system. The most intense is the $A-B$ interaction. The antiferromagnetics are characterized by the critical temperature – Néel temperature T_N. After heating beyond T_N the partial or total decomposition of the AFM phase might occure. A short-range order (a tendency of atomic moments to be coupled, which are near each other in the lattice), or long-range order (a tendency of atomic moments to be coupled in the lattice, over many lattice spacings – which is responsible for ferromagnetism and which disappears at T_C).

4. The effective methodical procedures

The magnetic behaviour of the Fe-Ti FriM-AFM chemical phases (ChPs) can be studied by the: 1) temperature dependent measurements of magnetic susceptibiliy (κ) of a powdered sample during continual heating (Curie temperature measurements), 2) temperature dependent measurements of κ of compact sample during stepwise heating, 3) temperature dependent partial

thermoremanent magnetization (PTRM) and demagnetization of compact sample during stepwise heating. The Fe-Ti FriM-AFM ChPs are characterized by a Néel temperature (T_N, in the Fe-Ti FriM-AFM ChPs cubic spinels at about 450 °C). The results of these methods have shown that their characteristics and the features of the curves have reflected the two sublattice (A and B) composition. The temperature dependent behaviour of κ and the magnetization of the two sublattice FriM-AFM systems are governed by their Curie constants C_A and C_B, proportions of their quantities, and also with the forces of three types $n_{AA}J_A$, $n_{AB}J_AJ_B$ and $n_{BB}J_B$ exchange interactions. The most intense is the $A-B$ interaction. We can say that their behaviour has reflected the principles of the two sublattice FriM-AFM alignment, respecting the the principles of the local molecualar field, according to *Néel (1971)*.

4.1. The measurements of Curie temperatures and the detection of the Fe-Ti minerals in the rocks

The analysis of the magnetic minerals of rocks was dominantly done by the Curie temperature measurements in air. The first prototype of CS-1 device combined with the KLY-2 susceptibilitymeter was used (the CS-1 device was originally suggested and dominant part of the instrument was also constructed by the author of this article (*Orlický, 1990*). Several samples were measured in argon atmosphere by Tiu Elbra, Geological Institute of Czech Academy of Sciences, Prague, Czech Republic. The results of X-ray diffraction analysis, the electron microprobe analysis and that of the Mössbauer spectroscopy analysis were used as the complementary methods. The demonstration of the behaviour of the powdered sample is in Fig. 1.

The Curie temperature measurements of softly grinded sample somska3a (κ versus temperature) was mesured in air (Fig. 1 A) and sample Šomoška3a1g was measured in inert argon gas (Fig. 1 B). The following magnetic phases were detected: a) heating of sample Fig. 1 A: $T_C = 230$ °C = Ti-Mt (only partly oxidized), $T_{C1} = 570$ °C = Ti-Mgh; the Néel temperature $T_N = 450$ °C of Ti-Mt/Ti-Mgh AFM phase was mostly detected; $T_{N^*} = 530$ °C corresponds to Ti-Mgh/Ti-He AFM phase; b) cooling of sample: $T'_{C1} = 570$ corresponds to Ti-Mgh, $T_N = 450$ °C reflects the Ti-Mt/Ti-Mgh AFM phase. **B**: a) heating of sample: $T_C = 230$ °C = Ti-rich Ti-Mt (only partly oxidized), $T_{C1} = 580$ °C = Ti-Mgh, T_{N^*} = Ti-Mgh – Ti-He AFM

phase; b) cooling of sample: $T'_{C1} = 580\,^{\circ}C$ = Ti-Mgh, T'_{N^*} = Ti-Mgh + Ti-He AFM phase; $T'_C = 120\,^{\circ}C$ = Ti-rich Ti-Mt phase; magnetic susceptibility of magnetic mineral was about twice enhanced of κ before heating to 700 °C and cooling of sample to room temperature. It appeared due to the partial decay of the Fe-Ti AFM phase and its breaking down to the two constituents, Ti-rich Ti-Mt and that of Ti-Mgh. No such or similar behaviour appeared in the case of sample after heating it to 700 °C and cooling to room temperature in air (Fig. 1, A). Instead, a partial oxidation of the sample took place. A partial decay of the Fe-Ti AFM phase took place. A dominant part of this AFM phase has been preserved. The Ti-Mt/Ti-Mgh AFM phase has been then considered as the Fe-Ti FriM-AFM chemical phase.

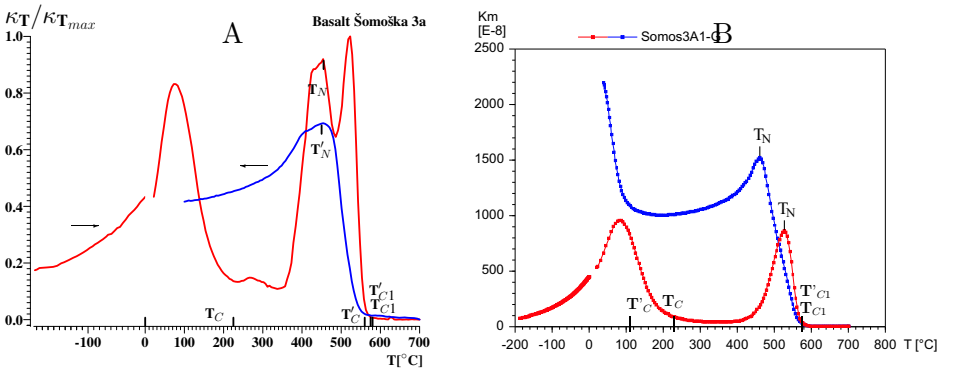

Fig. 1. Demonstration of magnetic behaviour of AFM Ti-Mt – Ti-Mgh phase during continual heating to 700 °C and cooling of coarsely grinded samples; κ versus temperature of grinded olivine basalt sample Šomoška3a1g mesured at air (A) and in inert argon gas (B). (Curie temperature measurements).

5. The description of the different magnetic behaviour of κ of the rocks versus temperature

I have described below the newly established categories of κ versus temperature behaviour, dependently on the inducing fields: 1) The rocks containing only the ferrimagnetic Fe-Ti oxides; 2) The rocks containing the Fe-Ti FriM-AFM ChPs cubic spinels; 3) The rocks containing the Fe-Ti FriM-AFM ChPs tetragonal spinels. This knowledge, together with the derived Eqs. (6), (7), (see below), have provided a complete new approach to

interprete the results in the rock magnetism, paleomagnetism and in the geomagnetism.

I have pondered the results of the samples like the rhyolite from Malý Kamenec locality (Fig. 2) having the only normal RM. There is present only ferrimagnetic phase. I deduce that there is a dominant magnetite in this rhyolite. The two different cation sites in the structure form two magnetic sublattices with a strong antiferromagnetic couping. The spin arrangement can be: $(Fe^{3+}\downarrow)_A(Fe^{3+}\uparrow)_B(Fe^{2+}\uparrow)_BO_4$. We see from a formula that the spins of the Fe^{3+} in A and B sublattices are cancelled, so, the resultant magnetic moment of the magnetite is that of the $Fe^{2+}\uparrow$ of B sublattice. In that case the internal field $|H_{T,int}|$ will be of a positive orientation and it will contribute to the normal field. So, the κ of this rock will decrease gradu-

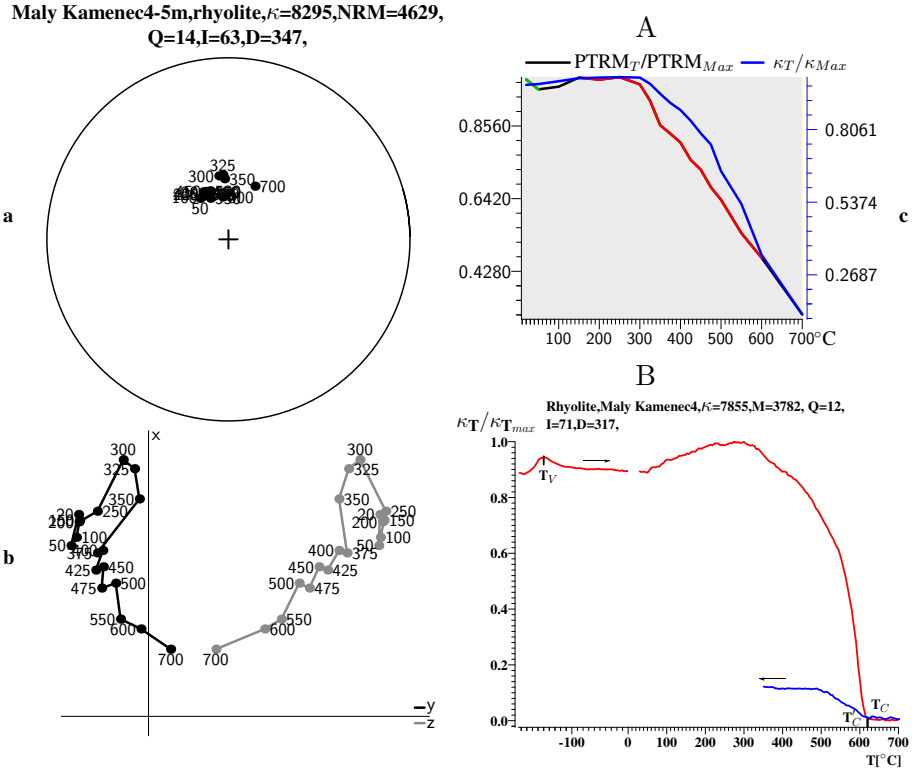

Fig. 2. A: The PTRM and κ versus temperature of rhyolite, sample malkam45, B: Curie temperature measurements of powdered sample mkamerh4, both from locality Malý Kamenec, Coordinates: 48.360 N, 21.790 E, Easthern Slovakia.

ally, according to the Eq. (7). There are dominantly the magnetite and the hematite in this rhyolite sample, respecting the Verwey temperature T_V, corresponding the magnetite and the Curie temperature T_C, corresponding to the non-stoichiometric hematite (see in Fig. 2).

5.1. The type of the κ curve versus temperature for the rocks with the ferrimagnetic alignment

The behaviour of the κ versus temperature can be very effectively applied to define the magnetic state of magnetic mineral. The equations (6) is the basic one to express the physical nature.

$$\kappa = \mu \frac{J_m}{H_{ef}} \tag{6}$$

μ – permeability (for (6) and (7) equations $\mu = 1$); J_m – magnetization of sample; H_{ef} – the effective inducing magnetic field, in our cases the geomagnetic field H.

We substitute the J_m with the PTRM, and the H_{ef} with the $H_{ef} = H + |H_{int}|$; then it can be expressed by the Eq. (7); H_{int} – internal molecular field.

$$\kappa = \mu \frac{PTRM}{H + |H_{T,int}|} \tag{7}$$

PTRM – magnetizations acquired during the temperature dependent magnetization of rock.

I have pondered the results of the samples like the rhyolite from Malý Kamenec locality (Fig. 2) having the only normal RM; the FriM-AFM ChPs has been missed or it has been completely desintegrated. There are dominantly the magnetite and the hematite in this rhyolite sample, respecting the Verwey temperature T_V, corresponding the magnetite and the Curie temperature T_C, corresponding to the non-stoichiometric hematite (see in Fig. 2).

I computed the relation of κ/PTRM data versus temperature in the interval from 25 to 700 °C. The data of the 16 individual temperature intervals are in the range 0.558 to 0.493. This relation has shown that the intensity of the inducing field H_{ef} does generate non-variable, nearly constant κ versus temperature. The Eq. (7) is valid for the rocks containing the pure

magnetite or quasi pure magnetite, the Ti-rich Ti-Mt, or the hematite containing rocks (*Orlický, 2010a*). The interanal field $H_{T,int}$ is of the normal orientation with respect to the magnetic field H. It is possible to suppose that the elementary magnetic moments (spins) of these minerals are parallel in the state of the lowest energy of the system. So, the field H will get gradually more intense, thanks to appearance of the positive internal field $H_{T,int}$. The magnetic behaviour of this Fe-Ti ferrimagnetic system will be similar to that of the ferromagnetic material.

5.2. Short background for magnetic behaviour of the κ versus temperature for the two sublattice Fe-Ti FriM-AFM cubic spinel ChPs

The results of samples of olivine basalt from a small lava dyke of Šomoška Castle locality; Coordinates: 48.171 N, 19.857 E, Southern Slovakia. The results have been applied for an explanation of the antiferromagnetic behaviour of the Fe-Ti FriM-AFM ChPs of the cubic spinels (Fig. 3).

5.3. The processing of the data in Fig. 3

The sample Som3A – the olivine basalt was of the reversed RM *in situ state*, without demagnetization of sample before its magnetization. There are the basic descriptions of the respective data, the quantities and the curves below the Fig. 3. The value of κ NRM, the differences Δm1,2,3,4 of PTRM of the sample are above, on the top in Fig. 3. The respective values were computed from the basic data. But I derived the real data, taking into account the law of additivity of the PTRM after cooling of the sample in the interval from an applied temperature T_n to room temperature. They are: The Δm1 corresponds to original reversed RM (spontaneous magnetization). It was completely removed during magnetization by the geomagnetic field and by the heating of the sample in the interval 25 to 150 °C. The Δm2 has a real value of 905 mA/m, because no other magnetic phase has lower blocking temperature below this phase. The Δm3 phase has shown the value = 779 mA/m of a reversed sense. But, its net value has been summed from the m3 = −779 and the m2 = −905, because the measured value −779 is a result of reduction of 905 mA/m due to cooling o sample through the m2 phase

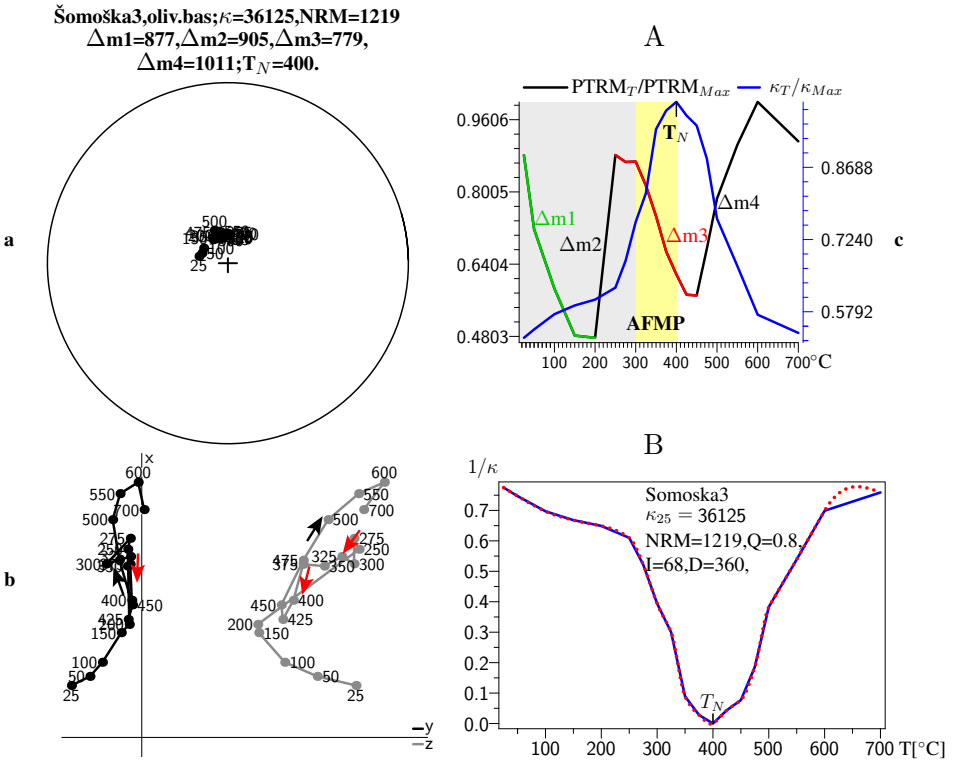

Fig. 3. A: The PTRM and κ versus temperature of olivine basalt from lava dyke, sample Som3A; locality Šomoška Castle; **a** – stereographic projection; **b** – Zijderveld diagram: arrows along the lines – a direction of either increase (black colour) or decrease (red colour) of the PTRM within a respective interval; **c** – susceptibility versus temperature curve (κ, blue curve) and partial thermoremanent magnetization – PTRM: Δm1,2,4 – the differences in PTRM between minimal and maximal values within the respective temperature intervals; Δm1 (green colour) – removal of original reversed spontaneous magnetization; Δm2 (black colour) – normally oriented magnetic moment of ferrimagnetic titanomagnetite (Ti-Mt) constituent of the AFM phase; Δm3 (red coloured curve) – reversally oriented magnetic moment of titanomaghemite constituent of the AFM phase; Δm4 (black colour) – normally oriented magnetic moment of more oxidized Ti-Mt (Ti-He) constituent of the AFM phase; soft yellow coloured area – the AFM phase; T_N – Néel temperature at 400 °C; κ values are in $\times$ 10^{-6} SI units; all NRM and PTRM data are in milli Ampere over meter, mA/m; AFMP – antiferromagnetic phase; B: $1/\kappa$ versus temperature of sample Somos3A1; curves of red, blue colour – the measurements at discrete temperatures and after smoothing of curve respectively.

to room temperature, respecting the additivity rule. It means that the net PTRM of Δm3 should be $-779 + (-905) = -1684$ mA/m. The Δm4 = 1011 contains the Δm3 = -1684 and the Δm2 = 905 = 1790 (106 + 1684).

5.4. Shortly about the law of additivity

According to *Stacey and Banerjee (1974)*, a specimen will acquire a PTRM if it is cooled in a field through a limited temperature range, being cooled in a zero field through the remaining ranges. Those grains whose blocking temperatures are within the range of field cooling acquire the thermoremanence, other do not, the resulting magnetization of the specimens, a whole being known as the PTRM. Tellier first noticed that the PTRMs acquired in different temperature intervals are independent. This means that the total TRM acquired by cooling a specimen in a field from the highest Curie point of its magnetic minerals to laboratory temperature is equal to the sum of the PTRMs acquired separately in several temperature intervals which together make up the whole temperature range. This is known as the *law of additivity* of PTRM (*Nagata, 1961*). The sum of PTRM:

$$\sum_{T_{i-1}=T_0}^{T_i=T} J_{T_i,H_{ex}}^{T_i-1}(T_0) = J_T, H_{ex}^{T_0}$$

Only normal polarity of the PTRM at individual temperature steps was detected in the stereographic projection. I have presented above also the corresponding κ and $1/\kappa$ curves versus temperature with the $T_N \approx 450\,^{\circ}$C. These types of Fe-Ti ChPs are characterized by the domain structure in magnetic grains (*Orlický, 2009*). The volume κ of this Fe-Ti FriM-AFM ChPs of the cubic spinels versus temperature has been governed by the above quantities of A and B sublattices, but also by the internal field $H_{T,int}$, at the temperature T, except of the normally oriented magnetizing field (H) during induction of the PTRM in the laboratory. I deduce that $H_{ef} = H + H_{T,int}$ are actual for this process.

The internal field $H_{T,int}$ is generated due to an activation of domains (or spins) and the exchange interction with the two sublattice systems (the $H_{T,int}$ is a function of the volume of domains in the respective material).

The orientation of this field is always antiparallel against the normal geomagnetic field. There is gradually generated the spontaneous magnetization of a value proportional to the intensity of the internal field $H_{T,int}$. The intensity and the direction of the net magnetization ($PTRM_{net}$) will be the vector sum of the normal PTRM ($PTRM_{nor}$), corresponding to the magnetizing geomagnetic field and that of the reversally oriented PTRM ($PTRM_{rev}$), corresponding to the intensity and the orientation of the internal field $H_{T,int}$, during the laboratory magnetizing of the Fe-Ti FriM-AFM cubic spinel ChPs containing rock sample.

We can see an elegant example of a certain mutual coupling of both, the κ and the PTRM magnetic behaviour (the shape of the PTRM curve and that of the reciprocal $1/\kappa$ curve versus temperature are nearly similar in the interval of temperatures where the AFM character of the sample has appeared. These characteristics were generated in the same sample during temperature dependent magnetization. The behaviour of κ versus temperature has been governed by the Eq. (7), dominantly by the gradual change of the internal magnetic field $H_{T,int}$, while the geomagnetic field H held sustained nearly in a constant level. We see a sharp increase of κ in the interval 250 to 400° C, with a maximum at T_N temperature, whereas the PTRM sharply decreased itself in the same interval, with a minimum at 400 °C (Fig. 3 A, B). This decrease of a previous positive value of the PTRM corresponds to the gradual increase of the negatively oriented internal magnetic field in the sample. The PTRM has becommed gradually of the reversed magnetization of the sponataneous origin in the sample. The behaviour of the κ and the PTRM is an opposite behind of the T_N of the Fe-Ti AFM phase. The internal field $H_{T,int}$ has gradually disappeared behind the T_N. It has been detected by the rapid decrease of κ and increase of the PTRM in Fig. 3. So, the internal field $H_{T,int}$, figured in the equation (7) has playied the decisive role in the magnetizing of the Fe-Ti FriM-AFM cubic spinel containing rocks in the nature and in the laboratory.

5.5. The transition of the Fe-Ti FriM-AFM cubic spinel ChP to the Fe-Ti FriM-AFM of the tetragonal spinel ChP

The Fe-Ti AFM cubic inversion spinel phase is supposed to be in a metastable state. It can be either partly or completely desintegrated, or it can be trans-

formed for tetragonal symmetry Fe-Ti oxide, due to alteration-transition mechanism, during heating of a previous material to temperatures about 600–700 °C in the field. I have revealed the Fe-Ti FriM-AFM ChPs of a tetragonal symmetry, or a combined cubic-tetragonal spinel, in the rocks. One could detect a less striking κ curve versus temperature (mostly only some remnant of previous phase has been preseved), frequently with a higher T_N than the previous a cubic symmetry Fe-Ti FriM-AFM ChPs. The physical and chemical features of this Fe-Ti FriM-AFM ChPs have shown that this type has arisen due to a transition of the previous Fe-Ti FriM-AFM ChPs of the spinel cubic phase. There are the examples of magnetic behaviour during magnetization versus temperature of samples (Figs. 3–5). The results have shown that the reversed RM has been inparted from the respective Fe-Ti FriM-AFM cubic spinel ChPs to the Fe-Ti FriM-AFM tetragonal spinel ChPs.

The results of the sample Pohanský vrch in Fig. 4 A, sample Trebelovce1-5 in Fig. 5 A and the sample Lošonec 4m in Fig. 6 have shown a very complex behaviour of the PTRM and the κ versus temperature. The samples in Figs. 4, 5 belong to the grouping involving 9 localities in Cerová vrchovina of southern Slovakia. About 76 samples of the olivine basalts were studied. All these samples have shown the physico chemical features similar to that like the Pohanský vrch and Trebelovce1-5 samples. In all these samples the AFM behaviour and the reversed RM was either partially or totally preserved during magnetization of the sample by normally oriented geomagnetic field of intensity H = 47.5 μT in the laboratory (in sample Pohanský vrch up to 300 °C, Fig. 4). The κ curve has shown also the AFM behaviour up to the Néel temperature T_N = 500 °C. The samples of rocks with these Fe-Ti FriM-AFM ChPs have shown the presence of T_N and T_{N1} different points. The peaks of the T_{N1} and T_N are suppose to be a rather less conspicuous than that in the Fe-Ti FriM-AFM cubis spinel ChPs. These types have more Ti-Hem containing composition. The rocks containing this type of the Fe-Ti FriM-AFM ChPs do have the reversed polarity of RM, more consistent direction of RM and a higher magnetic stability than those of the previous cubic spinel phases. A very low κ and a relatively high RM are the dominant chracteristics for the older rocks. Some of them do possess only one AFM phase with only one T_N temperature, others do have the two AFM phases and the two T_N (see in Fig. 6).

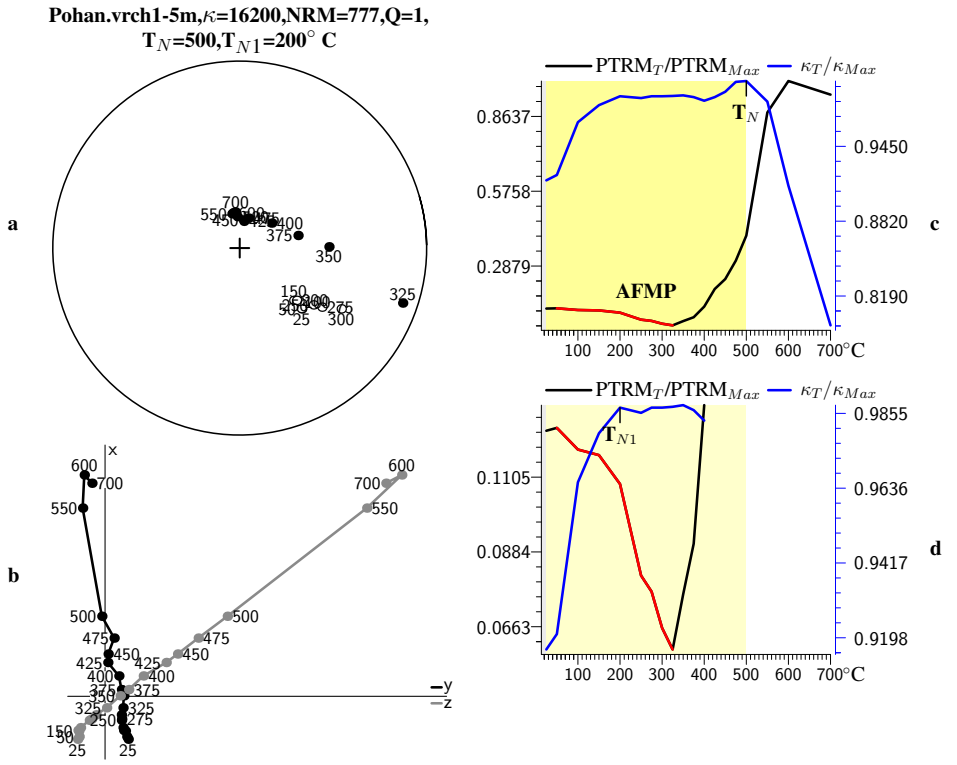

Fig. 4. PTRM and κ versus temperature of olivine basalt, sample Pohanský vrch, locality Pohanský vrch; Coordinates: 48.200 N, 19.922 E, Southern Slovakia; **d** – a magnification of the behaviour of a limited part of the PTRM and κ versus temperature of the sample.

The Fe-Ti FriM-AFM tetragonal spinels are dominantly characterized by the T_N near to 500 °C, but in many cases also with the intermediate T_N between 450 to 500 °C. I present the example of the combined, the Fe-Ti FriM-AFM tetragonal spinel and the Fe-Ti FriM-AFM cubic spinels, which are there in the olivine basalt from the Trebelovce locality, belonging to the grouping of 9 localities (a description see above).

The Eq. (7) is valid also for this type. But we need to respect some influence of the RM on the κ behaviour of the sample (the κ versus temperature is lagging behind the RM behaviour versus temperature). This effect is probably the reflection of the extreme high hysteresis of the RM of these rocks. I have selected only three examples in the Figs. 4–6, but

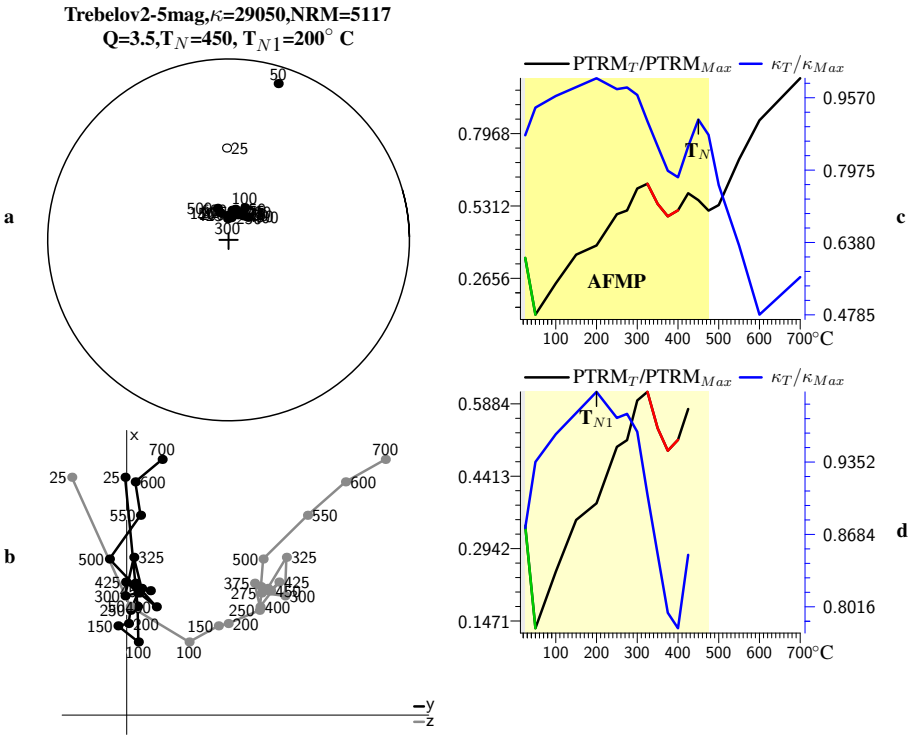

Fig. 5. PTRM and κ versus temperature of olivine basalt, sample Trebelovce2-5, locality Trebelovce; Coordinates: 48.287 N, 19.716 E, Southern Slovakia; **d** – a magnification of the behaviour of a limited part of the PTRM and κ versus temperature of the sample.

I have identified many such types of rocks so far. We see that the stable RM is linked with the AFM phases of the rock. The hysteresis of the RM is evident on nearly unchangeable values of the vector projections onto the $x-y$ and $x-z$ plains versus temperature, in the interval from 25 to 500 °C, (see on the Zijderveld diagrams in Figs. 4–6). The high stability and the reversed direction of the RM of the sample has been preserved up to 500 °C (see in Fig. 6). The reversed RM of the high Fe-Ti FriM-AFM tetragonal spinel ChPs in the rocks have been imparted from the Fe-Ti FriM-AFM cubic spinel ChPs containing rocks during the alteration transition processes in nature.

Many laboratory tests have shown that the oxidation and partial decomposition of minerals in the rocks take place rather regularly in the field. The

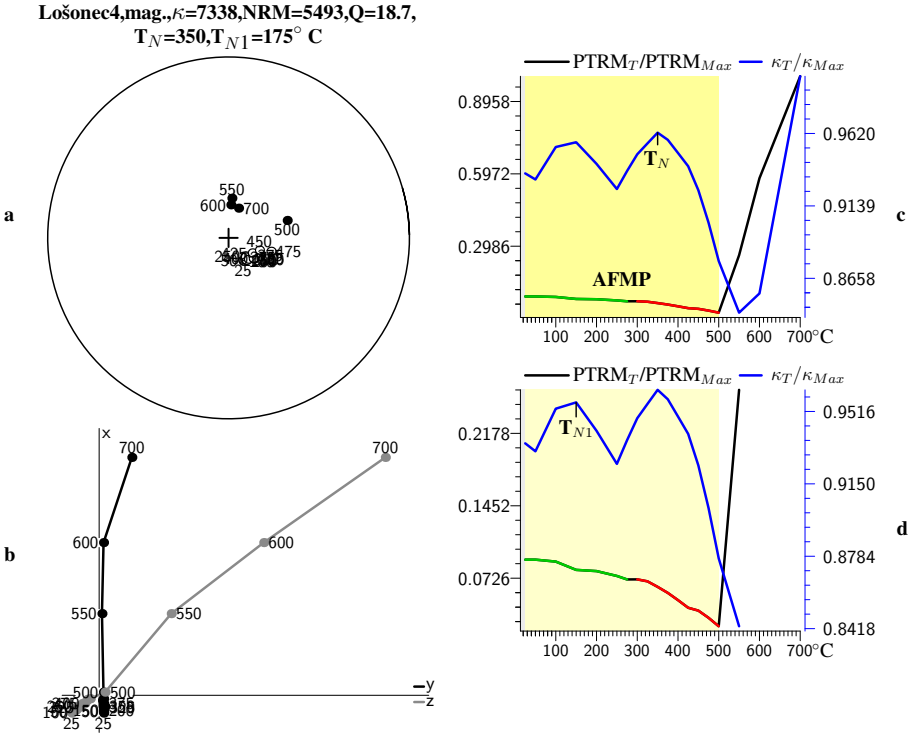

Fig. 6. PTRM and κ versus temperature of the melaphyre (the age about 270 My, the Upper Permian, the sample Lošonec 4m, the locality Lošonec; Coordinates: 48.438 N, 17.302 E, Low Carpathian Mts., Westhern Slovakia; **d** – a magnification of the behaviour of a limited part of the PTRM and κ versus temperature of the sample; green and red part of the PTRM curve differ the individual AFM phases.

decomposition of the Fe-Ti FriM-AFM cubic spinel phases has taken place at the temperatures close to T_N, or over 450 °C to 500 °C in the field (the temperature about 475 °C was derived as a typical for the decomposition of the AFM phase).

6. The summarized results of laboratory magnetization of rocks

The results were previously published, but not complete explanation of all characteristics was done. Generally, the pure ferromagnetic and the pure

ferrimagnetic Fe and Fe-Ti minerals of rocks should acquire a normally oriented RM under normally oriented magnetizing field. But if there are the Fe-Ti FriM-AFN ChPs in the rocks, the acquirement of the reversed sponataneous magnetization can be expected during their magnetization in laboratory. The reversed magnetization was only seen in the rocks having the Fe-Ti AFMP, according to *Orlický (2014)*. Generally, the chemicophysical features and the characteristic behaviour of κ versus temperature described above can be effectively applied for the interpretation of the results.

I studied the rocks from Kremnické vrchy Mts., Poľana-Javorie Mts., Zemplínske vrchy Mts., Vihorlat Mts., and Bohemian massif (*Orlický, 2001; 2002a; 2002b; 2002c; 2002d; 2002e; 2003a; 2003b; 2003c; 2003d; 2003e*). I applied the laboratory induction of PTRM in the rocks by normally oriented geomagnetic field. The samples were heated to 670 °C in a non-magnetic furnace under a fully compensated field and they were kept there for 30 minutes at this temperature. The PTRM was induced during the cooling of samples from 640 °C to 580 °C; the external field was fully compensated in the interval from 580 °C to laboratory temperature; later it was modified; the geomagnetic field was compensated from 520° C during the cooling of the samples (the description of procedures is in the literature cited above). The magnetization of samples by the external magnetic field should be active only within the delineated interval of 640 to 580 °C, temperatures the geomagnetic field, but it has taken place also at lower temperatures. Together 210 samples were magnetized (194 basaltic andesites and other types of andesites and 16 samples of rhyolites, all of them aged 9 to 15 My). Together 119 samples were of reversed polarity and 91 were of normal polarity of RM before laboratory magnetization. The results after the magnetization of the samples were the following: 102 samples acquired reversed magnetization (63 samples were originally of reversed polarity, 39 were of normal polarity of RM). Other 108 samples acquired normal PTRM (91 samples were originally of normal polarity and 17 of reversed polarity of RM). It is evident from a review that 39 samples acquired reversed magnetization which were originally of normal RM before laboratory magnetization. Many other samples of rocks were magnetized as well, but I have analysed only the results described in papers cited above. Why some samples of rocks, originally of reversed magnetization have not been magnetized reversally again,

and why some samples, originally of normal polarity acquired reversed magnetization by a normally oriented magnetic field in the laboratory? I have dominantly applied the results of the temperature dependent measurements of the magnetic susceptibility of a powdered sample and the compact sample versus temperature (Figs. 4–9) to explain the answers above. I presented many such evidences and the thermomagetic curves of selected rocks in the papers cited above.

I present now a short background to explain a more complex magnetic behaviour of the magnetic susceptibility versus temperature for the two sublattice systems, for the Fe-Ti FriM-AFM cubic spinel ChPs.

The Fe-Ti FriM-AFM cubic spinel ChPs probably contains the titanomagnetite, Ti-Mt, partly oxidized, of a ferrimagnetic alignment, and the titanomaghemite, Ti-Mgh, of the antiferromagnetic alignment. A partial oxidation and partial decomposition of minerals in the rocks took place rather regularly in the field. The results have shown that the state of the Fe-Ti FriM-AFM phases in the rocks has been influenced by the level of the thermal heating and its time duration. The decomposition of the Fe-Ti FriM-AFM phases has taken place at the temperatures close to T_N, or over 450 °C to 500 °C in the field (the temperature about 475 °C was derived as typical for the decomposition of the AFM phase. The specific measurements of a change of the κ of powdered sample at a constant temperature during 100 minutes, at different selected temperature intervals were done to derive a critical temperature of the probable decomposition of the AFM phase in the rock. The instrument and the procedure according to *Orlický (1990)* were used for these measurements. Most of rocks have been found in the field with a partly decayed AFM phase. This state of the AFM phase is then reflected in the intensity and the non-consistent directions (I and D) of RM of the magnetite and hematite containing rocks and of M_s containing dominantly the AFM titanomaghemite. The results have shown that there are present in the rock the individual constituents, as magnetite, hematite, pseudobrookite and ilmenite, after an alteration and a complete desintegration of the Fe-Ti AFM phase. Such rocks have possessed dominantly normal RM. There exists a second type of alteration and a transition of the Fe-Ti spinel AFM phase to the tetragonal spinel phase in the rocks of our interest. These effects have appeared on the deformed shapes of κ and PTRM curves versus temperature.

I have selected five groupings of rocks, respecting their different magnetic behaviour. The results for two samples from the different volcanic fields are presented in the respective figurere. There are considered the results of the polarity of magnetization (M) in the "in situ state" and the M′ "after the laboratory magnetization" of sample: 1) Normal, normal, Fig. 7; 2) Reversed, reversed, Fig. 8; 3) Normal, reversed, Fig. 9; 4) Reversed, normal, Fig. 10; 5) Anomalous directions and intensities of M of the autometamorphed rocks, Fig. 11.

6.1. Curie temperature measurements, a detection of the magnetic phases

The results of measurements of a change of κ of a powdered sample during a continual heating and a successive cooling of the sample have detected the Ti-Mt and the Ti-Mgh, which are the constituents of the Ti-Mt/Ti-Mgh AFM phase. The mentioned constituents were also detected by the X-Ray diffraction analysis. This is a completely new knowledge. The individual inversion spinel-cubic constituents Ti-Mt and Ti-Mgh have been coupled into the Ti-Mt/Ti-Mgh AFM (the Fe-Ti FriM-AFM phase during their existence in nature. This has allowed to establish a completely new category in rock magnetism, which has been based on the existence of antiferromagnetically aligned chemical compounds in nature.

6.2. The self-reversed origin of RM of rocks was proven by the results of the Curie temperature measurements of rocks

I firstly start with the characteristic features of the thermomagnetic curves. The presented thermomagnetic curves have concerned the natural sister samples of the respective rock. The results concern the measurements of a change of κ of a powdered sample of rock. These curves are combined from a low-temperature interval (– 190 to 0 °C) and a hihg-temperature interval (25–700 °C). Characteristic features: (heating curve, red colour), Low-temperature interval: an increase of κ from −190° C) to a peak T_V (Verwey transition temperature) detects the magnetite (Fe_3O_4); a gradual increase of κ from −190° C to laboratory temperature detects the titanomagnetite; a gradual decrease of κ from −190° C, mostly to laboratory temperature detects ilmenite. The ilmenite is an antiferromagnetic mineral with T_N about

$-205°$ C (maximum κ at an ordering temperature). It does not contribute to the RM of rocks. During heating over T_N a κ of the samples decreases. High temperature interval: The Curie temperatures: T_C = 120–230 °C – Ti-rich titanomagnetites; $T_C \approx 560°$ C – magnetite (mostly non-stoichiometric), with the same or very near T'_C and a reversible or, nearly reversible cooling curve, after heating of the sample to 700 °C and successive cooling; the Fe-Ti antiferromagnetic phase is characterized on the curves with the Néel temperatures T_N for an original state, and T'_N after heating of the sample to 700 °C and a successive cooling of the sample; $T_{C''}$ and T''_C correspond to the Curie temperatures of these Fe-Ti AFM phases, respectively; T_{C1}, T'_{C1} correspond to the Curie temperatures of the most oxidized magnetic phase, dominantly of the hematite enriched by maghemite. A rapid decrease of κ within the interval 300 to 450 °C, sometimes more (hump) in many samples corresponds to a transition and alteration of magnetite to maghemite (in some rocks it is a natural state, in some of them it is due to heating of samples in the laboratory; also a combined effect).

The interpretation of the results of magnetized rocks call for a detailed study of each respective sample. We need to pay an attention for the basic features and magnetic properties of the Fe-Ti FriM-AFM cubic and and the tetragonal spinels. If they are the stable enough ad they have not been decomposed during heating and cooling of the sample, the reversed RM should be preserved. If it has been either partly or a fully decomposed, the FriM-AFM alignment was disturbed and it was desintegrated in favour of individual constituents. The shape of the κ curve versus temperaure should be deformed in such cases (it is actual near to 475 °C).

The Fe-Ti FriM-AFM tetragonal spinels are dominantly characterized by the T_N near to 500 °C, but in many cases also with the intermediate T_N between 450 to 500 °C and there exist the combined, the Fe-Ti FriM-AFM tetragonal spinels and the Fe-Ti FriM-AFM cubic spinels in some rocks. These types of rocks contain two critical temperatures, the T_{N1}, haracterizing the tetragonal spinel and the T_N, characterizing the cubic spinel (see in Fig. 6). The curves of the κ and $1/\kappa$ versus temperature and the respective N éel temperatures are readable from the figures. A very characteristic feature is the very stable reversed RM (surviving to about 300 °C, in many types of rocks to about 500° C, during heating and the magnetizing of samples in the laboratory. This reversed RM is so stable, that it was

not removed, or remagnetized totally during cooling of the samples in the laboratory. The repeated heating of rocks to 670 °C did not destroy the previous RM of the rocks. Some rocks have shown a soft differences in the inclination (I) and the declination (D) values after heating to 670 °C and cooling to room temperature (see above), but the reversed polarity of the sample was preserved due to high hysteresis (high coercivity) of the Fe-Ti FriM-AFM tetragonal spinel ChPs in the rock. This is the basic explanation for the rocks which possessed the reversed RM before the laboratory magnetization and the reversed RM was preserved also after its magnetization by the normally oriented geomagnetic field in the laboratory.

These characteristics have been used to differ the cubic spinel types of Fe-Ti FriM-AFM phase carrying rocks from those of the tetragonal types of the Fe-Ti FriM-AFM phase carying rocks. in general.

As it was mentioned above, the temperature dependent measurements of κ of the two sublattice Fe-Ti FriM-AFM phase systems are governed by their Curie constants C_A and C_B, proportions of their quantities, and also with the forces of three types $n_{AA}J_A$, $n_{AB}J_AJ_B$ and $n_{BB}J_B$ exchange interactions. The most intense is the $A-B$ interaction. The actual Eqs. (6) (7) are above. The isolated ferrimagnetic Fe-Ti oxides are dominantly the products of both, the oxidation-alteration process of the Ti-Mt containing rocks, or the products of the decomposition of the Fe-Ti FriM-AFM ChPs in the rocks. There are present magnetite, hematite as the dominant minerals, except of the Ti-Mt and the non magnetic ilmenite and pseudobrookite in the rocks. If the isolated ferrimagnetic products are as dominant magnetic phases there in the rock, they carry dominantly normal RM. We can detect them at about 565–570 °C for magnetite, and at about 600–640 °C for hematite on the thermomagnetic curves during heating to 700 °C. If they have survived after heating, under duration of about 30 minutes. they are able to acquire the normal RM again.

6.3. Normal before, normal after magnetization (Fig. 7)

I took into account the polarity of the inclination of the RM of rocks. A similar behaviour concerns the 91 studied samples. All samples of rocks of this grouping have possessed the more oxidized Fe-Ti magnetic phases, the hematites, in some of them with magnetites. These hematites are of

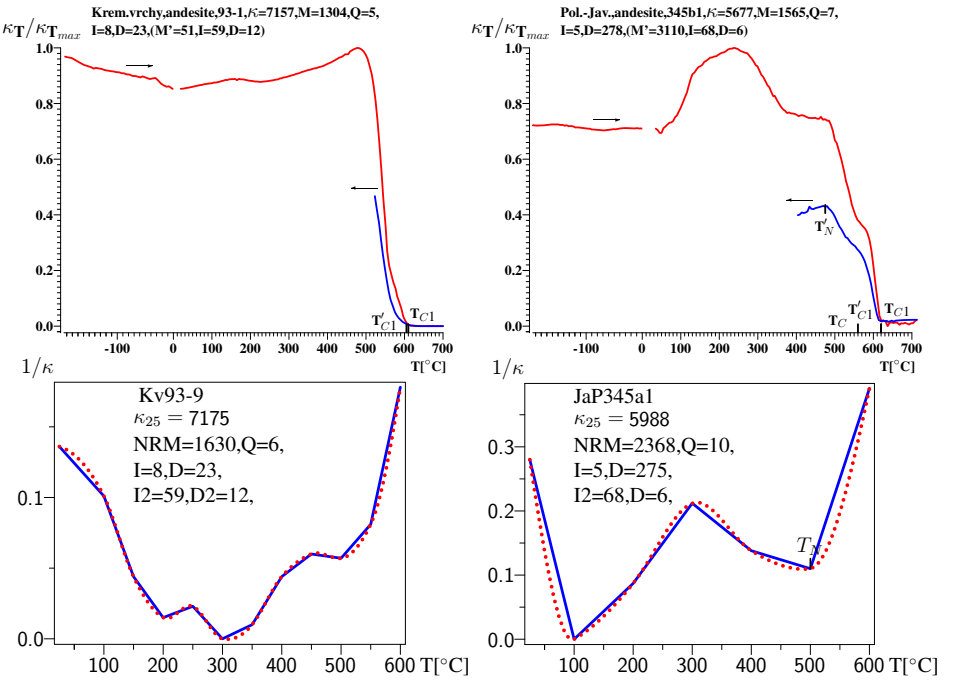

Fig. 7. **Normal before, normal after magnetization:** The temperature dependence of κ of sotfly powdered sample during heating to 700 °C and cooling to lower temperatures. Samples: krv93-1 (93-6, $1/\kappa$ curve) – andesite, Sielnica Formation, Kremnické vrchy Mts.; poj345b1, (jap345a1, $1/\kappa$ curve) – andesite Detva Formation, Poľana-Javorie Mts.; data in a picture: κ – magnetic susceptibility $\times 10^{-6}$ in SI Units; M – magnetization (remanent magnetization for the rocks of normal polarity and spontaneous for the rocks of reversed polarity) in mA/m – milli Ampere over meter; Q – Koenigsberger coefficient; I – inclination, D – declination of magnetization, respectively in a °; data in a round bracket – data after laboratory magnetization of the samples; M′ – a value of magnetization in mA/m, I, D – inclination and declination of RM of sample respectively after magnetization of sample in thelaboratory; T_C, T'_C – Curie temperatures after heating and cooling, respectively after magnetization of sample; T_V – Verwey transition temperature of the magnetite; T_N, T'_N – Néel temperatures of the Fe-Ti antiferromagnetic phase after heating and cooling of sample respectively; T''_C – Curie temperature of the Fe-Ti antiferromagnetic phase after cooling of the sample.

secondary origin and they originated due to the decay of the Fe-Ti AFMP, the titanomaghemite during its heating over T_N in the field. The magnetite, or the Ti-Mt are the products of the decay of the Fe-Ti AFMP. A successive alteration of the magnetite, through the maghemite occurs and the hematite

is the resulting and final product of this alteration. The magnetization is mostly of chemical (CRM) origin, only in the rare cases could be acquired as the thermoremanent (TRM) origin in the basaltic and the andesitic rocks. It means, that if there are present these hematite and the magnetite as the dominant minerals in the rocks, only the normal magnetization can be induced in the field and also in the laboratory, during magnetization by a normally oriented magnetic field. There are 17 samples which possessed reversed magnetization before laboratory magnetization. We see from Fig. 9 that the Fe-Ti AFM phase has not been preserved during heating to 700 °C and a successive cooling of the samples. So, the Fe-Ti AFM phase was decayed in the field and the secondary magnetite through maghemite to hematite were transformed. So the only normal magnetization was induced in these rocks in the laboratory.

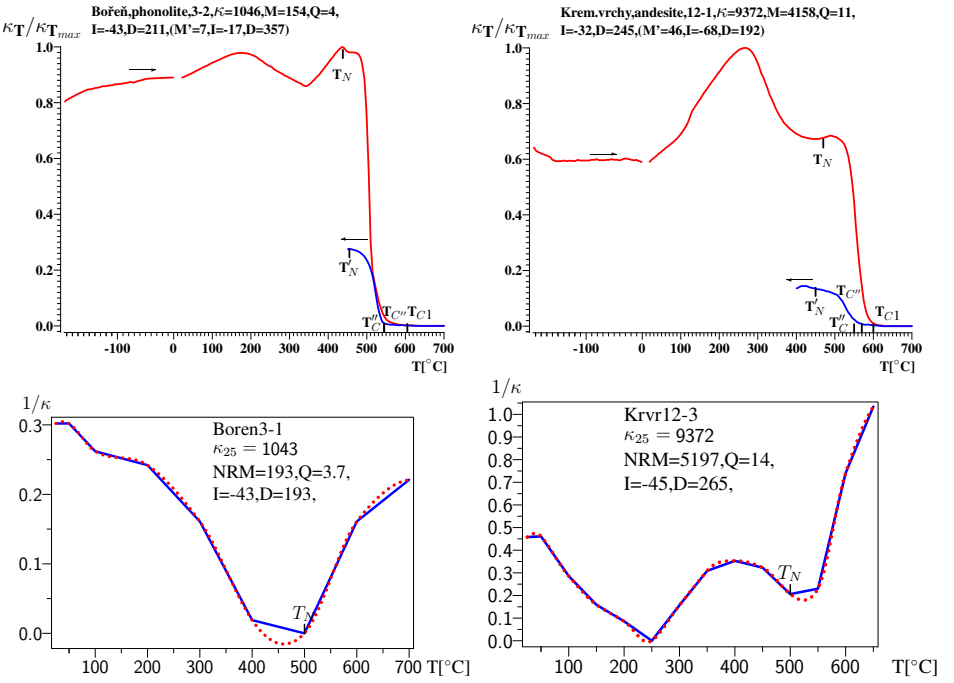

Fig. 8. **Reversed before, reversed after magnetization:** The samples: (Bořen3-2, Bořen3-1, $1/\kappa$ curve) – nepheline phonolite, North Bohemia; (krv12-1, krv12-3, $1/\kappa$ curve) – andesite, Turčok Formation, Kremnické vrchy Mts. For further descriptions and explanations see in Fig. 7.

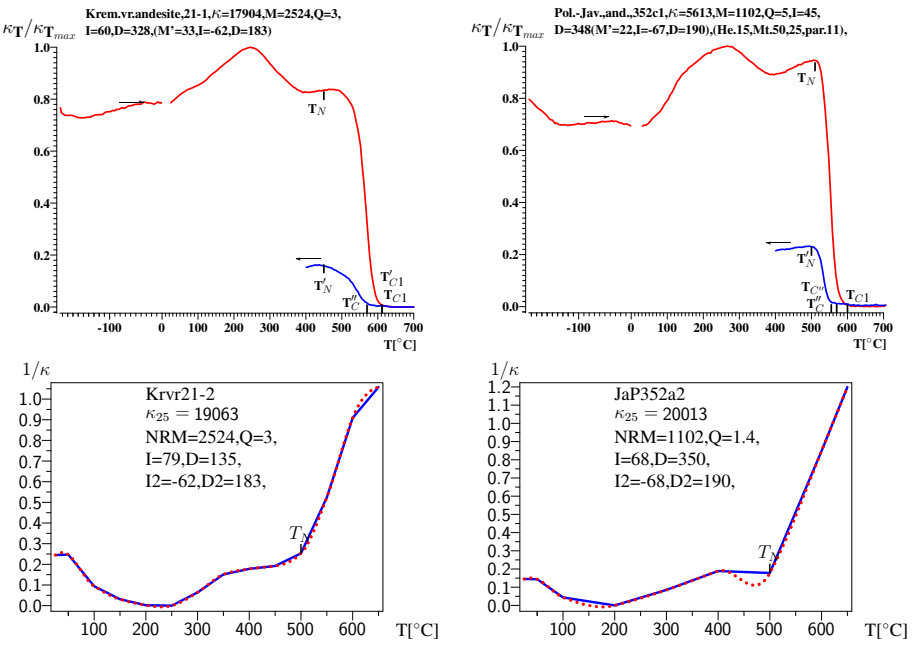

Fig. 9. **Normal before, reversed after magnetization:** The samples: (krv21-1, Krvr21-2, $1/\kappa$ curve) – andesite, Turčok Formation Kremnické vrchy Mts.; poj352c1, Jap252a2, $1/\kappa$ curve) – andesite, Veľká Detva Formation, Poľana-Javorie Mts. For further descriptions and explanations see in Fig. 7.

6.4. Reversed before, reversed after magnetization (Fig. 8)

A role in these samples plays the Fe-Ti AFM phase with its magnetic behaviour. The Fe-Ti FriM-AFM phase was there in the sample before laboratory magnetization and it has been preserved also after the laboratory magnetization in the sample. A similar behaviour have shown 63 samples having the reversed magnetization. In 39 samples of rocks, having a normal RM before magnetization possessed also a more oxidized phase, mostly magnetite. This was partially transformed to hematite before the magnetization of the sample. But during its heating to 700 °C and cooling this portion was reduced and dominantly the Fe-Ti AFM phase was preserved in the sample. During repeated heating of the sample a transition of the Fe-Ti FriM-AFM cubic spinel phase to the Fe-Ti FriM-AFM tetragonal spinel phase took place in the system. Such behaviour was seen in 39 samples (an example see in Fig. 9). From Fig. 8 we see that the shape of the $1/\kappa$ curve

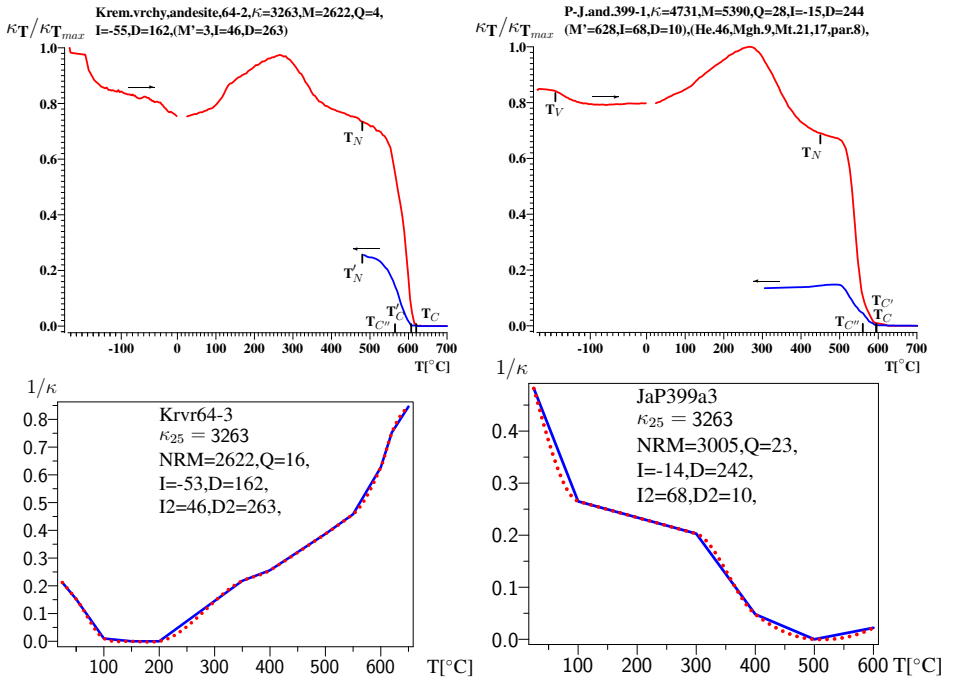

Fig. 10. **Reversed before, normal after magnetization:** The samples: (krv64-2, Krvr64-3, $1/\kappa$ curve) – andesite, Zlatá Studňa Formation, Kremnické vrchy Mts.; poj399-1, JaP399a3, $1/\kappa$ curve) – andesite, Rohy Formation, Poľana-Javorie Mts. For further descriptions and explanations see in Fig. 7.

of sample Boren3-1 is very near to that of a parabola like shape, characteristic for the reversed RM of samples. These more oxidized minerals are of a secondary origin. There are frequently present some combined Fe-Ti FriM-AFM phases in these chemical compounds, having partially the Fe-Ti cubic spinels and those of the Fe-Ti FriM-AFM phase tetragonal spinels. This feature is indicated by an enhanced T_N point from about 450 to about 500 °C and by a missing of domain structure in such samples of rocks. But the preservation of the reversed RM in these types of the Fe-Ti tetragonal spinel containing rocks is the most characteristic feature (see in Figs. 4–6).

6.5. Normal before, revered after magnetization

There were originally present both, the cubic spinel and the tetragonal spinel ChPs in these rocks. A partial destroying of these antiferromagnetic phases

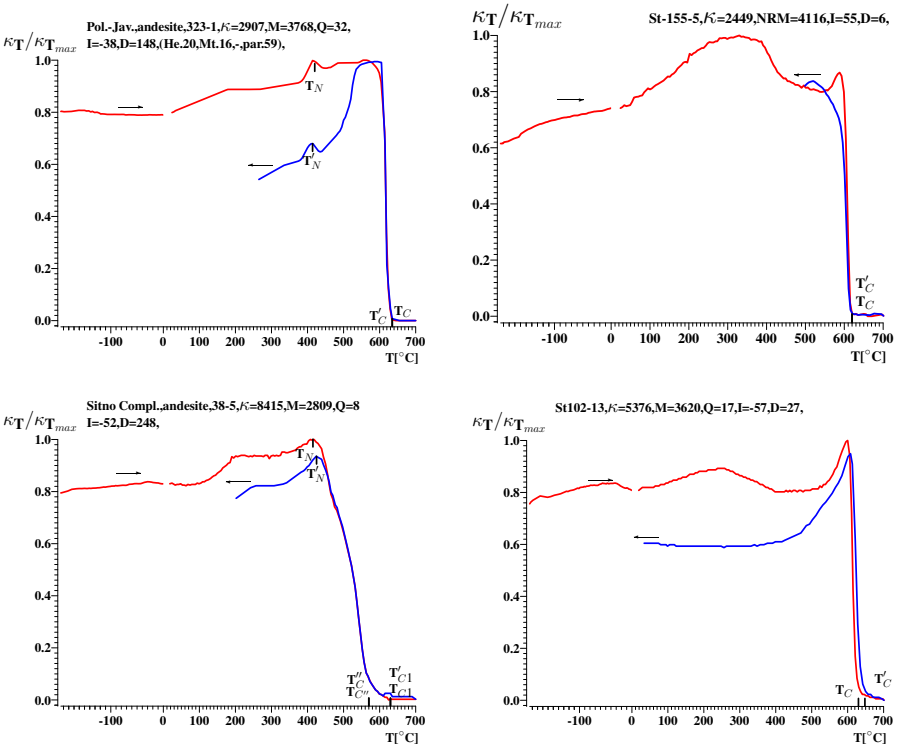

Fig. 11. **An anomalous magnetic behaviour:** The samples: PoJ323-1, autometamorphed andesite, Abčina Formation, Poľana-Javorie Mts.; Stf155-5, biotite-hornblrnde andesite of Studenec Formation; Sk38-5, autometamorphed andesite, Sitno effusive Complex, Štiavnické vrchy Mts.; St-102-13, biotite-hornblrnde andesite of Studenec Formation, Štiavnické vrchy Mts.; For further descriptions and explanations see in Fig. 7.

produced the individual Fe-Ti oxides which were remagnetized in the field. The directions (I, D) of the RM are mostly anomalous ones. A high stability of a previous reversed RM is a main characteristic which remagnetized the secondary components and the resultant RM has becommed to be as the reversed RM of the rocks, after heating in the laboratory. The thermomagnetic curves detected the T_C of over 600 °C and the T_N temperatures at about 450° and 500°, respectively during heating (red curve), and of about T'$_C$ about 550 to 570 °C during cooling of sample (blue curves). The T_N temperatures were detected at about 450°, 500 °C, respectively during cooling of samples. The $1/\kappa$ versus temperature curves have shown the anti-

ferromagetic Fe-Ti FriM-AFM behaviour with a T_N temperatures at about 599 °C.

6.6. Reversed before, normal after magnetization

There were originally present both, the cubic spinel and the tetragonal spinel ChPs, differing the T_N temperatures in these rocks. A partial destroying of these antiferromagnetic phases produced the individual Fe-Ti oxides which were remagnetized in the field in favour of normal directions of the RM (the directions are close to the direction of the geomagnetic field in the laboratory). The thermomagnetic curves detected the T_C of over 600 °C during heating (red curve), and during cooling of sample (blue curves). The $1/\kappa$ versus temperature curves have not detected the antiferromagetic Fe-Ti FriM-AFM behaviour, no T_N temperatures were detected. The X-ray diffraction analysis identified the tetragonal γ-Fe_2O_3 spinel, rhombohedral α-Fe_2O_3 in the samples of autometamorphed andesites PoJ323-1, Sk38-5, and in the biotite-hornblende andesite St-102-13. Low portion of magnetite (in the A sublattice) was also detected by the Mössbauer spectroscopy. The high portion of FeO and mostly low portion of TiO_2 were identified by the electron microprobe analysis in these samples. We can deduce that the rocks, as that represented by the samples in Fig. 11 survived the alteration-transition process in nature. They had originally the reversed RM, which was dominantly preserved also after the alteration-transition process.

7. Discussion and conslusions

So far, nearly all authors in a study of the magnetism and the paleomagnetism of rocks have accepted an explanation that the reversed RM of the rocks originated due to reversally oriented geomagnetic field in the time the rocks originated. An attractivity of this hypothesis was enhanced after the publication of geophysical measurements under the seas and oceans and the interpretation of marine magnetic anomalies. Many variable Geomagnetic Polarity Time Scales (GPTS) have been constructed, e.g. *Heirtzler et al., 1968; Kent and Grantstein, 1986; Berggren et al., 1995; Candl and Kent, 1995; Kent and Olsen, 1999; Huestis and Acton, 1997;* and others. The Pleistocene to Early Miocene Time Scale (*Berggren et al., 1995*)

is a very complex one. It is based on the RM polarity intervals of rocks, complemented by the Planctonic foraminifera and Calcareous nanoplancton data, ranging in the age from present time to 24.6 My. The GPTS of *Kent and Olsen (1999)* was constructed using the stratigraphic and magnetostratigraphic analyses from approximately 5000 m thick composite section obtained by scientific coring in the Newark rift basin of eastern North America. Only normal polarity was found in approximately 1000 m of interbedded volcanics and continental sediment of earliest Jurassic age but a total of 59 normal and reverse polarity magnetozones are delineated underlying 4000 m of the Late Triassic continental sediments. Generally the polarity timescale intervals are very irregular, reflecting also a very irregular dynamics of the geomagnetic field in the past. The GPTS have been frequently applied by specialists for the magnetostratigraphic interpretations. As we have known, the field-reversal theory was applied as a dominant in the paleomagnetism and in the study of magnetism of the rocks. The geomagnetic polarity timescales have provided one of the few lines of the empirical evidence of the geodynamo dynamics (*Kent and Olsen, 1999*). We do exactly know only today's orientation of the field with its short period and long period variations, applying the observatory measurements. Some known model see in *Olsen and Mandea (2007*).

There are presented above the complete new, original approaches for the explanation of the origin of the reversed remanent magnetization of rocks on Earth. The explanation is based on the existence of the Fe-Ti ferrimegnetic-antiferromagnetic chemical phases of the two sublattice systems in the rocks. There exist the interactions of these Fe-Ti FriM-AFM ChPs with the Weiss molecular field-Heinsenberg forces, generating the reversally oriented internal magnetic field. A production of the reversed spontaneous magnetization is a consequence of these processess. So, the Fe-Ti FriM-AFM ChPs in the rock, the local molecular fields with so called Weiss-Heisenberg forces (*Néel, 1971*) are decisive for the acquirement of the reversed magnetization in the rock. The basic ChPs in the rocks is supposed to be the Fe-Ti FriM-AFM cubic spinel. But it has a tendency to be altered and transitioned in favour of the tetragonal spinel. A very important knowledge is that the reversed magnetization is supposed to be imparted from the cubic spinel to the tetragonal spinel during this alteration-transitopn process in the rock. As a result, more stable RM has been preserved in these tetragonal spinels

(this part of my new idea call for more complex evaluation of knowledge about this problem). The central point of the above mentioned processess is the internal field, which is generated by the Weiss molecular field in the system.

More complex explanation of the reversed magnetization of rocks will be complemented in a future by analyzing the magnetizing processes applying the available knowledge (*Brož, 1962; Hajko et al., 1982; Vonsovskij, 1971*). From the results we see that there have been generated two different types of mechanisms during magnetizing of samples versus temperature. The shifting of the domain walls and the magnetizing vector of spontaneous magnetization rotation. If it is so, the magnetizing vector of spontaneous magnetization rotation is exclusively actual only for Fe-Ti FriM- AFM ChPs in reck.

The effective laboratory methods for the detection of the magnetic behaviour of the Fe-Ti FriM-AFM ChPs containing in the rocks are described as well. I need to empasize that the application of the magnetic methods and procedures has played the very important role to reveal the presented new phenomena. A very favourable knowledge is that we are able to study the Fe-Ti FriM-AFM ChPs containing rocks also by the Curie and the T_N temperature measurements of powdered rocks (see above).

The presented results have allowed to establish a complte new model:

1) Only the normal RM can be find in the rocks, containing the isolated Ti-rich titanomagnetite, the isolated non-stoichiometric, or pure magnetite, the isolated non-stoichiometric, or pure hematite.
2) Only the reversed RM can be find in the rocks, containing the Fe-Ti FriM-AFM ChPs, either of the cubic, or the tetragonal symmetry. The complementary are the results of the self-reversal origin presented in a review above.

My final statement: the above presented results have shown that we do not need to apply the field reversal theory, because I have revealed the realistic mechanism which is able to generate the reversed RM of rocks under a presence of the normal geomagnetic field. The presented results have shown that we do not need to apply the field reversal theory, because I have revealed the realistic mechanism which is able to generate the reversed RM of rocks under a presence of the normal geomagnetic field.

Acknowledgements. The author is graetful to Ladislav Bittó from the Earth Science Institute SAS, Bratislava, for a willing help in technical works, namely for the modification of some graphical softwers; the author is grateful to Dr. Tiu Elbra, the Geological Institute of Czech Academy of Sciences, Prague, Czech Republic, for the measurements of the Curie temperatures of some samples in argon atmosphere.

References

Balsley I. R., Buddington A. F., 1954: Correlation of remanent magnetism and negative anomalies with certain minerals. - J. Geom. Geoel. **6**, 4, 176–181.

Berggren W. A., Kent D. V., Aubry M. P., Hardembol J., 1995: Geochronology, Time Scales and Global Stratigraphic Correlation. SEPM Special Publication, **54**, Society for Sedimentary Geology, 129–212.

Bina M., Tanguy J.C, Hoffmann V., Prévot M., Listanco E. L., Keller R., Fehr K. Th., Goguitchaichvili A. T., Punongbayan R. S., 1999: A detailed magnetic and mineralogical study of self-reversed dacite pumices from the 1991 Pinatubo eruption (Philippines). Geophys. J. Int., **138**, 159–178.

Brož J., 1962: Modern problems of ferromagnetism. Publisher of Czechoslovak Academy of Sciences. In Czech, pp. 186.

Candl S. C., Kent D. V., 1995: Revised calibration of the geomagnetic polarity timescale for the Late Cretaceous and Cenozoic. J. Geophys. Res., **100**, 6093–6095.

Carmichael C. M., 1961: The magnetic properties of ilmenite-hematite crystals. Proc. Roy. Soc., A263, 508.

Carvallo C., Sainctavit P., Arrio M. A., Guyodo Y., Penn R. I., Forsberg B., Rogalev A., Wilhelm F., Smekhova A., 2010: Self-reversal of magnetization in oceanic submarine basalts studied with XMCD. Geophys. Res. Lett., **37**, L11306, doi: 10.1029/2010GL043390.

Doubrovine P. V., Tarduno J. A., 2004: Self-reversed magnetization carried by titanomaghemite in oceanic basalts. Earth Planet. Sci. Lett., **222**, 959–969.

Goguitchaichvili A. T., Prévot M., 2000: Magnetism of oriented single crystals of hemoilmenite with self-reversed thermoremanent magnetism. J. Geoph. Res., **105**, B2, 2761–2780.

Goodenough J., 1963: Magnetism and the Chemical Bond. Interscience Publishers, a division of John Wiley and Sons, New York-London, pp. 393.

Haag M., Heller F., Carracedo J. C., Soler V., 1990: Remanent magnetization of andesitic and dacitic pumice from the 1985 eruption of Nevado del Ruiz (Colombia) reversed due to self-reversal. J. Volc. Geotherm. Res., **41**, 369–377.

Hajko V., Potocký L., Zentko A., 1982: Magnetizing Processes. Publisher of of Technical and Economical Literature (Alfa), Bratislava, pp. 318 (in Slovak).

Havard A. D., Lewis M., 1965: Reversed partial thermo-magnetic remanence in natural and synthetic titano-magnetites. Geophys. J., **10**, 59–68.

Heirtzler J. R., Dickson G. O., Herron E. M., Pittman W. C., Le Pichon X., 1986: Marine magnetic anomalies, geomagnetic field reversals, and motions of the ocean floor and continents. J. Geophys. Res. **73**, 2119–2136.

Heller F., Petersen N., 1982: Self-reversal explanation for the Lashamp-Olby geomagnetic field excursion. Phys. Earth and Planet. Interior, **30**, 358–372.

Heller F., Carracedo J. C., Soler V., 1986: Reversed magnetization in pyroclastics from the 1985 eruption of Nevado del Ruiz. Colombia. Nature, bf 324, 241–242.

Hoffmann V., Fehr K. Th., 1996: Micromagnetic, rockmagnetic and mineralogical studies on dacitic pumice from the Pinatubo eruption (1991, Philippines), showing self-reversed TRM. Geophys. Res. Lett., **23**, 2835–2838.

Hoffman K., 1975: Cation diffusion processes and reverse thermoremanent magnetization in the ilmenite-hematite solid solution series. Geophys. J. R. Astr. Soc., **41**, 65–80.

Huestis S. P., Acton G. D., 1997: On the construction of geomagnetic timescales from non-prejudical treatment of magnetic anomaly data from multiple ridges. Geophys. J. Int., **129**, 176–182.

Irving R., 1970: The mid-Atlantic ridge at 45° N. XIV. Oxidation and magnetic properties of basalts: review and discussion, Can. J. Earth Sci., **7**, 1528–1538.

Ishikawa Y., Syono Y., 1963: Order-disorder transformation and reverse t thermoremanent magnetism in the $FeTiO_3$-Fe_2O_3 system. J. Phys. Chem. Solids, **24**, 517–528.

Kelso P. R., Richter C., Pariso J. E., 1996: Rock Magnetic Properties, Magnetic Mineralogy and Paleomagnetism of Peridotites from Site 895 Hess Deep. Mével C., Gillis K. M., Allan J. F., Meyer P. S. (Eds.), 1996: Proceedings of the Ocean Drilling Program, Scientific Results, **147**.

Kennedy L., 1981: Self-reversed thermoremanent magnetization in a late Brunhes dacite pumice. J. Geomag. Geoelctr., **33**, 429–448.

Kent D. V., Grandstein F. M., 1986: A Jurassic to recent chronology. The Geology of North America, Vol. M., Geological Soc. of America, 45–50.

Kent D. V., Olsen P. E., 1999: Astronomically tuned geomagnetic polarity timescale for the Late Triassic. J. Geophys. Res., **104**, B6, 12831–12841.

Kirkpatrick R. J., 1979: 33. Leg 46 Cruise Synthesis: The Petrology, Structure, and Geologic History at Site 396. Initial Reports of the Deep Sea Drilling Project, **46**.

Krása D., Shcherbakov V. P., Kunzmann T., Petersen N., 2005: Self-reversal of remanent magnetization in basalts due to partially oxidized titanomagnetites. Geophys. J. int., **162**, 115–136.

Lawson C., Nord G. I., Dowty E., Hargraves R. B., 1981: Anti phase domains and reverse thermoremanent magnetism in hematite-ilmenite minerals. Science, **2013**, 1372–1374.

Lawson C., Nord G. I. Jr., Champion D. E., 1987: Fe-Ti oxide mineralogy and the origin of normal and reverse remanent magnetization in dacitic pumice blocks from Mt. Shasta, California. Phys. Earth Planet. Inter., **46**, 270–288.

Lindsley D. H., 1991: Oxide minerals: Petrologic and Magnetic significance, Reviews in Mineralogy, **25**. Series Editor: Ribble P. H., Mineralogical Society of America, 698 p.

Lowrie W., Lowlie R., Opdyke N. D., 1973: The magnetic properties of Deep See Drilling Project basalts from the Atlantic Ocean, Earth Planet. Sci. Lett., **17**, 338–349.

Marshall M., Cox A., 1972: Magnetic changes in pillow basalt due to sea-floor weathering. J. Geophys. Res., **77**, 6459–6469.

Nagata T., Akimoto S., Uyeda S., 1951: Reversed thermo-remanent magnetism. Proc. Jap. Acad., **27**, 643–645.

Nagata T., 1952: Reverse thermo-remanent magnetism. Nature 169, 704–705.

Nagata T., 1961: Rock Magnetism. Marusen Company Ltd., Tokyo. 341 p.

Néel L., 1948: Magnetic properties of ferrites: Ferrimagnetism and antiferromagnetism. Ann. Phys., **3**, pp. 137.

Néel L., 1971: Magnetism and the local molecular field (Nobel Lecture, December 11, 1970), 318–341.

Nord G. I., Lawson C. A., 1989: Order-disorder transition-induced twin domains and magnetic properties in ilmenite-hematite. Am. Mineral., **74**, 160–176.

Nord G. I., Lawson C. A., 1992: Magnetic properties of ilmenite$_{70}$ – hematite$_{30}$ effect of transformation-induced twin boundaries. J. Geophys. Res., **97**, 10897–10910.

Olsen N., Mandea M., 2007: Investigation of a secular variation impulse using satellite data: The 2003 geomagnetic jerk. Earth Planet. Sci. Lett., **255**, 94–105, doi: 10.1016/j.epsl.2006.12.008.

Orlický O., 1990: Detection of magnetic carriers in rocks: results of susceptibility changes in powdered rock samples induced by temperature. Physics of the Earth and Planetary Interiors, **63**, 66–70.

Orlický O., Funaki M., Pagáč P., 2000: Study of the self-reversal thermoremanent and partial thermoremanent magnetization of the Haruna dacite from central Japan. Contr. Geoph. Geod., **30**, 4, 323–342.

Orlický O., Funaki M., 2000a: An origin and mechanism of the self-reversed TRM or PTRM of rocks. A study of the Rhyodacite from the Haruna Locality (Japan). Geol. Carpathica, **51**, 201–204.

Orlick'y O., Funaki M., 2000b: Detection of Fe-Ti magnetic phases in the Haruna dacite from central Japan. An application of the Curie temperature measurements of samples. Contr. Geoph. Geod., **30**, 4, 359–372.

Orlický O., Funaki M., 2001: Magnetic study of individual Fe-Ti oxides separated from the rhyodacite of the Haruna Volcano (Japan) and the dacite ash of Mount Pinatubo (Philippines). Contr. Geoph. Geod. **31**, 3, 537–556.

Orlický O., 2001: Field-reversal versus self-reversal hypothesis: Paleomagmetic properties and magnetic mineralogy of the Neogene andesites of central Slovakia (Part I). Contr. Geoph. Geod., **31**, 4, 653–681.

Orlický O., 2002a: Field-reversal versus self-reversal hypothesis: Paleomagmetic properties and magnetic mineralogy of selected Neogene hornblende pyroxene andesites of central Slovakia (Part II). Contr. Geoph. Geod., **32**, 1, 1–40.

Orlický O., 2002b: Field-reversal versus self-reversal hypothesis: Paleomagnetic properties, magnetic mineralogy and the reproducible self-reversal RM of the Neogene andesites from the Javorie and Poľana mountain range (Part III). Contr. Geoph. Geod., **33**, 2, 91–128.

Orlický O., 2002c: Field-reversal versus self-reversal hypothesis: Paleomagnetic properties, magnetic mineralogy and the reproducible self-reversal RM of the Eocene to Miocene volcanic rocks from České Středohoří Mts. – North Bohemia (Part IV). Contr. Geoph. Geod., **32**, 2, 129–149.

Orlický O., 2002d: Field-reversal versus self-reversal hypothesis: Paleomagnetic properties, magnetic mineralogy and the reproducible PTRM of the Neogene andesites from the Kremnické vrchy mountain range (Part V). Contr. Geoph. Geod., **32**, 4, 309–333.

Orlický O., 2002e: Field-reversal versus self-reversal hypothesis: Paleomagnetic properties, magnetic mineralogy and the reproducible PTRM of the Neogene andesites from the East-Slovak Lowlands, Zemplínske vrchy Mts., and Slanské vrchy Mts., (Part VI). Contr. Geoph. Geod., **32**, 4, 359–373.

Orlický O., 2003a: Field-reversal versus self-reversal hypothesis: Paleomagnetic properties, magnetic mineralogy and the reproducible PTRM of the Neogene andesites from the Vihorlat Mts., (Part VII). Contr. Geoph. Geod., **33**, 1, 57–76.

Orlický O., 2003b: Field-reversal versus self-reversal hypothesis: Paleomagnetic properties, magnetic mineralogy and an origin of the reversed RM of the Neogene rhyolites from central and eastern part of Slovakia (Part VII). Contr. Geoph. Geod., **33**, 2, 77–97.

Orlický O., 2003c: The origin of RM, and magnetic mineralogy of the Cretaceous to Jurassic nepheline basanites from Nigeria and the Cretaceous basalts from the Syrian Arab Republic (Part XI). Contr. Geoph. Geod., **33**, 4, 309–332.

Orlický O., 2003d: The origin of RM and magnetic mineralogy of the Palaeozoic melaphyres from Western Carpathian Mts. and dominantly of intrusive volcanics from the Red Sea Hills, the Sudan Republic (Part X). Contr. Geoph. Geod., **33**, 4, 283–308.

Orlický O., 2003e: A study of magnetic properties and magnetic mineralogy of the Neogene volcanic and volcano-sedimentary rocks from Central Slovakia. Contr. Geoph. Geod., **33**, 2, 111–126.

Orlický O., 2006: Field-reversal versus self-reversal hypothesis: Different intensities of TRM of the reversely magnetized natural basalts and those of the same origin artificial samples magnetized in laboratory. Contr. Geoph. Geod., **36**, 1, 35–48.

Orlický O. 2009: The ionic reordering in Fe-Ti ferrimagnetics as a dominant source of the reversed RM in basaltic rocks. Contr. Geophys. Geod., **39**, 1, 55–82.

Orlický O., 2010a: On the demonstration of the normal polarity of remanent magnetization by volcanic rocks containing magnetite and hematite. Contr. Geophys. Geod., **40**, 3, 263–282.

Orlický O., 2010b: A realistic approach to explanation of the normal and reversed remanent magnetization of rocks: Application for submarine volcanics. Contr. Geophys. Geod., **40**, 2, 159–172.

Orlický O., 2011: The self-reversal origin of the reversed remanent magnetization in the igneous rocks containing the oxidized Fe-Ti oxide solid solutions. Contr. Geophys. Geod., **41**, 1, 19–44.

Orlický O., 2014: A strange antiferromagnetic phase has controlled the magnetic reversed remanent magnetization of rocks coming from the Earth globe. and paleomagnetic properties of the Fe-Ti inversion spinel bearing rocks Contr. Geophys. Geod. Paleo, Rocks and Environmental Magnetism, Book of on the whole Earth globe. Contr. Geophys. Geod., **44**, 2, 161–203.

Ozima M., Funaki M., 2001: Magnetic properties of hemoilmenite single crystals in Haruna dacite pumice revealed by the Bitter technique, with special reference to self-reversal thermoremanent magnetism. Earth Planet Space, **53**, 111–119.

Ozima M., Ozima M., 1967: Self-reversal of remanent magnetization in some dredged submarine basalts. Earth. Planet. Sci. Lett., **3**, 213–215.

Ozima M., Funaki M., Hamada N., Aramaki S., Fuji T., 1992: Self-reversal of thermoremenent magnetization in pyroclastics from the 1991 eruption of Mt. Pinatubo, Philippines. J. Geomag. Geoelectr., **44**, 979–984.

Ozima M., Larson E. E., 1968: Study of self-reversal of TRM in some submarine basalts. J. Geomagnet. Geoelectr., **20**, 4, 337–351.

Pan Y., Liu O., Deng Ch., Quin H., Zhu R., 2006: Thermally induced inversion of Al-substituted titanomagnetite in basalts: Evidence for partial self-reversal. J. Geophys. Res., **111**, B12S29, https://doi.org/10.1029/2006JB004576.

Petersen N., 1979: Rock and paleomagnetism of basalts from Site 396B, LEG 46, Initial Report DSDP 46.

Petersen N., Bleil U., Eisenach P., 1979: Low temperature alteration of the magnetic minerals in ocean floor basalts. In Talwani M., Harrison C. H., Hayes D. E. (Eds), Deep Drilling Results in the Atlantic Ocean: ocean crust. Am. Geophys. Union Maurice Ewing Series 2: Washington, 169–209.

Stacey F. D., Banerjee S. K., 1974: The physical principles of rock magnetism. Elsevier Scientific Company, 195 p.

Schult A., 1968: Self-reversal magnetization and chemical composition of titanomagnetites in basalts. Earth Planet Sci. Lett., **4**, 57–63.

Schult A., 1971: On the strenght of exchange interactions in titanomagnetites and its relation to self-reversal magnetization. Zeitschrift für Geophysik, Band **37**, 357–365.

Uyeda S., 1958: Thermo-remanent magnetism as a medium of paleomagnetism with special reference to reverse thermo-remanent magnetism. Jap. J. Geophys., **2**, 1–123.

Vonsovskij S. V., 1971: Magnetism. Magntic properties of dia-, para-, ferro-, antiferro-, and ferrimagnetics. Moscow, pp. 1032 (in Russian).

Wescott-Lewis M. F., Parry L. G., 1971: Thermoremanence in synthetic iron-titanium oxides. Aust. J. Phys., **24**, 735–742.

Xu W., Peacor D. R., Dollase W. A., Van Der Voo R., Beaubouef R., 1997: Transformation of titanomagnetite to titanomaghemite: A slow, two-step oxidation-ordering process in MORB. American Mineralogist, **82**, 1101–1110.

Zhou W., Van Der Voo R., Donald R., Peacor D. W., Zhang Y., 2001: Low temperature oxidation in MORB of titanomagnetite to titanomaghemite: A gradual process with application for marine magnetic anomaly amplitudes. J. Geophys. Res., **106**, B4, 6409–6421.